

University of Cincinnati

Date: 4/4/2017

I. Vishak Venkatraman, hereby submit this original work as part of the requirements for the degree of Doctor of Philosophy in Electrical Engineering.

It is entitled:

Optical and Power Source Integrated Paper Microfluidic Devices for Point of Care Systems

Student's name: **Vishak Venkatraman**

This work and its defense approved by:

Committee chair: Andrew Steckl, Ph.D.

Committee member: Fred Beyette, Ph.D.

Committee member: Leyla Esfandiari, Ph.D.

Committee member: Kenneth James Kozak, B.A.

Committee member: Ian Papautsky, Ph.D.



24650

Optical and Power Source Integrated Paper Microfluidic Devices for Point of Care Systems

A dissertation submitted to the
Graduate School
of the University of Cincinnati
in partial fulfillment of the
requirements for the degree of

Doctor of Philosophy

in the Department of Electrical and Computer Engineering
of the College of Engineering

by

Vishak Venkatraman

B.S. Anna University, India 2011

Submitted on April 4, 2017

ABSTRACT

The goal of this project is to create a point-of-care (POC) diagnostic device with several desirable characteristics, combining high sensitivity and semi-quantitative output in a cost effective and disposable package. Another important component of a POC system is power, and in this thesis, several options were explored. The biosensor used in this project is lateral flow immunoassay (LFIA), which is a paper based device. LFIAs have several desirable characteristics such as capillary action for fluid transport and affinity to proteins that makes them ideal candidates for Lab-on-Chip (LOC) applications.

The POC described in this paper is a combination of LFIA and organic optoelectronics as the signal detection component. Organic light emitting diodes (OLEDs) and organic photodiodes (OPDs) have been found to be desirable candidates over their inorganic counterparts for POC applications. Organic devices provide the distinct advantages of having planar form factor and large active area in nature which is suitable for the integration with LFIAs.

First, phosphorescence-based green OLEDs fabricated on plastic substrates were integrated as excitation light sources for fluorescent quantum dot (QD)-based LFIA devices. A 10× improvement in visual signal intensity was achieved compared to conventional LFIA, resulting in a 7× improvement in the limit-of-detection (LOD) of 3 nM concentration.

For power source options, a zero-power (on board) system was designed on a flexible plastic substrate. The system utilized the power provided by near field communication (NFC) antenna to an LED array formed on the same substrate using hybrid manufacturing techniques. Such a

system can harvest power from smartphones, which are a ubiquitous presence in this digital century. The NFC LED chip was used to excite the QD-based fluorescent LFA, which demonstrated again a $\sim 10\times$ higher sensitivity compared to conventional commercial devices. The hybrid manufacturing approach using roll-to-roll manufacturing and integration has the potential to significantly decrease the fabrication cost.

Finally, the LFIA was integrated with organic optoelectronics devices on plastic as the detector component as a step toward a fully integrated lab-on-chip device. An organic photodiode (OPD) that absorbs at green wavelengths has been used. The quantitative measurements have utilized optical transmission mode through an LFIA strip that forms red colored lines by the accumulation of gold nanoparticles (AuNP). In this configuration, the amount of transmitted light decreases as the number of Au NPs accumulate on the test line, which directly correlates with the analyte concentration. This change in optical intensity results in a change as change in the OPD photocurrent. We have successfully created such a prototype and have done a quantitative measurement of the analyte.

Acknowledgements

I would like to start by thanking my family, parents and sister, without whom this tough journey of my PhD tenure would have been tougher. Without their emotional support and constant motivation, this work would not have been possible.

Next, I would like to thank the funding and material supply sources for this project. NSF and CADMIM provided major funding for several goals accomplished in this thesis work. We gratefully also acknowledge the test kits provided by Meridian bioscience Inc. Cincinnati.

I would like to thank various staff at UC starting with Julie from Graduate office, Nicole from UC International, Janie and Dorothy from Electrical engineering department for their assistance in administrative procedures over the years. I would like to also thank Gisela for coordinating the work done in this thesis with CADMIM center at Irvine.

I would like to acknowledge Prof. Heikenfeld's support by giving me access to NDL lab's facilities and equipment. Thanks to Jeff Simkins for training me and giving me access to various facilities in the ERC central clean room.

I would like to thank all the current (early 2017) Nanolab members; Daewoo, Hua, Eric, Prajokta, Shima, Ashkan and Sam for their conversations and advice over the years. Many thanks to former lab members Eliot, Jerry and Hans for helping and guiding me in the initial several years where I had a chance to learn a lot.

I would like to acknowledge Ken Kozak from Meridan bioscience, Ralph from VTT Finland and Xiaole Mao from P&G for collaborating and guiding me in several parts of this thesis work.

I would like to thank Prof. Cahay and Prof. Mantei from EECE department who taught me various classes as well as having me as a TA for various courses they taught from which I gained incredible experience as well as knowledge. I am grateful to Dr. Ahn and Dr. Paputsky for teaching me courses which were essential to the work done in this thesis. Dr. Ahn's lab course also helped me acquire equipment as well as fabrication skills for experimental work in this project.

I would like to thank my PhD committee members Dr. Steckl, Dr. Papautsky, Dr. Beyette, Dr. Esfandiari and Mr. Kozak for guiding me through this work on a regular basis.

Finally, I am very grateful to my advisor Dr. Andrew Steckl. More than just an advisor I would like to thank him for being a great mentor. I would like to also specifically also thank him for his trust in me and accommodating me into his lab and preparing me for a professional career ahead.

TABLE OF CONTENTS

ABSTRACT.....	ii
Acknowledgements.....	v
TABLE OF CONTENTS.....	vii
List of Figures	xi
Common Abbreviations & Symbols	xvii
Chapter 1 : Introduction.....	1
1. Project Introduction and Overview	1
2. Paper Microfluidics for the Point of Care	3
3. Organic Electronics for LOC Applications	7
4. Proposed Contribution	11
Chapter 2 : Materials and Methods	15
1. Introduction	15
2. Organic electronics	15
2.1 Overview.....	15
2.2 OLEDs.....	16
2.3 OPDs	17

3.	Fabrication and Properties	18
4.	Organic Electronics at the Nanolab	22
4.1	Substrates and Anode patterning.....	22
5.	OLED and OPD Characterization	27
5.1	OLED Characterization.....	28
5.2	OPD Characterization	30
6.	Lateral Flow Immunoassays (LFIA).....	32
7.	Summary	36
Chapter 3 : Integration of OLED with Lateral Flow Immunoassays.....		37
1.	Introduction:	37
2.	Fluorescent LFIAs	38
3.	OLED Fabrication.....	42
4.	LFIA Assay Fabrication	44
5.	Integration	46
6.	Summary	51
Chapter 4 : Integrated NFC Power Source in Lateral Flow Immunoassays		52
1.	Introduction	52
2.	NFC LED Chip Fabrication.....	56
3.	LFIA Assay Fabrication	60

4. Results & Discussion	62
5. Summary	66
Chapter 5 : Integration of OPD Detector in Lateral Flow Immunoassays	67
1. Introduction	67
2. Device Fabrication & Characterization	73
3. LFIA Diagnostics	78
4. Integration	81
5. Conclusions	87
Chapter 6 : Conclusions and Future Work	88
1. Concluding Remark	88
2. Future Work	90
2.1 Flat Battery Power Source	90
2.2 Hybrid Microelectronics Circuits	94
Appendix A – Devices on NC Membrane	97
Appendix B – Clearblue device teardown	99
1. Components inside the device:	99
2. Cost analysis:.....	100
Appendix C: Cost analysis of proposed approach	102

1. OLED and OPD Fabrication cost	102
1.1 Layers Cost.....	102
1.2 Substrate Cost.....	103
2. Microelectronics on PET Fabrication	103
3. LFIA Test kits:	103
REFERENCES.....	105

List of Figures

Figure 1-1 Artistic rendering of an ideal microfluidic based POC system	2
Figure 1-2 Rapid diagnostics and its diverse fields of applications.	4
Figure 1-3 Paper microfluidics channel fabrication using Wax Printing technique.....	5
Figure 1-4 Paper based microfluidic devices; (a) Simple form of electrochemical sensor on paper fabricated using PR ⁵ ; (b) LFIA biosensor based on immunochemistry.....	6
Figure 1-5 Organic electronics: (a) A simple OLED structure; (b) OLED on a flexible plastic substrate; (c) OPV structure; (d) OPV device as a solar cell.	7
Figure 1-6 Organic optoelectronic applications in LOC devices; (a) Two part fabrication; (b) PDMS encapsulated photo detector.	9
Figure 1-7 Both OLED and OPD integrated with a fluorescence microfluidic system.....	10
Figure 1-8 Goals of this thesis work.....	13
Figure 2-1 OLED working principle; (a) First heterostructure OLED; (b) Physics underlying in an OLED.....	16
Figure 2-2 OPD working principle; (a) First heterostructure OPD; (b) Physics underlying in an OPD	18
Figure 2-3 Solution processing equipment; (a) Spin coating; (b) Inkjet printing; (c) Screen printing.	19
Figure 2-4 Thermal evaporation system; (a) Concept illustration; (b) Equipment at Nanolab....	21
Figure 2-5 Fabrication on flexible and unusual substrate; (a) OLED on transparent paper; (b) Flexible display wrapped around a pencil.	21

Figure 2-6 Energy band diagram of devices fabricated in this thesis; (a) OLED multi-layered stack; (b) OPD single layer stack.	22
Figure 2-7 ITO coated sheet obtained from Sigma Aldrich (blue color due to liner).	23
Figure 2-8 UV exposure tool used for Photolithography.....	24
Figure 2-9 MDB system for thermal evaporation of organic layers (operated by myself).....	25
Figure 2-10 Glass substrates and shadow masks used for various layer patterning during thermal deposition	26
Figure 2-11 Typical characteristics of an OLED; (a) Current-Voltage (I-V) characteristics; (b) Brightness-Voltage (L-V).	28
Figure 2-12 OLED chracterization setup; (a) LabVIEW PC control; (b) Brightness measurement meter (minolta).....	29
Figure 2-13 Spectral measurements; (a) Spectral measurement instrument; (b) Typical spectral shape of a green emitting OLED	29
Figure 2-14 OPD characteristics (typical); (a) Typical I-V characteristics of an OPD fabricated; (b) Photocurrent pulsing with puled light input.	30
Figure 2-15 OPD characterization; (a) LabVIEW program and power supply for OPD measurements; (b) Probe station for I-V measurement, alignment stage under microscope	31
Figure 2-16 Absorption spectra measurement; (a) Instrument Perkin-Elmer for measurements; (b) Absorption spectra measured of a thin film of CuPC (layer used in OPD).....	32
Figure 2-17 LFIA working principle; (a) Typical LFIA test strip; (b) Sandwich immunoreaction in such assays.....	34

Figure 2-18 Line formation in an LFIA; (a) As a function of time; (b) Gray value of line contrast plotted vs time 35

Figure 3-1 Fluorescent visualizer device showing illuminated test lines⁵¹ 39

Figure 3-2 QD based LFIA (right) in comparison to Au NP based conventional device (left) ⁶⁰ ... 40

Figure 3-3 Schematic of OLED/LFIA integration approach. 41

Figure 3-4 OLED details: (a) constituent layers and their respective HOMO/LUMO energy levels; (b) photo of emitting green OLED pixel on a PET substrate 43

Figure 3-5 OLED characteristics: (a) current and brightness vs. voltage; (b) emission spectrum.43

Figure 3-6 Optical spectra of the components of the integrated OLED/QD-LFIA device: (a) Absorption and emission spectra of quantum dots. OLED peak excitation wavelength also indicated; (b) Transmission of green and red filters..... 44

Figure 3-7 Spectral response showing the effect of light filters in the OLED/LFIA device: (a) OLED emission through input light filter; (b) OLED +QD emission through input and output light filter 45

Figure 3-8 LFIA working principle: (a) dipstick assay format; (b) UV excitation after assay process shows emission from QDs captured on test lines 46

Figure 3-9 Fabrication steps of integrated OLED/LFIA device 48

Figure 3-10 Comparison of LFIA operation - emissive integrated OLED-QD approach vs. reflective Au-NP approach: (a) side-by-side photo of the two types of LFIAs; (b) equivalent grey scale contrast comparison 49

Figure 3-11 Visual characteristics of QD and Au NP-LFIA as a function of concentration of conjugate solution: (a) Photographs of Au based LFIA compared with QD based LFIA at same

concentrations; (b) signal intensity; dashed lines indicate signal sensitivity in linear region; (c) signal-to-noise ratio; LoD concentrations indicated by the arrows. 50

Figure 4-1 Smartphone use in diagnostic devices: (a) Smartphone camera microscopy; (b) Colorimetric detection using smartphone's camera. 54

Figure 4-2 Hybrid manufactured flexible NFC powered LED chip (powered using a Samsung smartphone) 55

Figure 4-3 Schematic showing NFC power harvesting and integration with LEDs, optical filters and LFIA..... 56

Figure 4-4 NFC chip design tailored to fit dimensions of the LFIA kit test and control lines. 57

Figure 4-5 Hybrid manufacturing setup at VTT; (a) Roll-to-Roll fabrication equipment; (b) Actual equipment and setup; (c) Die attachment using “pick and place” and adhesive glue..... 58

Figure 4-6 NFC power harvesting for LED operation: (a) demonstration of smartphone powering LEDs (insert – photo showing LEDs surface mounted on plastic sheet); (b) emission spectrum of the green LED; (c) LED output optical power vs. input current, separately measured 59

Figure 4-7 LFIA working principle: (a) immunochemistry of the LFIA showing capture of both Au-NP and QD at test and control lines; (b) captured Au-NPs reflection under room light; (c) captured QD particles fluorescence excited under UV light. 61

Figure 4-8 Spacers used in integration: (a) Thicker spacer for uniform illumination; (b) Thinner spacer that shows non uniformity due to point source nature of LED. 62

Figure 4-9 LFIA capture test line results: (a) fluorescence of QDs excited using NFC powered LEDs; (b) room light reflectance of Au NPs; (c) gray value contrast comparison between QD and Au-NP as baseline..... 64

Figure 4-10 Wash step to remove non-specific binding: (a) No wash step performed; (b) Wash step using DI water.	65
Figure 5-1 External LFIA reader: (a) Qiagen reader with a LCD display; (b) Reader with slot to insert an LFIA strip.....	69
Figure 5-2 Portable POC devices and readers: (a) Clearblue packaged LFIA digital device; (b) Alignment error intensity loss; (c) Handheld reader for LFIA strips; (d) Basic underlying reflection mechanism in all the devices.	70
Figure 5-3 Schematic of organic optoelectronics and LFIA integration approach	71
Figure 5-4 Organic devices details: (a,c) Energy band diagrams for devices used in this project; (b,d) OLED and OPD devices fabricated on PET.....	75
Figure 5-5 OLED characteristics: (a) Current vs. Voltage; (b) Brightness vs. Voltage; (c) Lifetime testing measuring Brightness over time.	76
Figure 5-6 OPD characteristics: (a) Absorption spectra of the active layer; (b) Reverse bias dark current characteristics and breakdown; (c) Photo-current response of the OPD in reverse bias excited with a green laser source.	77
Figure 5-7 LFIA details: (a) Test and control lines formation in an LFIA; (b) Different densities of test line illuminated under green light; (c) Measured brightness of light transmitted through different densities of LFIA lines.	80
Figure 5-8 Quantitative LFIA measurements: (a) LFIA strip with test lines of various concentration of analyte (in %); (b) Measured OPD photocurrent for various concentration of analyte; (c) Intensity of photocurrent (area under curve) plotted for various concentrations of analyte.....	82
Figure 5-9 Integration of organic devices with LFIA strip inside the cassette.....	84

Figure 5-10 Integrated device results; (a) Measure OPD photocurrent as the line in the LFIA forms over time; (b) Relative OPD photocurrent plotted over time; (c) Gray value measure as a line forms over time (visual contrast)..... 86

Figure 6-1 Attractive feature of POC designed at Nanolab. 90

Figure 6-2 Flat battery options (Credit: Eric Frantz): (a) Few options of batteries available in the market; (b) Side view of extremely thin STMicro battery. 91

Figure 6-3 Flat battery integration concept..... 92

Figure 6-4 Preliminary experiment with flat battery powering integrated device; (a) Experimental setup showing series connection of flat battery; (b) OPD current response with and without test line case..... 94

Figure 6-5 All component integrated concept: (a) Microelectronic reader circuit with indicator LED for qualitative readout; (b) A similar microelectronic circuit hybrid manufactured on plastic (Credit: Eric Frantz). 95

Figure 6-6 All integrated package concept: (a) Approach at Nanolab; (b) Commercially available device with same components. 96

Common Abbreviations & Symbols

POC	Point of Care
LOC	Lab-on-Chip
LOD	Limit of Detection
LFIA	Lateral flow Immunoassay
LFA	Lateral flow Assay
ELISA	Enzyme-linked Immunosorbent Assay
hCG	Human Chorionic Gonadotropin
NPs	Nanoparticles
AuNPs	Gold Nanoparticles
QDs	Quantum dots
OLED	Organic Light Emitting Diodes
LED	Light Emitting Diode
OPD	Organic Photo Diodes
PD	Photo Diode
NFC	Near Field Communication
EBL	Electron blocking layer
HBL	Hole blocking layer
OPV	Organic Photovoltaic

OTFT	Organic thin film transistor
HOMO	Highest occupied molecular orbital
LUMO	Lowest unoccupied molecular orbital
PDMS	Poly(dimethylsiloxane)
ITO	Indium tin oxide
PEDOT:PSS	Poly(3,4-ethylenedioxythiophene)-poly(styrenesulfonate)
NPB	N,N'-Di(1-naphthyl)-N,N'-diphenyl-(1,1'-biphenyl)-4,4'-diamine
CBP	4,4'-Bis(N-carbazolyl)-1,1'-biphenyl
Ir(ppy) ₃	Tris[2-phenylpyridinato-C ₂ ,N]iridium(III)
BCP	Bathocuproine
Alq ₃	Tris-(8-hydroxyquinoline)aluminum
MBD	Molecular beam deposition
XPS or UPS	X-ray or Ultraviolet photoemission spectrometer
UV	Ultraviolet
SEM	Scanning electron microscopy
AFM	Atomic force microscopy
eV	Electron volts

V	Voltage
I	Current
J	Current density
L	Luminance
cd	Candelas
lum	Luminous flux

Chapter 1 : Introduction

1. Project Introduction and Overview

The Point-of-Care (POC)¹ diagnostic system development has been a popular area of research for several decades and is of even more significance in the developing countries². This can be achieved by developing a Lab-on-Chip (LOC) system having several desirable characteristics such as low Limit-Of-Detection (LOD), high sensitivity, low power, rapid, cheap and being disposable³. Microfluidic technologies have made this realization possible. Figure 1-1 below depicts an artistic rendering of an idea POC system which uses microfluidics for fluid manipulation in the heart of the device. Also, depicted in the figure are other parts of a LOC system:

- Sample processing: Includes filtering, cell separation and sample wicking.
- Microfluidic Chip: Handling and manipulating fluids in small quantities, this include channels, valves and bio-recognition elements.
- Signal Transduction: Transducers to read and sense bio-recognition regions. Can be electrical, optical or magnetic.
- Electronics: Microelectronic digital/analogue circuits to process signals and output in meaningful form for result interpretation.
- Packaging: Houses all the components of the system in a small and robust integrated package. Typically contains indicator LEDs and/or LCD to display results.

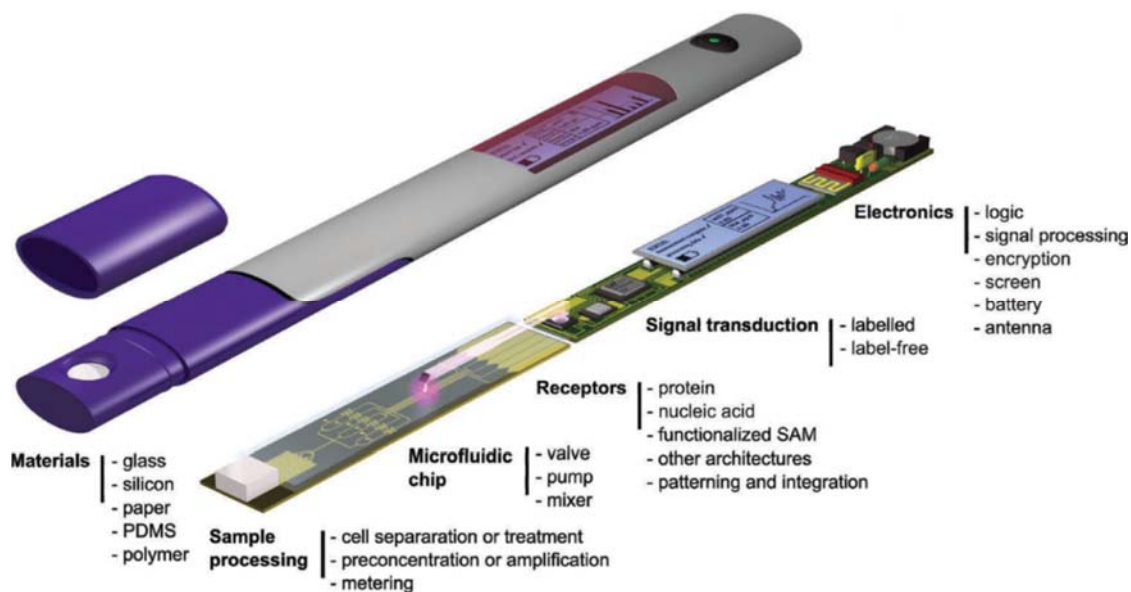


Figure 1-1 Artistic rendering of an ideal microfluidic based POC system⁴

Paper microfluidics possess several of these traits such as integrated capillary pump and simple device fabrication enabling reduced costs as well as being disposable⁵⁻⁷. Lateral flow Immunoassay (LFIA) devices have been a successful application of paper based microfluidics for qualitative rapid visual analysis⁸, however, optical systems can also be integrated to interpret the results for improving sensitivity and making the device quantitative in nature as well^{9,10}. Organic optoelectronics (OLEDs and OPDs) have been found to be ideal candidates for integrated LOC diagnostic systems by several groups¹¹, however, investigating their integration in LFIAs has not been done before. Such an integration would bring best of both the worlds to have a better LOC research vehicle. In this work, the integration of organic optoelectronics with paper based microfluidics has been explored in an effort for improving LOC for POC applications. The hypotheses was formulated by first conducting literature survey on advantages of using paper based microfluidic devices and application of organic optoelectronics in LOC applications. Hence,

we believe by integrating organic optoelectronics with paper based microfluidics, a LOC vehicle with many desirable traits will be created.

At Nanolab, I have had the opportunity to work on several other projects to gain skills and knowledge that include fabrication and characterization of organic devices. Further, at UC, I have had the opportunity to take several courses such as BioMEMS, Microfabrication, etc. which has equipped me with sufficient knowledge to make this project a success. Several former and current Nanolab members have conducted research works in OLEDs^{12,13} and paper based diagnostic devices^{14,15}, which form a critical foundation for this project.

2. Paper Microfluidics for the Point of Care

Diagnosis is the first step of treatment and hence delivering simple, low cost, robust and portable diagnostic systems is essential and especially of critical importance in developing economies all around the world¹⁶. Rapid diagnostics has impact in several fields shown in Figure 1-2.



Figure 1-2 Rapid diagnostics and its diverse fields of applications¹.

Microfluidics is a key underlying technology that has many of the above desirable traits³. PDMS based microfluidics have been subject to extensive research in the past decade, however, they have made very little progress in becoming real world products⁸. This is due to several factors such as limited diffusion and/or needing of external equipment such as pumps and detection systems¹⁷. Some of these problems can be negated by using capillary based microfluidics, however they require complex fabrication procedures.

Paper, a natural thin material which can be produced by pressing together cellulosic fibers, can be used as a vehicle for capillary based transport of fluids. Various types of papers having different flow characteristics have been extensively used in paper based diagnostic devices. Several fabrication techniques are also available for channel fabrication in paper based devices.

These channels can be fabricated using wax printing techniques, one of which is shown in Figure 1-3.

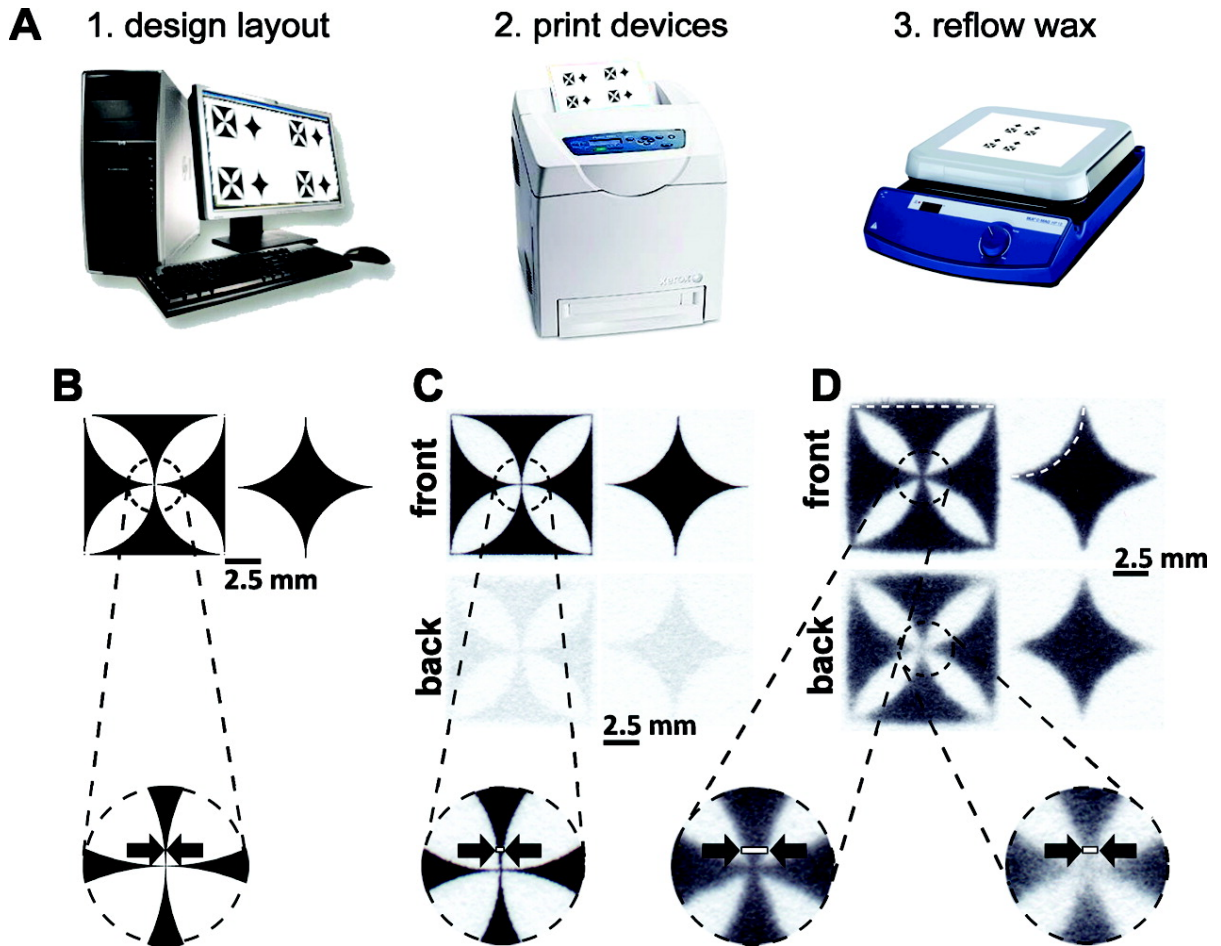


Figure 1-3 Paper microfluidics channel fabrication using Wax Printing technique¹⁸

Whitesides group at Harvard University has done extensive research on paper based microfluidic devices for biosensors, one of them is shown in Figure 1-4a, a device whose channels were fabricated using photolithography. The group has developed several techniques to fabricate channels using wax as well as other layering techniques¹⁹⁻²⁶. Dipsticks and lateral flow are the established assay formats in paper microfluidics for point-of-care testing. Lateral flow immunoassay (LFIA) use immunoreactions to detect an analyte. A typical LFIA format consists of

a sample pad, conjugate pad, analyte membrane and wicking pad can be seen in Figure 1-4b. The reactions, antibody sandwich capture happen at the immobilized antibodies at the test and control line regions.

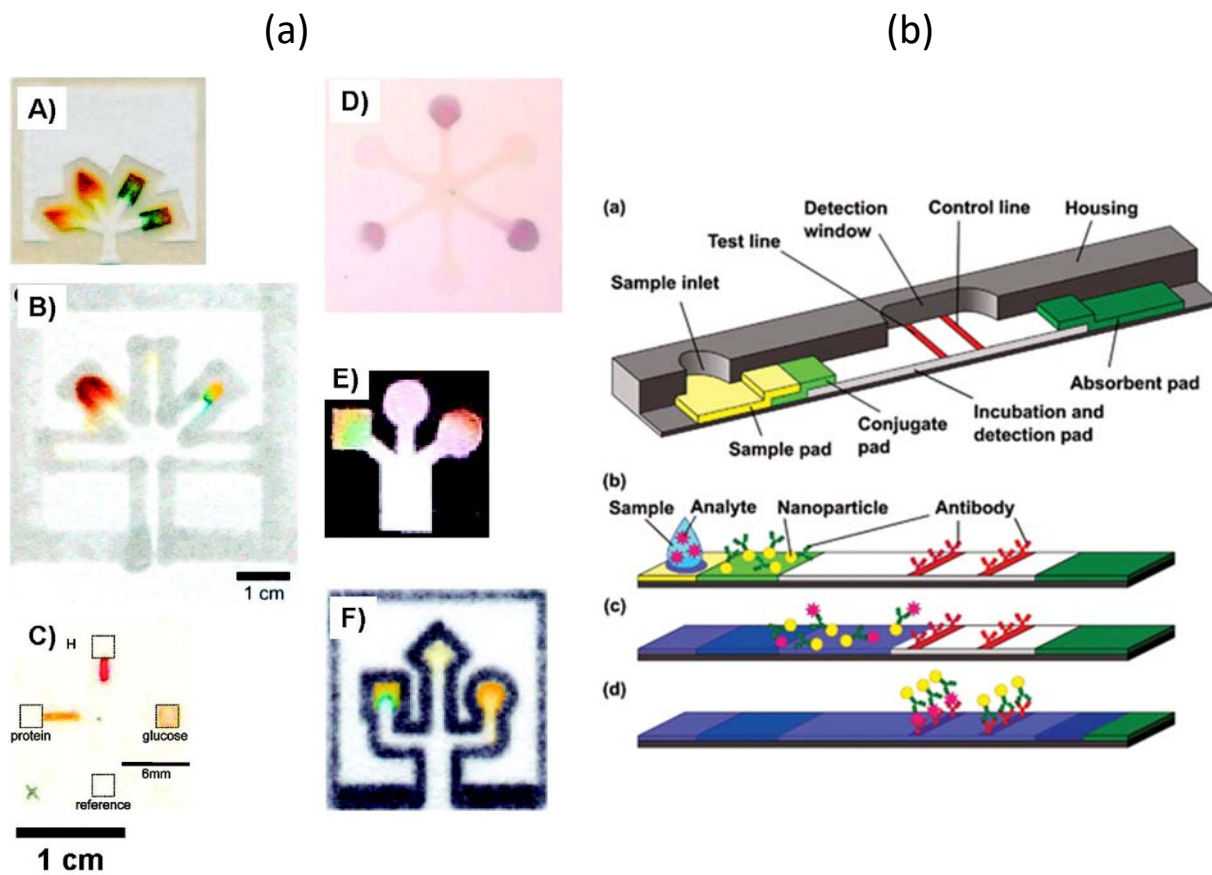


Figure 1-4 Paper based microfluidic devices; (a) Simple form of electrochemical sensor on paper fabricated using PR⁵; (b) LFIA biosensor based on immunochemistry²⁷.

Several commercial LFIA devices use gold nanoparticle which gets accumulated in the test line/control line which is visible as a band of line²⁸. The results are typically qualitative (yes/no) in nature, which is still a valued asset in several applications due to the ease of interpretation of the results¹⁷. Like any other technology, the potentiality of LFIA can be improved by trying to improve its visual sensitivity and making it more quantitative in nature.

3. Organic Electronics for LOC Applications

The Organic optoelectronic devices (OLEDs and OPDs) consist of a series of thin films (10-40 nm) of various organic materials deposited on substrates, resulting in devices that emit or detect light when biased²⁹. While OLEDs and OPDs are usually formed on glass substrates, the fact that the thin film deposition takes place at relatively low temperatures makes it possible to fabricate them on plastic films or paper substrates^{14,15,30}, some of such device is depicted in Figure 1-5 below.

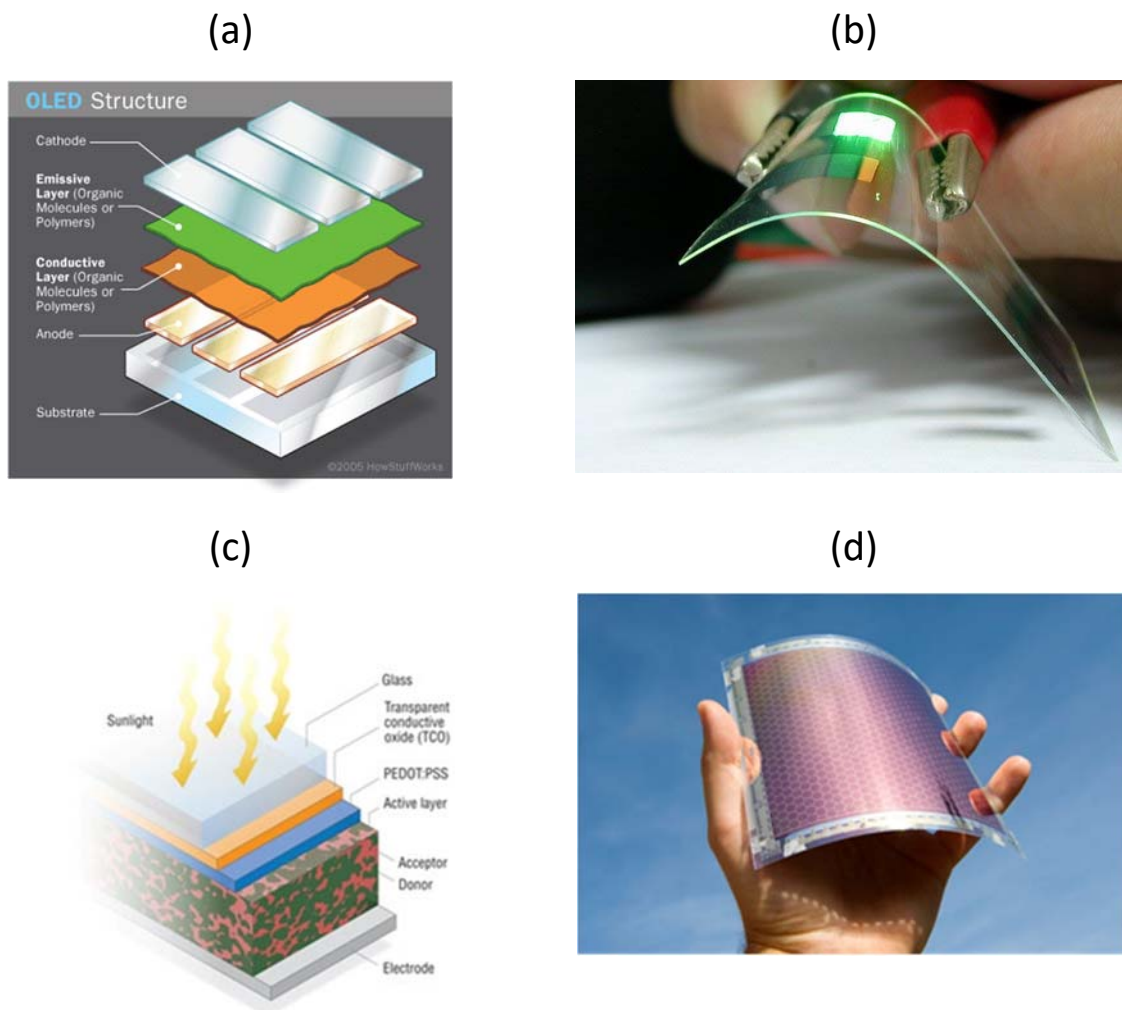


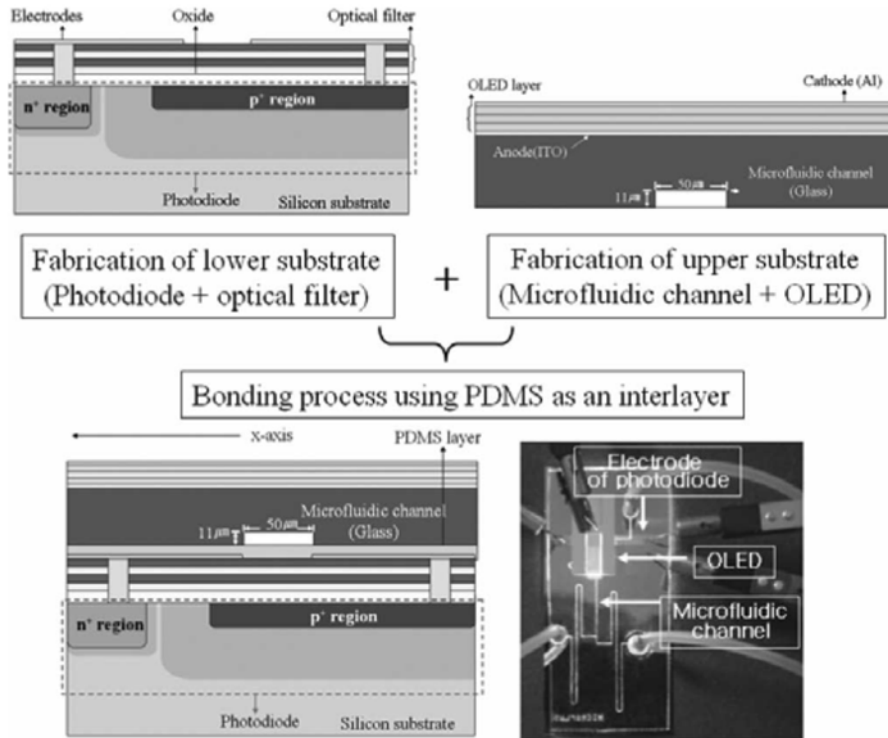
Figure 1-5 Organic electronics: (a) A simple OLED structure³¹; (b) OLED on a flexible plastic substrate³²; (c) OPV structure³³; (d) OPV device as a solar cell³⁴.

This facilitates integration with microfluidics devices for realizing LOC applications¹¹ for medical diagnostics. Organic devices also have several advantages compared to their inorganic counterparts (LED), including physical flexibility and large area fabrication capability for application in LOC¹¹.

For example, *Shin et al*³⁵, used OLED as light source integrated with glass based microfluidics system as shown in Figure 1-6a. However, an inorganic silicon PN junction was used as the photodetector. In their work, the two devices were prepared separately and integrated using a thin layer of PDMS as bonding layer. They were able to get a detection limit of 1 μ M. A similar work was done by Kim et al.³⁶, with a PDMS packaging design, in their work the photodiode (Si based) was embedded into a block of PDMS which acted as both bonding as well as an encapsulation chamber (

Figure 1-6b).

(a)



(b)

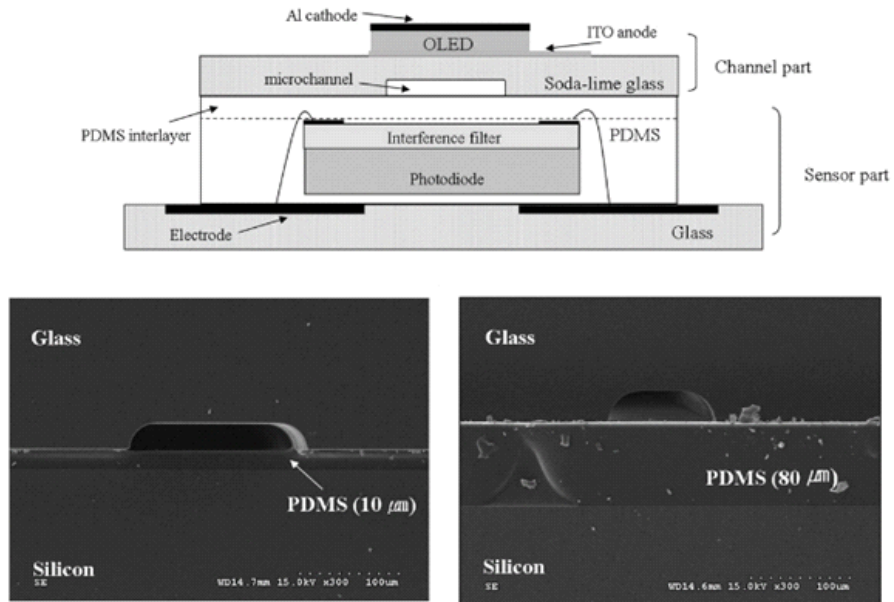


Figure 1-6 Organic optoelectronic applications in LOC devices; (a) Two part fabrication³⁵; (b) PDMS encapsulated photo detector³⁶.

Papautsky et al group at University of Cincinnati integrated both OLED and OPD with PDMS based microfluidics system (fluorescent)³⁷. To eliminate the excitation light source, the group used simple plastic polarizers aligned perpendicular to each other. Their devices were fabricated on glass and planar integrated with the microfluidic based chip. They demonstrated detection limit as low as 100nM with such an integrated device. Their configuration can be seen in the Figure 1-7 below.

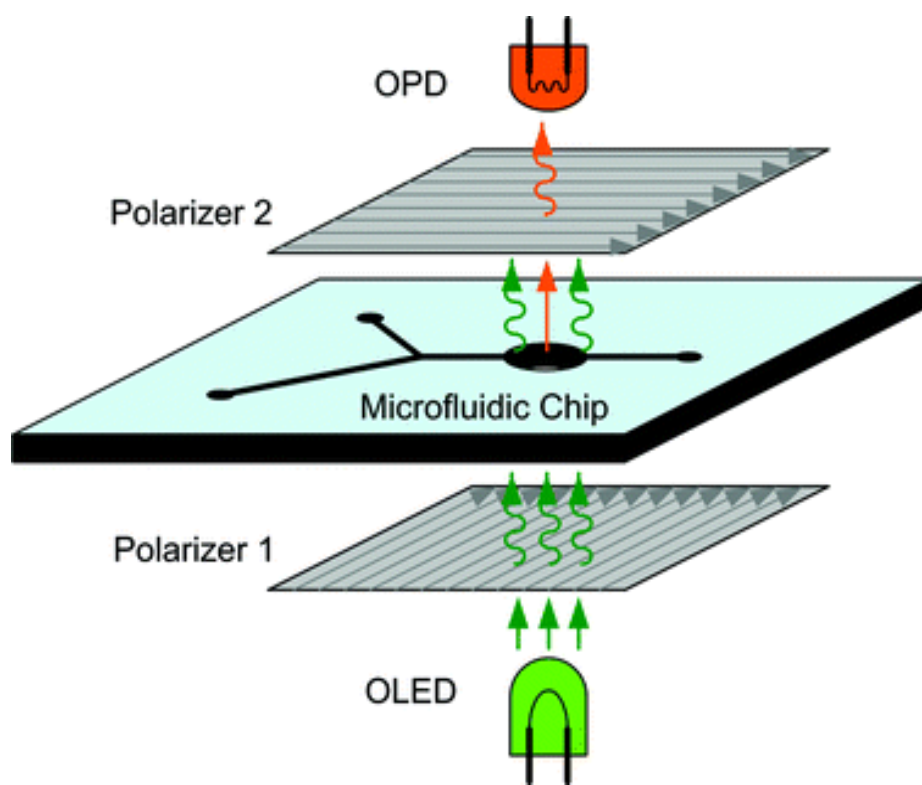


Figure 1-7 Both OLED and OPD integrated with a fluorescence microfluidic system³⁷.

Several other advantages by using organic devices, such as not requiring waveguides and the proximity of the source and detectors that can be achieved has been exploited by several other groups as well, some of which are tabulated in Table 1-1 below. However, the application has been limited to PDMS based microfluidics and utilizing for paper based devices has not been done before.

Application		Micro-Fluidic	OLED Details	Detector	Analyte	Dynamic Range
Dye conc	PL	PDMS channel	ITO/ α -NPD/Alq ₃ /LiF/Al	CCD w/ fibre	RhB	5–100 μ M
			ITO/ α -NPD/Alq ₃ :C6/Alq ₃ /LiF/Al			
Multi-analyte conc	PLq	film (non-MF), PP channel	ITO/CuPc/a-NPD/DPVBi/Alq ₃ /CsF/Al	PMT, Si PD + pre-amp	glucose, lactate, ethanol	0.02–0.3 mM
			ITO/CuPc/a-NPD/Alq ₃ /CsF/Al		O ₂	0–100%
			ITO/CuPc/NPD/Alq ₃ :C545T/Alq ₃ /LiF/Al		dissolved O ₂	2–40 ppm
EP sep'n, immune assay	PL	etched glass, PDMS channel	ITO/PEDOT:PSS/(PF emitter) or PPV)/LiF/Al	PMT, Si APD w/ filter, lens, fibre	fluorescein	1 μ M–10 mM
					HSA	10–100 mg/L
Dye conc, IEF	PL	PDMS channel	ITO/NPB/Alq ₃ /Mg:Ag/Ag	PMT, CCD w/ filter, lens	rhodamine 6G, Alexa Fluor 532	50–700 μ M
			commercial AM-OLED array		R-phycoerythrin	38 ng/mL–50 μ g/mL
Dye conc, immune assay	PL	etched glass, PDMS channel	ITO/CuPc/ α -NPD/Alq ₃ /LiF/Al	p-i-n, p+n PD	TAMRA	10–100 μ M
					Rh6G	1–100 μ M
Analyte conc	IV	droplet	ITO/TPD/Alq ₃ /Al	N/A	ethanol, methanol	10–1E3 ppm

Table 1-1 Applications of organic optoelectronics (OLED and OPD) for LOC devices¹¹

4. Proposed Contribution

In this work, integration of various active components with paper based microfluidics for improvements in sensitivity or better features is proposed. This work differs in the way that organic opto-electronics components are used for the various advantages it offers over its

inorganic counterparts. Importance is also given to power source and several prospective ideas are proposed with one explored in detail.

The main goal of this proposed project can be achieved by investigating several types of integration for different applications as detailed in the sub-goals below.

Goal 1: Light source integration

OLEDs were integrated as light source with fluorescent lateral flow immunoassays. Such an integration would improve the visual sensitivity and hence the limit of detection. OLEDs were fabricated on plastics which was then integrated within the LFIA device. Such an integrated device would also be self-contained, disposable and easily fabricated. The integrated device performed superior in comparison to conventional LFIA devices.

Goal 2: Power source integration

After the light source, has been integrated, the next step would be to look for on board power options. There are several candidates but we confined our option to zero on board power by utilizing antennas that can capture RF signals from smartphones (NFC) to generate power. Smartphones are ubiquitous in the modern world their application in diagnostic devices are being currently investigated by several groups. The antenna and LEDs can be fabricated on plastic substrates using hybrid manufacturing process.

Goal 3: Detector integration

Finally, a light source detector integration has been pursued for quantitative detection. Organic photodiodes (OPDs) have similar advantages as OLEDs and will be suitable candidates as the detector. For the light source, OLEDs will be used. All the devices will be fabricated on plastic which can be integrated with the LFIA by sandwiching them together. Such an integrated device can do quantitative analysis as well as digitize the data which can be easily processed and stored. Furthermore, by integrating the detector, human subjective interpretation can be eliminated and hence the results are more reliable.

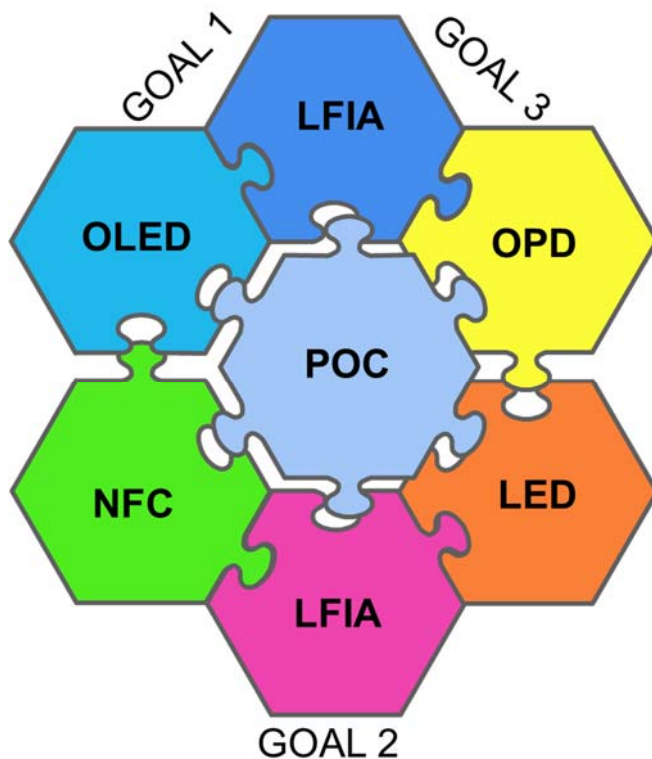


Figure 1-8 Goals of this thesis work.

Though integration of all the components is beyond the scope of this thesis, individual integration or partial combination still can provide valuable stepping stones for any future work in this area to realize such a POC device with many desirable characteristics. This is depicted in the Figure 1-8 above.

Chapter 2 : Materials and Methods

1. Introduction

In this chapter, a general introduction to fundamental and fabrication details of the devices used in this project are given. The chapter starts with some basic device physics of organic electronics followed by ways to fabricate them and their applications. After this general introduction, the focus will shift to devices fabricated at Nanolab specifically. The procedures described here are more general in nature with the specifics discussed in later chapters (such device dimensions, materials etc.). Further, the LFIA biosensor's materials and methods are also discussed in the end of this chapter. An introduction to immunoassays and paper based microfluidics devices followed by its implementation in Lateral flow assay format is described.

2. Organic electronics

2.1 Overview

Organic electronics are electronic devices with active layer composed of organic materials (made of C, H, N and O primarily). These thin films are held together by weak Van der Waals' forces and hence are amorphous in nature. These thin films can be polymers or small molecule based. This contrasts with conventional LEDs which contain crystalline inorganic materials with covalent bonds which also makes the device more rigid in nature. Such nature of organic thin films implies they can be low temperature processed and hence can be formed on any substrates and be subject to physical deformation (flexible). Further, owing to their flexible property, they can be

mass manufactured as well using roll-to-roll processing as well which leads to lower cost of production.

Organic thin films can be used to make many electronic devices including transistors and diodes. However, since in this work emphasis is on optical detection, only organic light emitting diodes (OLEDs) and organic photodiodes (OPDs) are discussed further.

2.2 OLEDs

Helfrich et al. first observed³⁸, in 1965, a recombination radiation from anthracene crystals which eventually gave birth to light emitting devices based on organic molecules. These devices consisted of organic thin films sandwiched between electrodes. When excited using a voltage source the charge carriers (electrons and holes) recombine in the organic layer and if such a layer is electroluminescent, light maybe emitted. Figure 2-1b below shows this concept.

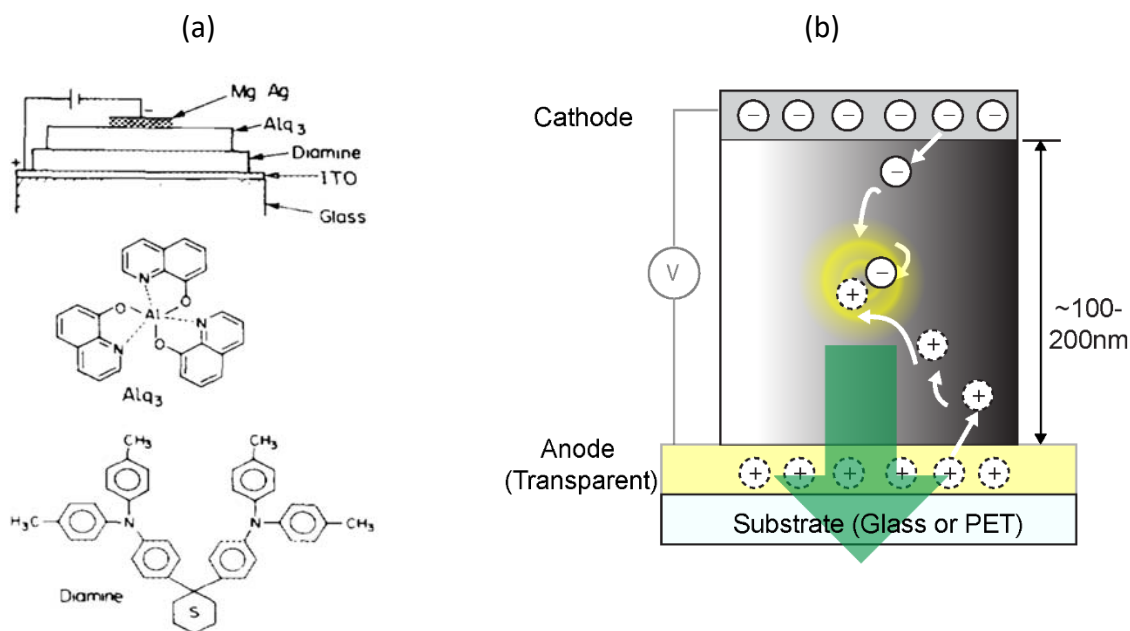


Figure 2-1 OLED working principle; (a) First heterostructure OLED³⁹; (b) Physics underlying in an OLED.

In theory, a single layer (~100-200 nm) of appropriate organic layer can make such a device (Figure 2-1), however, multilayer devices can be more efficient. First multilayer device, with two layers, was proposed by Tang and VanSlyke in 1987 (Figure 2-1a) that revolutionized the technology³⁹ due to its high efficiency. Bandgap engineering (HOMO-LUMO) using multi-layers of organic thin films can improve the efficiency of such devices significantly. In addition, choice of the emitting layer also affects the device performance significantly. Adachi et al discovered that by using a triplet exciton harvesting emitting material (phosphorescent) the efficiency of the device improved significantly⁴⁰. The work presented in this thesis is based on such materials and structures.

2.3 OPDs

Several organic thin films also absorb light, the wavelength of which is dictated by the HOMO-LUMO gap. Using chemical synthesis, these gaps can be modified to create organic compounds that absorb in specific wavelengths or range of wavelengths. An in-built electric field can be set up by using contacts of different work function which can be used to create OPV (organic photovoltaic) devices. Basic working principle of an OPD is shown in Figure 2-2b below. When photons of sufficient energy hit the material (greater than HOMO-LUMO gap), excitons are created (electron-hole pairs). In photodiodes, a reverse bias is applied to separate these charges and produce more reverse bias currents as shown in Figure 2-2b. In photovoltaics, however, no such bias is applied and the device acts as a battery instead. Like OLEDs, OPDs can also be made more efficient by using multi layered device stacks. Heeger et al discovered polymers that absorb in solar spectrum which can be solution processed and mass manufactured. The group also created a combination of polymers⁴¹ (Figure 2-2a), with different properties, to create networks

for charge separation eventually leading to a markedly improved efficiency. There is active research work in such solar cells due to its desirable characteristics such as flexibility, disposability and being cheap⁴².

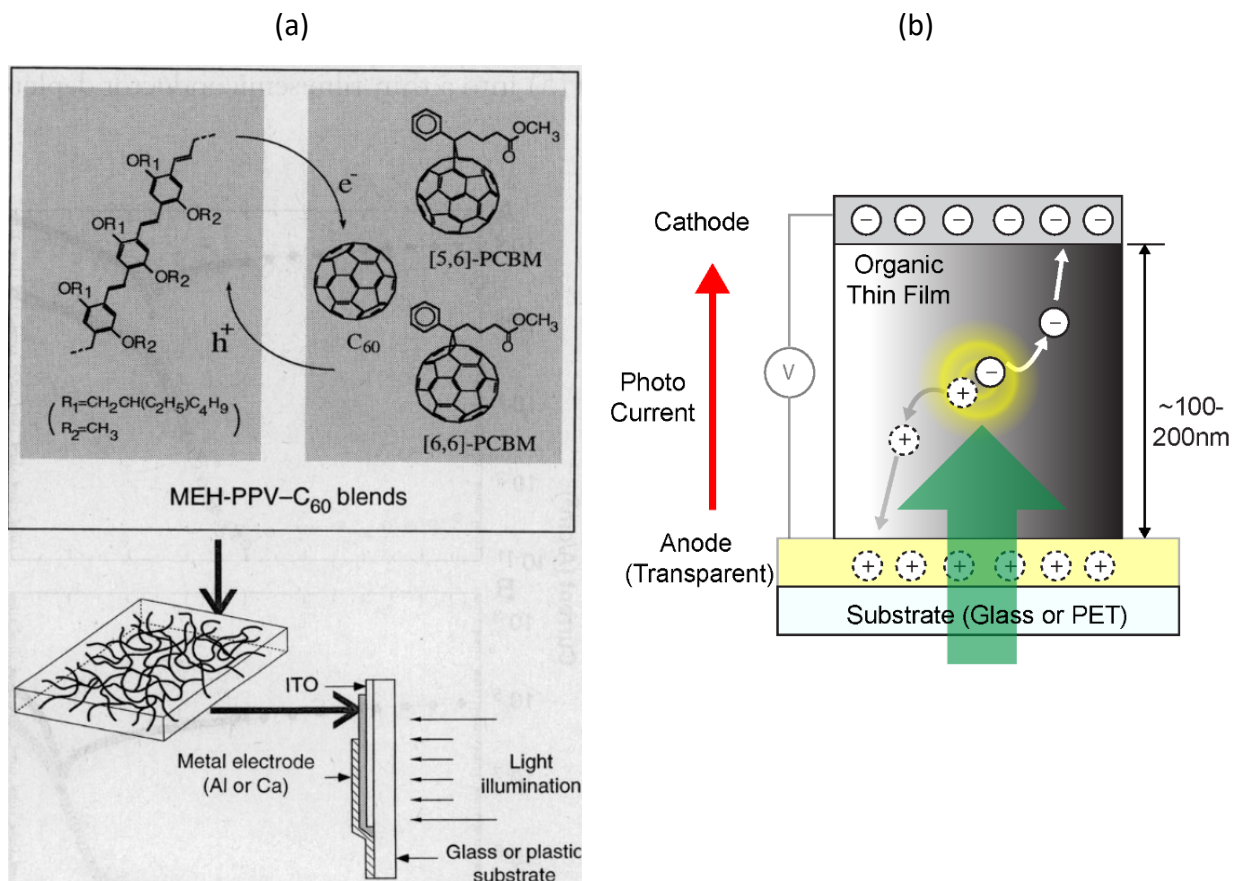


Figure 2-2 OPD working principle; (a) First heterostructure OPD⁴¹; (b) Physics underlying in an OPD

3. Fabrication and Properties

One major attractive feature of organic devices is the various ways available to fabricate them. These thin layers of organic films can be deposited predominantly by solution processing or thermal evaporation. Some solution processing methods include spin coating, blade coating, inkjet printing, and spray coating⁴³. Such processing is also usually roll-to-roll compatible, if the substrates are also flexible. Further solution processing typically only requires low temperature

(save for moderate temperature annealing) which is an attractive feature for using plastic substrates. Figure 2-3 below depicts some common ways to do solution processing of organic thin films. Of these, spin coating is predominantly the most common way. In this process, the thin film to be deposited is first dissolved in a solution and flooded on top a substrate. The substrate is then rotated at high speeds (~ 1500 rpm) which produces a thin liquid layer that then evaporates leaving to a thin film of the material (solute) on the substrate's surface. The film thickness can be controlled using both concentration of the original solution as well as the spin speed. Figure 2-3a shows an actual equipment used by our lab for this procedure. Though this form of solution coating is commonly used, it suffers from the disadvantage of not being roll-to-roll compatible and hence very large area manufacturing can be expensive and difficult.

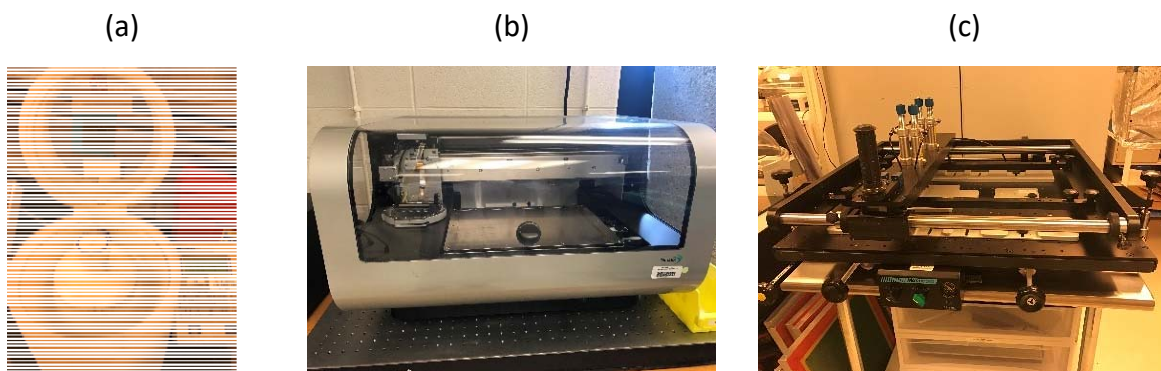


Figure 2-3 Solution processing equipment; (a) Spin coating; (b) Inkjet printing; (c) Screen printing.

The other common procedure is to print the solution using inkjet or screen printing methods. In inkjet printing, a piezoelectric head ejects the organic solvent in pico-liter sized droplets on top of the substrate. The drops then dry off leaving a thin film of material (solute) on the substrate. This procedure can be roll-to-roll compatible, however, due to the nature of the process, the throughput of this technique is low and mass manufacturing can be difficult. This disadvantage can be offset using a different printing technology called screen printing. In this technology, the

solution is percolated through a screen containing gaps using a squeegee similar to newspaper and magazine printing. The screen is also a way to generate patterns. This technique can give high throughput as well as manufacturing, however, it suffers from poor resolution and thickness control of the layer deposited. Figure 2-3b,c shows some equipment present in our labs for performing inkjet and screen printing respectively. Though solution processing can be done at ambient environment, due to sensitivity of organic devices to the elements, the fabrication is done in a controlled environment such as a nitrogen glove box to prevent degradation of the devices.

The other popular way to form the thin organic films is to use thermal vacuum deposition. In this process, powder form of the material to be deposited is sublimed by heating in a vacuum chamber. The sublimed vapors then condense back and deposit as thin films on the substrate. Figure 2-4a describes such a process. In this deposition technique, there is precise control of thickness of the layer. It is to be noted that the substrate can kept at room temperature or slightly warmed up to improve quality of the layer. Unlike solution processing, this procedure requires a high vacuum which increases complexity and hence manufacturing costs. However, the quality of the layer is better than solution processed and precision is also higher. Figure 2-4b shows an equipment that can be used to thermal deposit thin films. Both the above methods, solution and vapor processing, are compatible with plastic as well as several other substrates.

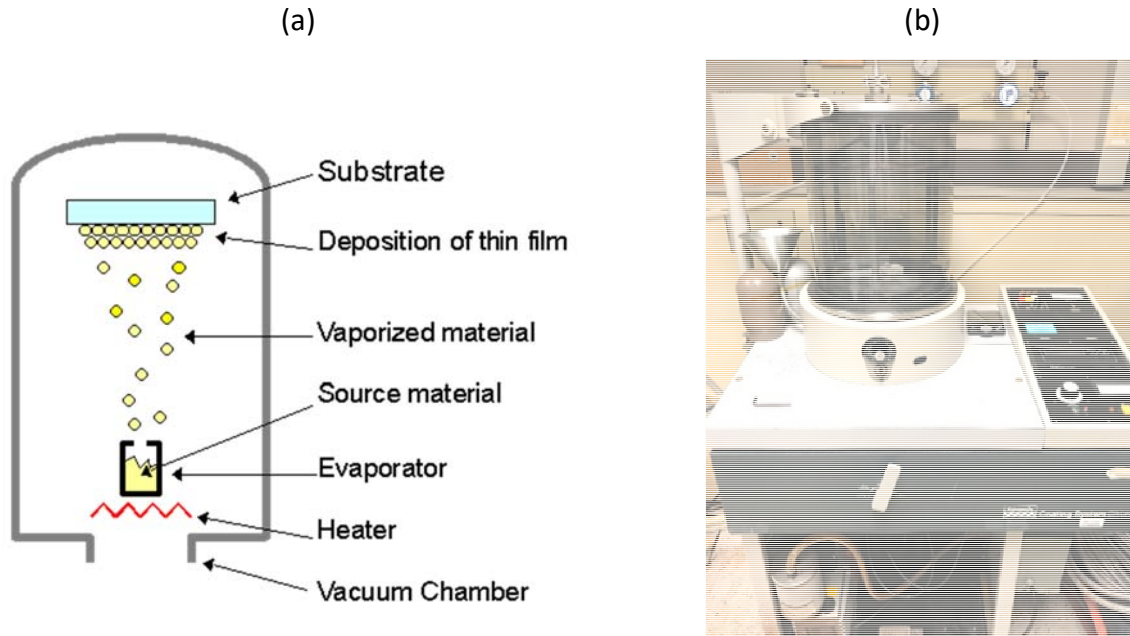


Figure 2-4 Thermal evaporation system; (a) Concept illustration⁴⁴; (b) Equipment at Nanolab

Figure 2-5b below shows an application of flexible displays that can be manufactured using this technology. At Nanolab, UC, work has been done in fabricating these devices on unconventional substrates, such as transparent paper (Figure 2-5a), which may have potential applications in biodegradable packaging and implantable biosensors.

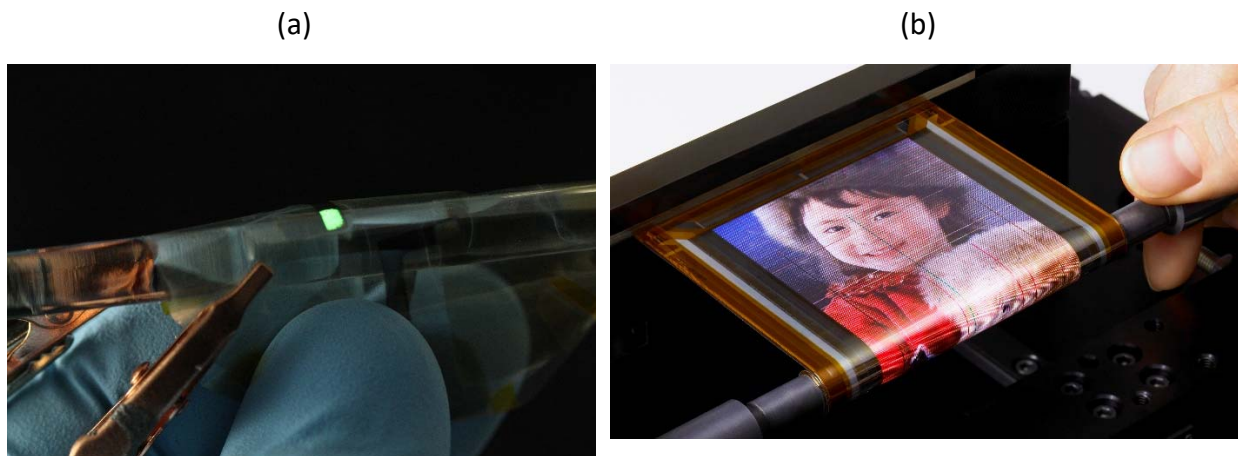


Figure 2-5 Fabrication on flexible and unusual substrate; (a) OLED on transparent paper¹⁴; (b) Flexible display wrapped around a pencil⁴⁵.

4. Organic Electronics at the Nanolab

At Nanolab, prior work has been done in fabricating and characterizing high efficiency OLEDs. In this work, hence, similar materials and stack choice were used. Figure 2-6a shows an optimized typical green emitting OLED device stack fabricated in our lab. However, for OPDs a single layer of light absorbing material (green wavelengths) sandwiched between the electrodes was used (Figure 2-6b). This configuration, even if not very efficient was chosen for its simplicity. The reasoning for choice of these stacks for respective applications has been described in later chapters.

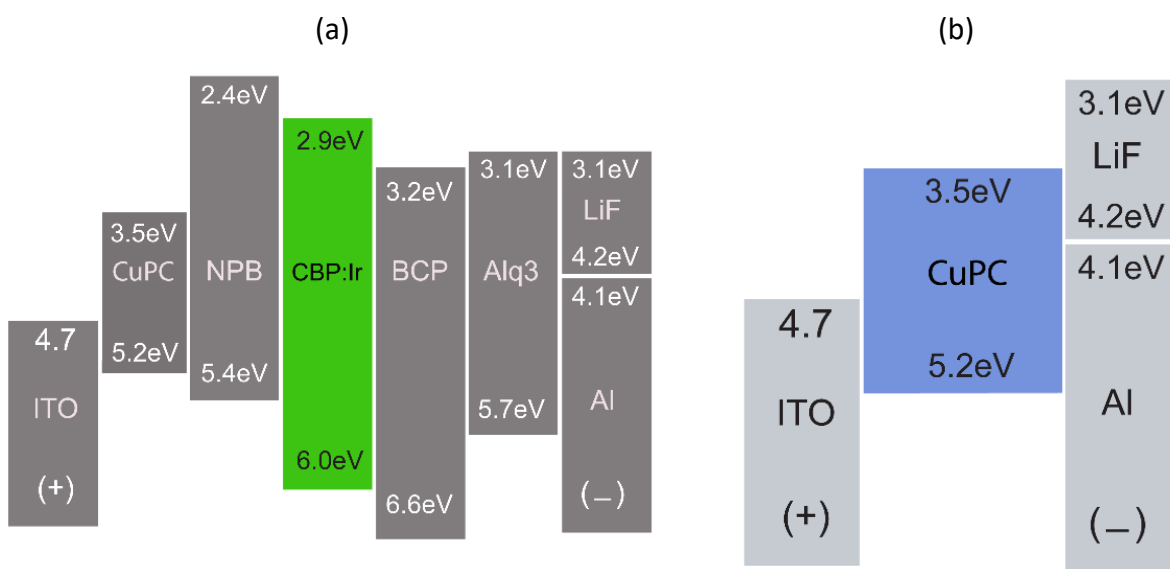


Figure 2-6 Energy band diagram of devices fabricated in this thesis; (a) OLED multi-layered stack; (b) OPD single layer stack.

4.1 Substrates and Anode patterning

In this work, the organic devices have been fabricated on two different types of substrates, glass and PET. The bottom electrode, ITO, can be procured pre-coated for both substrates. For the glass substrates, it was also purchased pre-patterned (90nm and 20 ohms/sq). It contained ITO

strips of 2mm width. For devices on PET, ITO coated PET sheets (unpatterned) were purchased from sigma Aldrich and patterned using photolithography in house.

The device fabrication on PET required extra handling procedures due its flimsy nature. Further, they are prone to solvent attack and hence only select organic solvents were used to clean the surface. The as received ITO coated sheets were first cut into square pieces measuring 30mm edge length. The ITO side of the sheet had a liner on it (pictured blue) in Figure 2-7 below.



Figure 2-7 ITO coated sheet obtained from Sigma Aldrich (blue color due to liner).

The cut PET squares were then attached to a glass substrate measuring same dimensions using a thin PDMS layer (~ 2 mm). The PDMS layer was fabricated using standard procedure by mixing 1:1 ratio of the polymer to curing agent. The mixture was then casted onto a small cover slip container and cured at 120 C for 3 hours. After cure, it was peeled off and placed on top of the glass substrate on top of which the PET was then placed. This way of attaching PET to the glass substrate was used as the bonding is not very strong and removing the PET sheet after device

fabrication is less damaging as well as easier. In contrast, removing it from a double-sided tape can introduce lot of strain on the PET and lead to deformation.

After attaching the PET to glass substrate, the surface was cleaned by scrubbing it with a IPA soaked wipe followed by a water rinse and drying in the oven at 120C. The devices are now subject to ITO patterning using photolithography. The procedure started by spin coating a thin layer of Microposit S1818 (~ 2-5 microns) photoresist at 1500 RPM for 30 secs followed by an exposure to UV (equipment used shown in (Figure 2-8)) through a mask (cut kapton tape).



Figure 2-8 UV exposure tool used for Photolithography

The photoresist layer, after the exposure was then developed using a microposit developer solution by dipping inside it for about 30 seconds. Then the devices were soaked into the ITO etching solution for 40 seconds which constituted a 50% diluted HCL solution. The ITO layer

exposed to the etching solution with no photoresist layer on top would be etched away leaving the ones unexposed under the photoresist intact. After the etching, the photoresist layer was removed by re-exposing it to the UV light (no photo mask) and developing.

The substrates are now ready for device growth. The substrates were cleaned once again using organic solvents and mechanically scrubbing with wipes. The wafers are also then exposed to oxygen plasma to further clean the surface as well as to modify the electrodes for organic layer contact. The wafers were then transferred to an ultra-high vacuum molecular beam deposition (MBD) system (refer to Figure 2-9) for the deposition of the organic layers and the cathode.

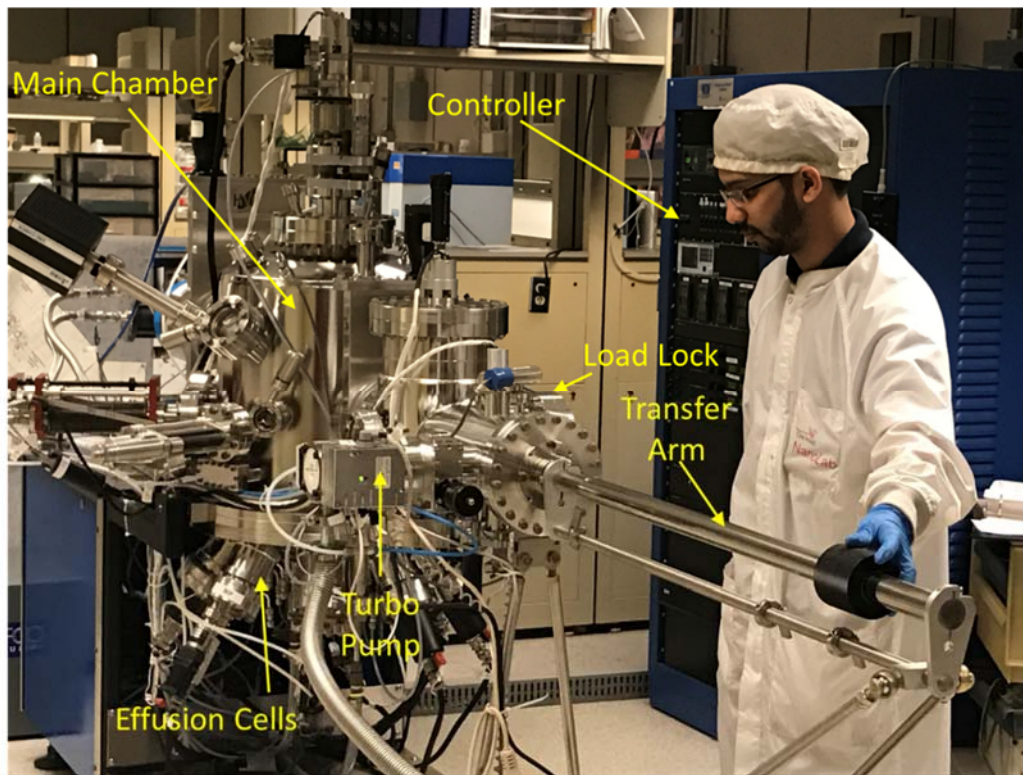


Figure 2-9 MBD system for thermal evaporation of organic layers (operated by myself)

Before loading into the vacuum system, shadow masks (Figure 2-10) are attached to the wafers to prevent deposition of the organics on the ITO contact pads to facilitate making electrical

contact. The organic masks are metal sheets with square holes in the middle. Due to the size of device dimensions, in the mm range, alignment of the masks can be made visually.

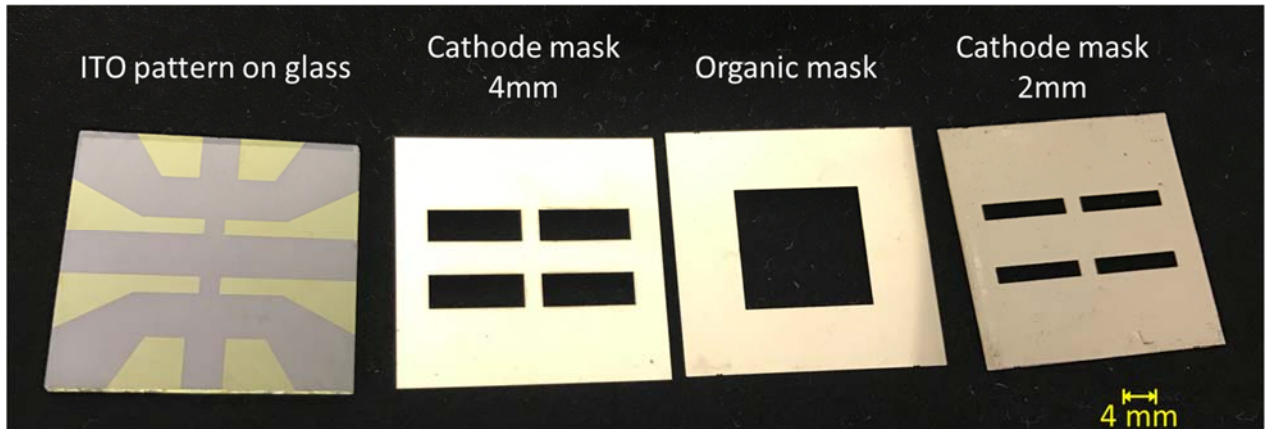


Figure 2-10 Glass substrates and shadow masks used for various layer patterning during thermal deposition

The wafers are loaded in the high vacuum main chamber using a load lock system. The main chamber of the MBD system consist of eight effusion cells in which the organic materials, in powder form, is loaded and can be controlled individually for heating. The cells also possess their own set of shutters with a separate shutter for the substrate stage. The wafers are transferred from the load lock to the main chamber using a mechanical arm which is coupled magnetically to an external handle. The substrate holder in the main chamber is rotated for uniform deposition of the organic thin films and equipped with an option for heating the substrates as well. After the transfer, the corresponding effusion cell of the layer to be deposited is heated to the sublimation temperature of the organic material loaded. Once the target temperature is reached, the shutter of the effusion cell is opened to measure the deposition rate, in situ, using a quartz crystal monitor. After the desired rate has been reached ($\sim 0.5 - 2$ A/s, depending on the layer), both the shutters (substrate holder and effusion cells) are opened to begin the layer deposition onto the substrate. After the desired thickness has been reached (measured using time), the shutter

to the substrate is closed to stop further deposition. The rate of deposition after the layer growth is then re-verified using the quartz crystal monitor to validate and confirm the layer deposition and its thickness. Other organic layers are then sequentially deposited using similar procedure until the desired multi-layer stack (if applicable) has been grown. Now the wafers are ready for the cathode deposition (LiF and Aluminum in this project).

For this, the wafers are first removed from the vacuum system briefly to apply a different mask (cathode pattern). This mask consisted of rectangular (thin line like) holes on a metal sheet (Figure 2-10). This would produce stripes of cathode deposited on the wafers perpendicular to the anode strips leading to square or rectangular shaped active device area. The width of these strips would dictate the dimensions of the final device fabricated. After the new masks are attached, they were loaded back into the system and the cathode LiF and Aluminum were deposited (sequentially).

The layer thickness and the organic layer stack details are dependent on the specific application and has been described in their respective later chapters. Also, no layers were solution processed due to which the devices were of good quality. The devices are now ready for characterization.

5. OLED and OPD Characterization

The devices were then removed from the MBD system for characterization. In this thesis work, due to the nature of instrument used, the OLEDs measurement were done inside a Nitrogen box to prevent moisture degradation and OPD measurements were done in ambient environment.

5.1 OLED Characterization

The OLEDs were characterized for its Brightness, Current and Voltage characteristics. Figure 2-11 shows some typical characteristic curves obtained for the devices.

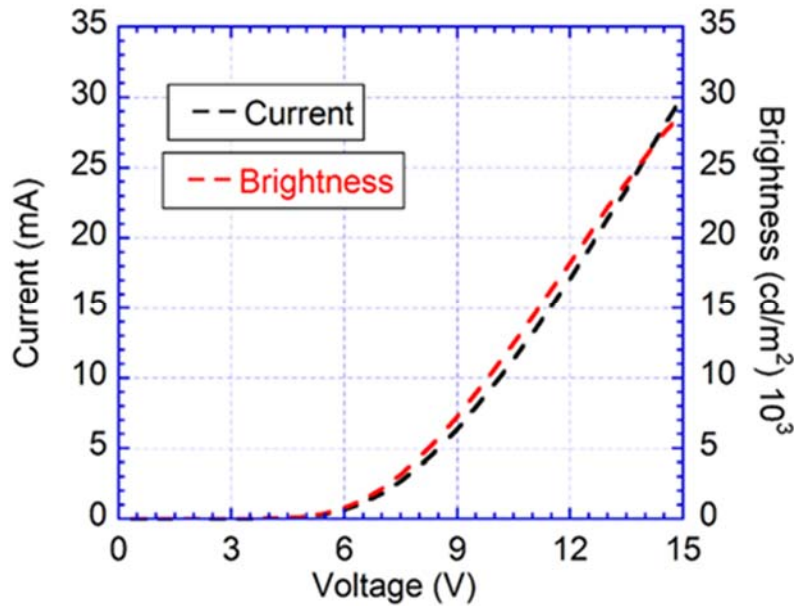


Figure 2-11 Typical characteristics of an OLED; (a) Current-Voltage (I-V) characteristics; (b) Brightness-Voltage (L-V).

This was done using a computer program (LabView), depicted in Figure 2-12a, controlling a DC power supply (HP 6634B) to power the OLED. The voltage was swept at 0.25V intervals and the corresponding current measured and recorded using the same program. The brightness is measured using a Konica Minolta CS-200 color and luminance meter (see Figure 2-12b). The luminance, in cd/m², is measured every 0.5s with the meter set at an angle of 1 degree, while OLED is kept on for 1 sec followed by turning it off for 3 seconds.



Figure 2-12 OLED characterization setup; (a) LabVIEW PC control; (b) Brightness measurement meter (minolta)

Other important characteristics of the OLED is its emission spectral curve. The importance of this will be evident in later chapters and is measured using Ocean Optics SD2000 (Figure 2-13a). The instrument and its measurement is also computer controlled. During the measurement, the OLED is biased at a constant voltage well above its turn on. Typical emission characteristics is shown below in Figure 2-13b.

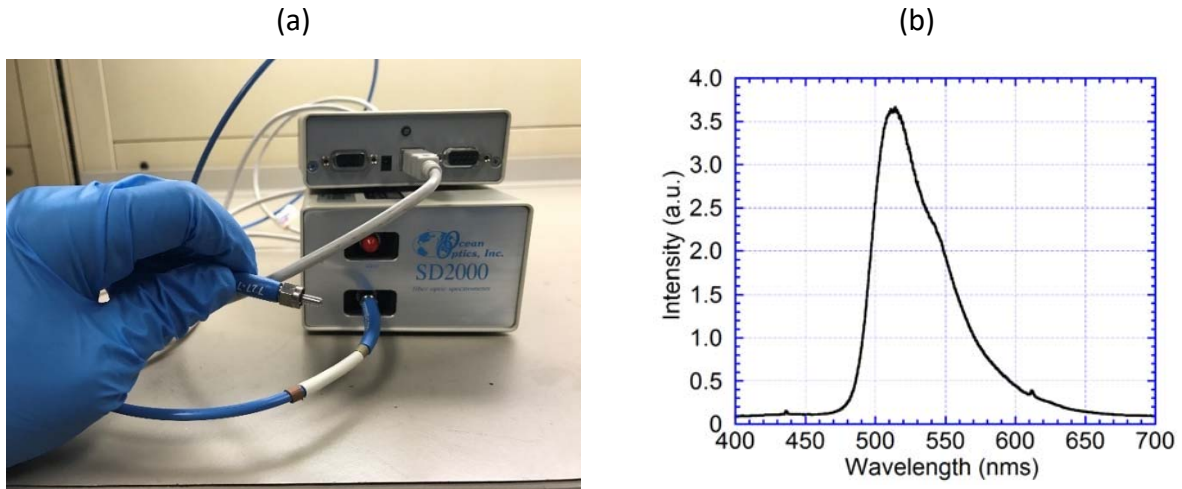


Figure 2-13 Spectral measurements; (a) Spectral measurement instrument; (b) Typical spectral shape of a green emitting OLED

5.2 OPD Characterization

The OPDs were characterized for its Current (Photo and dark) – Voltage characteristics in an ambient light controlled room. Figure 2-14 below shows typical characteristics of devices fabricated in our lab.

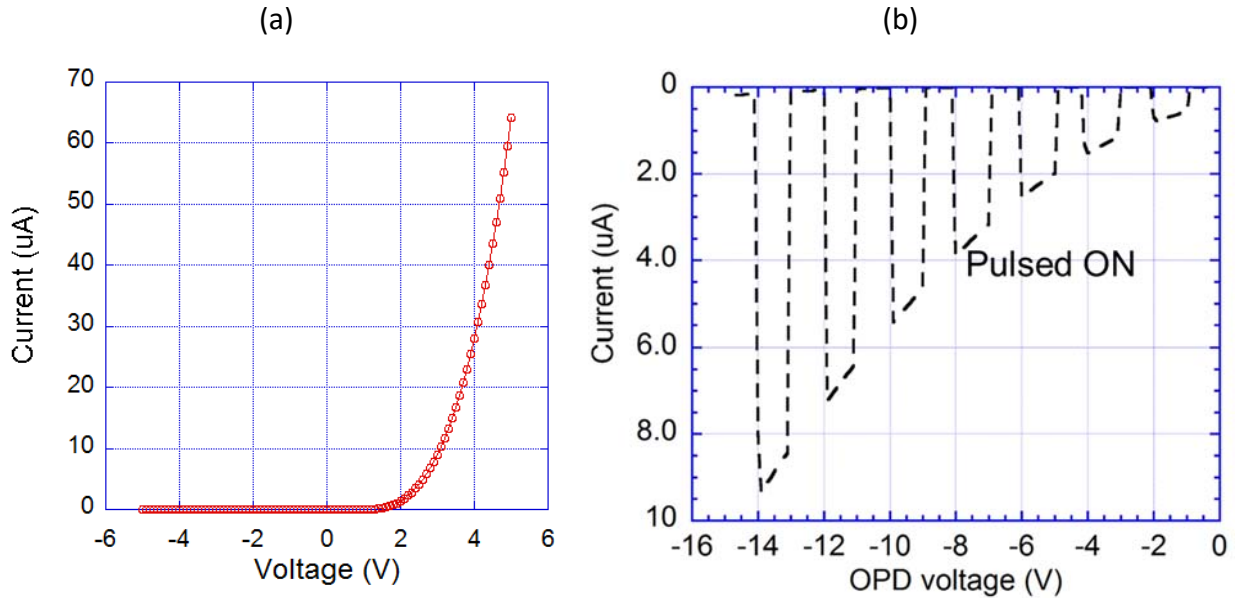


Figure 2-14 OPD characteristics (typical); (a) Typical I-V characteristics of an OPD fabricated; (b) Photocurrent pulsing with pulsed light input.

The power supply is a computer controlled (LabVIEW) Pico-ammeter (HP) with current measure, resolution at pico-amperes, as the voltage was swept at 0.1V intervals (Figure 2-15a). Contact to the devices were made using a probe station (Figure 2-15b). For photo current, a light source excited the OPD from the bottom (through the substrate) and current measured as the voltage swept at 0.1 V intervals.

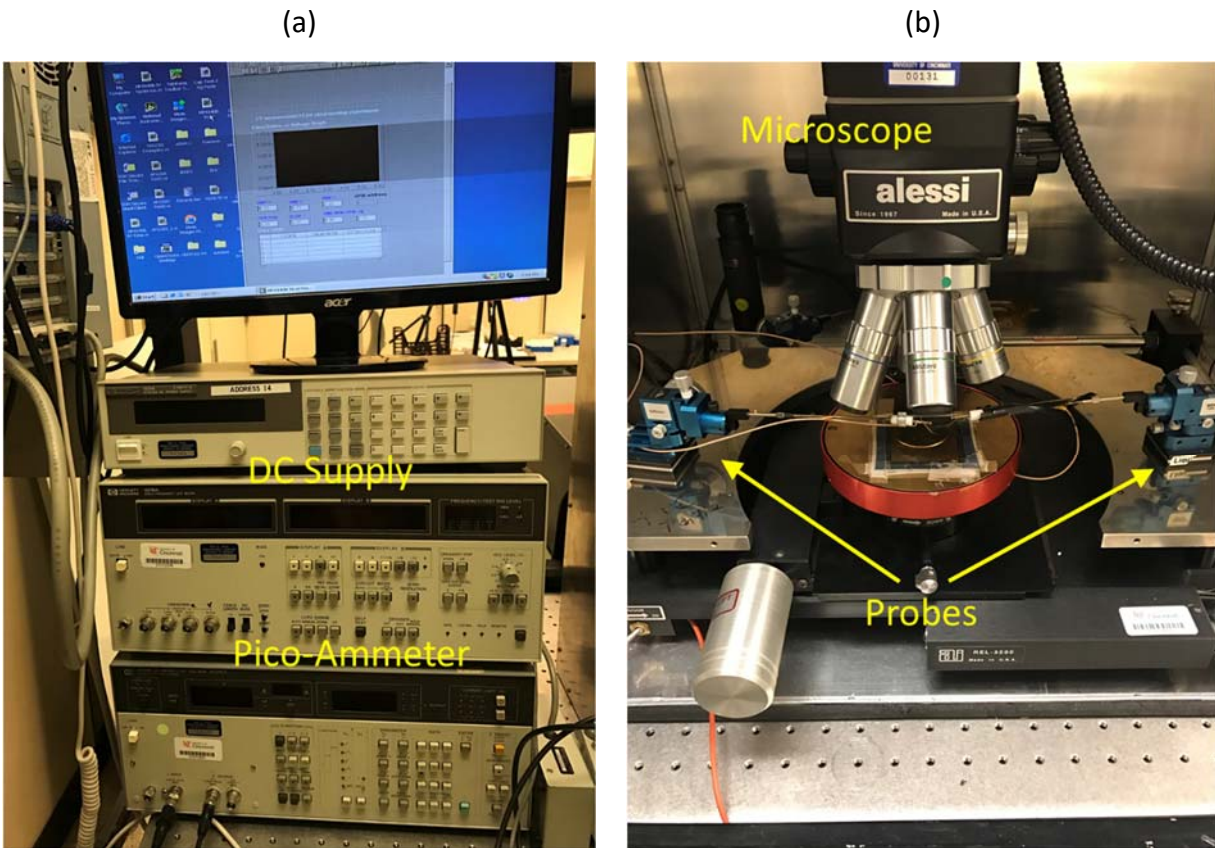


Figure 2-15 OPD characterization; (a) LabVIEW program and power supply for OPD measurements; (b) Probe station for I-V measurement, alignment stage under microscope

The absorption spectra of the active layer used in an OPD is important as it determines the photocurrent of the device for a specific wavelength. This was measured in our lab using a Perkin Elmer optical-spectroscopy equipment (Figure 2-16a). Figure 2-16b below shows one such characteristics.

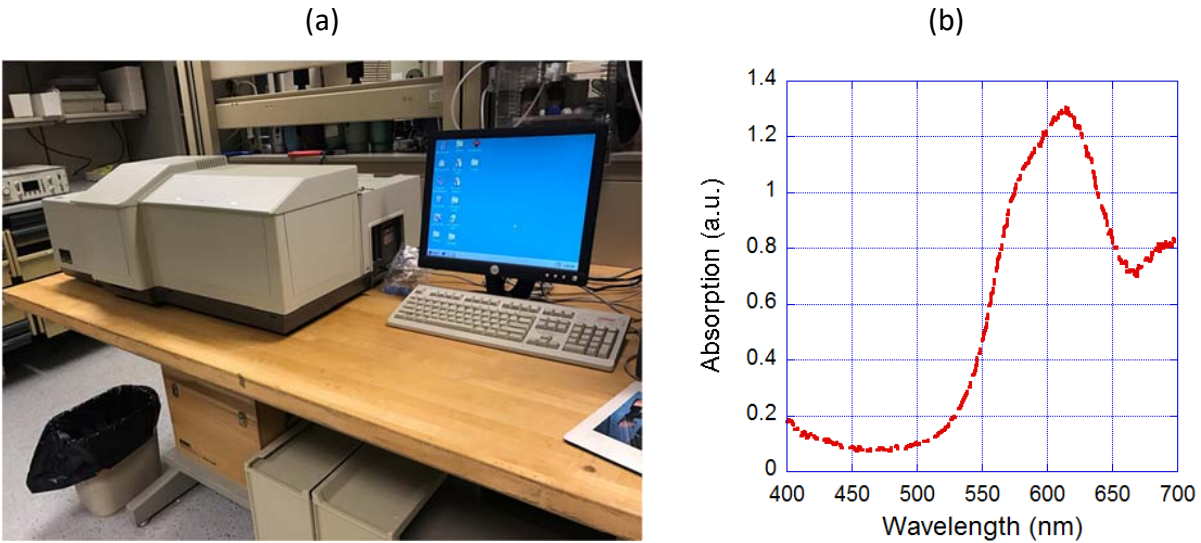


Figure 2-16 Absorption spectra measurement; (a) Instrument Perkin-Elmer for measurements; (b) Absorption spectra measured of a thin film of CuPC (layer used in OPD)

6. Lateral Flow Immunoassays (LFIA)

LFIA are the primary biosensors used in this research work. The basic sensing mechanism in such assays is immunoreaction chemistry. Typically, sandwich immunoassay format is employed in the LFIA. In this format, the analyte to be sensed is sandwiched between two antibodies, one immobilized and the other attached to a detector particle (enzyme in the case of ELISA). The antibodies are immobilized to substrates using surface chemistry binding. After immobilizing, the sample solution containing the target analyte is added, which gets attached to the immobilized antibody. Then the device is subject to a washing step in which all the unbound antigens are washed away. Finally, the second Abs (conjugated to detector particle) is added which binds to the antigen completing the sandwich followed by another washing step in which the unbound Abs are flushed away leaving only the conjugated Abs forming the sandwich, since the whole sandwich is immobilized by the first Abs. These procedures are typically carried out in a 96 well

microplate and the readout can be colorimetric or fluorescent depending on the type of detector particle being used.

The LFIAs fundamentally work similar to ELISAs done on micro well plate. In LFIAs however, the substrate is paper based and liquid flow through the capillary wicking of the paper. Further all the washing steps in an ELISA procedure occurs through sample flow of the solution which makes the process simple as well as rapid. The LFIAs consist of a sample pad, conjugate pad, Nitrocellulose (NC membrane) and the wicking pad. These components are attached to a backing card which is further enclosed in an outer plastic housing. The plastic housing also helps in holding sample (liquid) while it is being wicked by the paper strip. The NC membrane is impregnated with antibodies specific to the protein antigen to be diagnosed. These regions of the NC membrane are called the test and the control lines. The conjugate pad consists of antibodies conjugated to detector particles (typically gold) which target a specific antigen. In some cases, a conjugate solution may be employed instead of a conjugate pad. One such assay is shown in Figure 2-17a. When the sample solution is added, the liquid begins to flow by the capillary action, and, as it flows through the conjugate pad the conjugated antibodies are released from the pad and starts to flow along with the liquid toward the NC membrane. During this flow, in the presence of the target analyte, the conjugated Abs attach with the antigen and the complex flows through the NC toward the test and control regions. In the presence of the target analyte, the sandwich capture would occur in the test line region and the conjugated Abs with the detector particle will start accumulating a narrow region. This process is illustrated in Figure 2-17b.

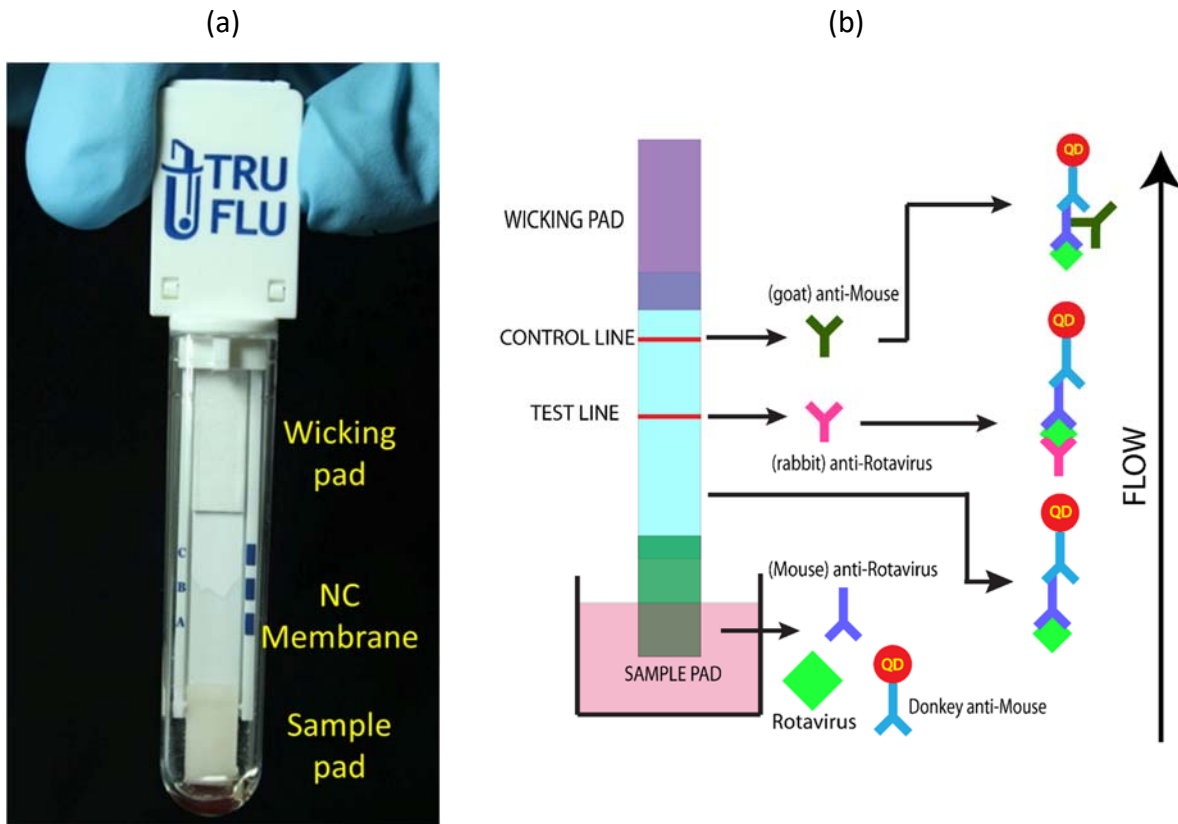
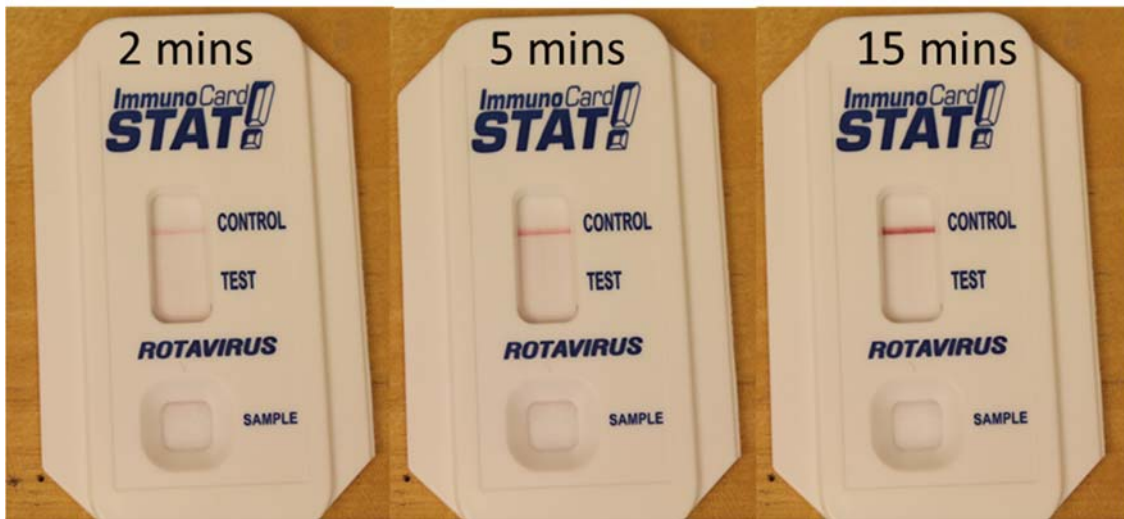


Figure 2-17 LFI working principle; (a) Typical LFI test strip; (b) Sandwich immunoreaction in such assays.

This manifests in the form of a dark colored line (red for gold nanoparticles). This can only happen in the presence of the target analyte, in the absence of which, the sandwich cannot form and hence no accumulation of the particle and the line formation. To validate the test, a second region of Abs line is impregnated in the NC membrane called the control line. These Abs would attach with the Abs present in the conjugate pad even in the absence of the analyte. Hence the detector particle aggregation occurs irrespective of the presence of target protein. Hence a control line forms even in the absence of the analyte Figure 2-17b. This line is critical to validate the authenticity of test results as the absence of it implies the test run was unsuccessful and no results may be interpreted from the run. Hence, two lines means positive test result (the presence of analyte) and one line (control line only) means the absence of the same and the test result is said to be negative (eg. Figure 2-18a). Absence of control line implies an invalid run. The

formation of lines typically take ten minutes and are to be visually interpreted. As the test is run, the accumulation continues to occur and the lines continue to darken, and this is the basis for quantitative analysis (optical detection). Figure 2-18b below shows a gray scale plot of the line darkening over time.

(a)



(b)

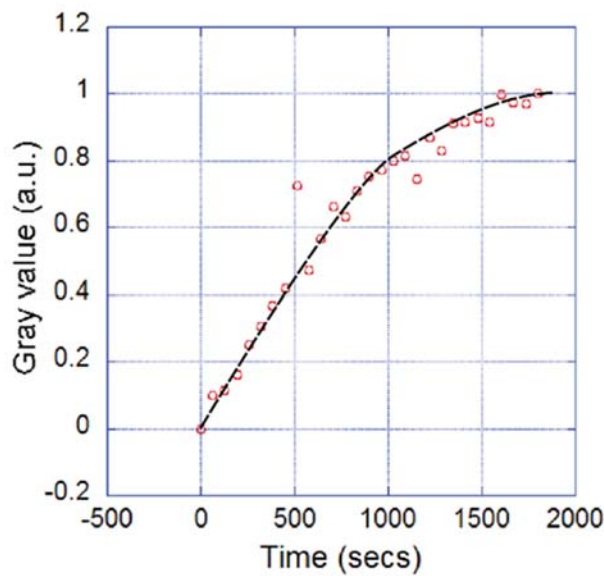


Figure 2-18 Line formation in an LFIA; (a) As a function of time; (b) Gray value of line contrast plotted vs time

The LFIA kits used in this thesis work were an in-kind donation from Meridian Bioscience Inc, Cincinnati. Two main kits were utilized, Tru-Flu and the Rotavirus. The Tru-flu kit had a different format than a conventional LFIA in which a conjugate pad was not present. It was replaced by a conjugate ball in a test tube which is dissolvable on adding a sample solution (Figure 2-17a). This format turned out to be convenient for us when we had to use a different detector particle (semiconductor QDs) in this test kit to form fluorescent based test lines (described in chapter 2).

7. Summary

In this chapter, a detailed description of all the procedures and methods have been discussed. The details are general in nature, specifics of which has been discussed in later chapters in their respective applications. In the beginning of this chapter, an overview of organic devices was given, followed by its fabrication methods and few applications utilizing its unique features and properties. The fabrication and characterization of the organic devices used for this project were then described. In which, details of the equipment and procedures used were also discussed. Finally, in the last section an introduction to working principles of LFIA and kits used for this project were described.

Chapter 3 : Integration of OLED with Lateral Flow Immunoassays

1. Introduction:

In this chapter, the first goal of this thesis is described. In the previous chapters a detailed description of lateral flow immunoassays (LFIAs) have been given with emphasis on its advantages and disadvantages over other formats of biosensors. We examined that one of the major limitations of this format is its qualitative nature and the need to visually interpret the results. However, it may be considered advantageous in a different sense, because, it makes the test procedure and interpretation of results much simpler. However, the problem of subjective interpretation error persists. This can be alleviated by improving the visual signal intensity. In this chapter, one way of achieving it has been described.

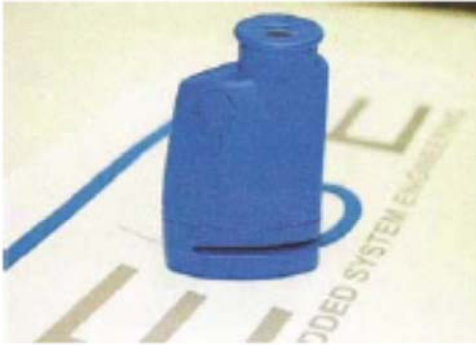
The integration of organic light emitting diodes (OLEDs) as excitation light sources for quantum dot-based fluorescent lateral flow immunoassay systems (LFIA) was investigated. This approach has the potential to deliver a sensitive visible detection scheme for low-cost, disposable lab-on-chip point-of-care (POC) diagnosis system. Thin film phosphorescent green OLEDs fabricated on plastic substrates were integrated on-chip to excite the test line of a quantum dot-based LFIA (QD-LFIA). OLEDs were fabricated by sequential deposition of organic thin films (total of ~100nm) onto ITO-coated PET substrates. CdSe/ZnS QDs emitting at 655nm and Au nanoparticles (NP - 10nm size) conjugated antibodies were used for the QD-LFIA and conventional reflection-mode Au NP-LFIA, respectively. Thin plastic color light filters were integrated for filtering the excitation

light source and, thereby, increasing the contrast of the emitted light for optimized visual detection. Integration of the OLED and color filters with the analytical membrane was achieved using adhesive techniques facilitated by the planar nature of the layers, which suggests possible large scale manufacturing using roll-to-roll processing. Grey scale analysis from digital images captured with a digital camera was used to quantify the visual sensitivity. The signal intensity, signal-to-noise ratio (SNR) and the limit of detection (LOD) of OLED integrated QD-LFIAs were compared to Au NP LFIAs. OLED QD-LFIA exhibited superior performance in all signal aspects: 7-8× higher signal intensity and SNR, and a 7× lower LOD of 3 nM (measured at S/N = 3). These results demonstrate the potential of OLED-integrated in LFIA devices for obtaining sensitive POC diagnostics.

2. Fluorescent LFIAs

The Use of fluorescent particles in LFIA (F-LFIA)⁴⁶⁻⁴⁹ are currently gaining high interest due to the resulting high sensitivity⁵⁰. Special readers which detect these signals can be used to make it quantitative also⁵¹. However, the visual sensitivity can also be increased, if, light sources or readers are used. Fluo visualizers (Figure 3-1) is one such commercial reader that contain light sources and filters which illuminates the test line. They are proven to be more sensitive than simple calorimetric based⁵¹. However, they are still not very cost effective and still be an additional equipment i.e not “integrated” into system. Commercially, there are LFIA kits with designed reader systems available. Sofia is one such technology by Quidel inc. which utilizes fluorescent immunochemistry for quantitative and rapid detection of several analytes including influenza⁵².

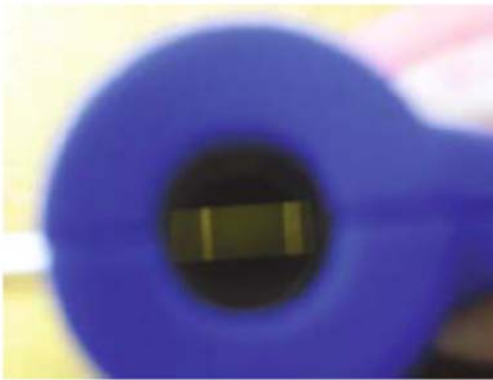
(a) The ESE FluoVisualizer



(b) Visualization of test results.



(c) View into the FluoVisualizer



(d) View of multiple dyes

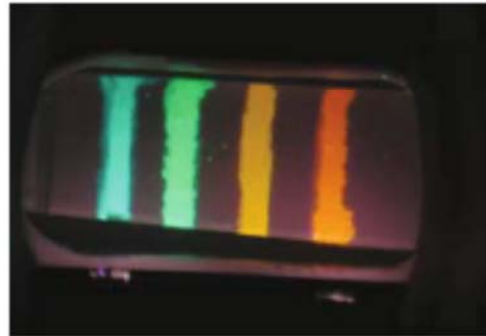


Figure 3-1 Fluorescent visualizer device showing illuminated test lines⁵¹

Sensitivity can further be improved by using high bright fluorescent particles such as Quantum Dots. Quantum dot (QD) fluorescent particles, owing to their high photoluminescence properties⁵³, as well as colloidal water soluble synthesis methods⁵⁴, are being increasingly explored in medical applications⁵⁵⁻⁵⁹. Recently, QDs have received attention for incorporation into LFIA devices. Syphilis detection using QD-LFIA reported by Yang et al. has shown 10× improvement in visual limit-of-detection (LOD) by using QDs over conventional Au NP-based system (Figure 3-2)⁶⁰.

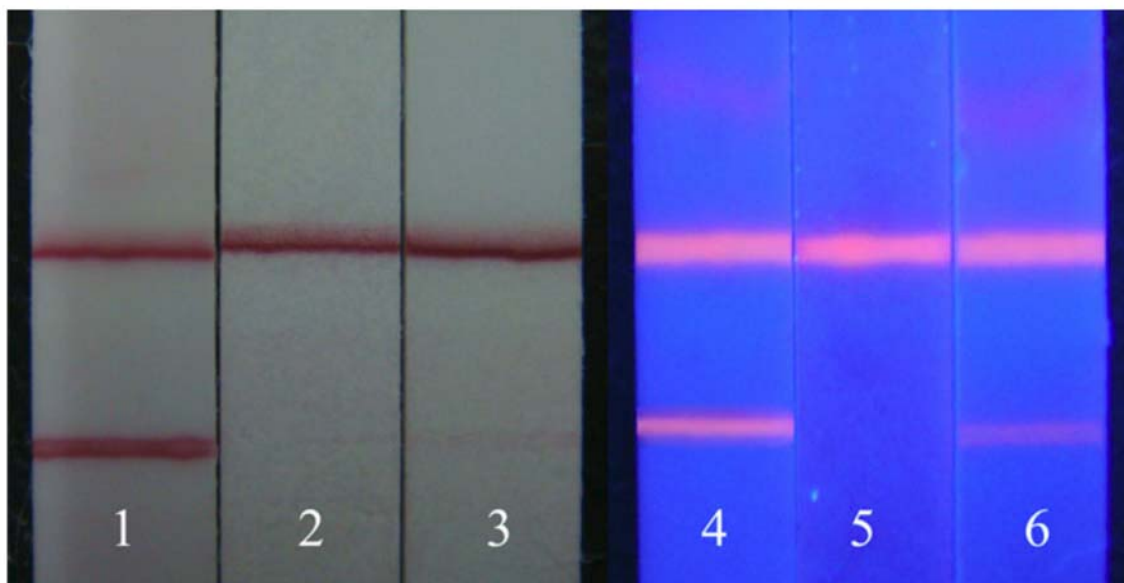


Figure 3-2 QD based LFIA (right) in comparison to Au NP based conventional device (left) ⁶⁰

Similar improvement of visual sensitivity, were reported by Li et al. in detecting human ceruloplasmin⁶¹. These results show the potential of fluorescent particles as visual indicators in LFIA devices. However, these LFIA systems also require separate readers with light sources and detectors, usually benchtop units that are not easily portable and thus harder to use in POC applications.

Organic light emitting diodes (OLED) consist of a series of thin films of various organic materials deposited on substrates, resulting in devices that emit and detect light when biased⁶². While OLEDs are usually formed on glass substrates, the fact that the thin film deposition takes place at relatively low temperatures makes it possible to fabricate them on plastic films or paper substrates^{14,15}. This facilitates integration with LFIAs for realizing LOC applications¹¹ for medical diagnostics. OLEDs have several advantages compared to their inorganic counterparts (LED), including physical flexibility and large area fabrication capability¹¹. The operation of LFIAs using separate OLED excitation has been reported³⁷ by Pais et al. to exhibit a fluorescent dye detection

down to the 100 nm level. However, a system that integrates OLED with paper microfluidic devices has not been realized yet. Such an integrated system would take the advantage of both paper-based diagnostics as well and the potential of organic optoelectronic devices.

In this manuscript, we explore the integration of OLEDs as the excitation source in QD-LFIA devices for high sensitivity, visual observation-based qualitative LFIA diagnosis. Red emitting (655 nm) QDs were used as fluorophores in the LFIA. Though these QDs have maximum absorption in the UV/blue region, the higher efficiency and brightness of green OLEDs compared to blue OLEDs, led us to choose the former. To enhance the visual signal from the QDs in the test line of the LFIA, two color filters were also incorporated in the device. Figure 3-3 below shows an overall sketch of this integration concept.

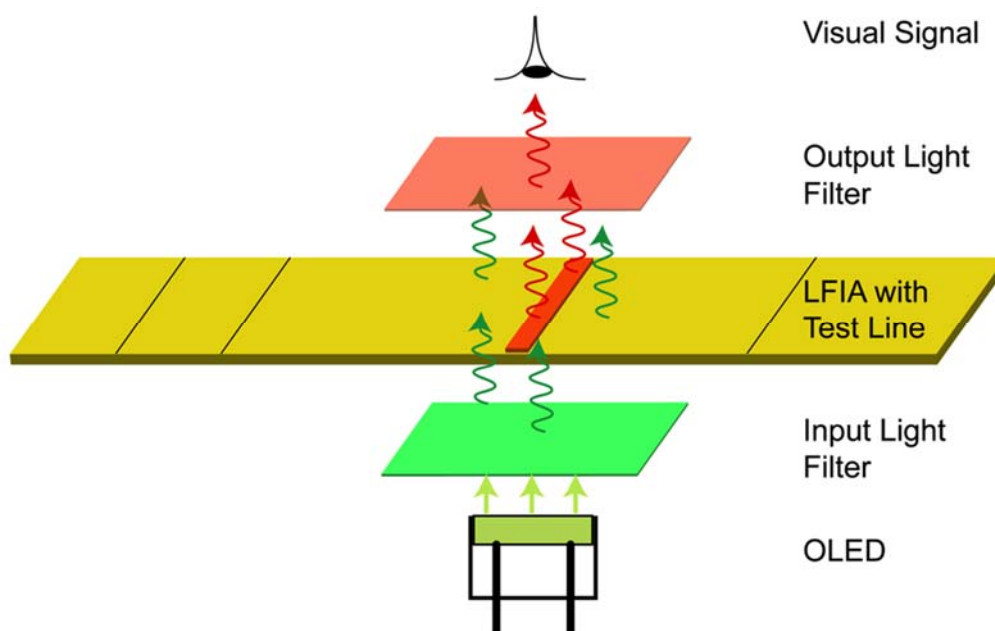


Figure 3-3 Schematic of OLED/LFIA integration approach.

The QD-LFIA was compared with conventional Au NP-based LFIA operated under similar conditions to ascertain improvements in contrast and LOD. A high sensitivity system will improve

the LOD in several LFIA systems that provide qualitative (i.e. yes/no) analysis, such as home pregnancy test kits and flu kits.

3. OLED Fabrication

A phosphorescence based green emitting OLED stack, ITO/NPB/CBP:Ir/BCP/ALQ3/LiF/Al, was chosen due to its inherent high efficiency and brightness, as demonstrated by the Forrest group⁴⁰.

Energy levels of the organic layers stack are shown in Figure 3-4a.

OLEDs were fabricated on ITO coated PET sheets (5 mils) having a sheet resistance of 60 ohm/sq (Sigma Aldrich). To facilitate ease of fabrication, PET sheets were attached to rigid glass substrates before processing. The fabrication process starts by lithographically patterning the ITO to produce 4 mm wide strips of ITO. After patterning the ITO, the surface was cleaned using O₂ plasma for 2 min. The substrates were then transferred to a high vacuum deposition system and the organic layers were sequentially deposited through a shadow mask at an operating pressure of 5×10^{-7} Torr. The thickness of the total organic stack was ~ 100 nm. Next, the substrates were very briefly removed to load the anode mask. Lithium fluoride (LiF) and aluminum were then deposited (total of ~ 40 nm) in the vacuum system, forming the anode electrode in devices with an active area of 4 mm \times 4 mm. After the OLED fabrication was completed, the PET sheet was removed from the glass substrate in order to integrate with the LFIA. Each OLED substrate measured 15mm \times 15mm, as shown in Figure 3-4b. It is important to note that in these bottom-emitting OLEDs, the emission that is utilized in the overall device is through ITO layer and the PET sheet.

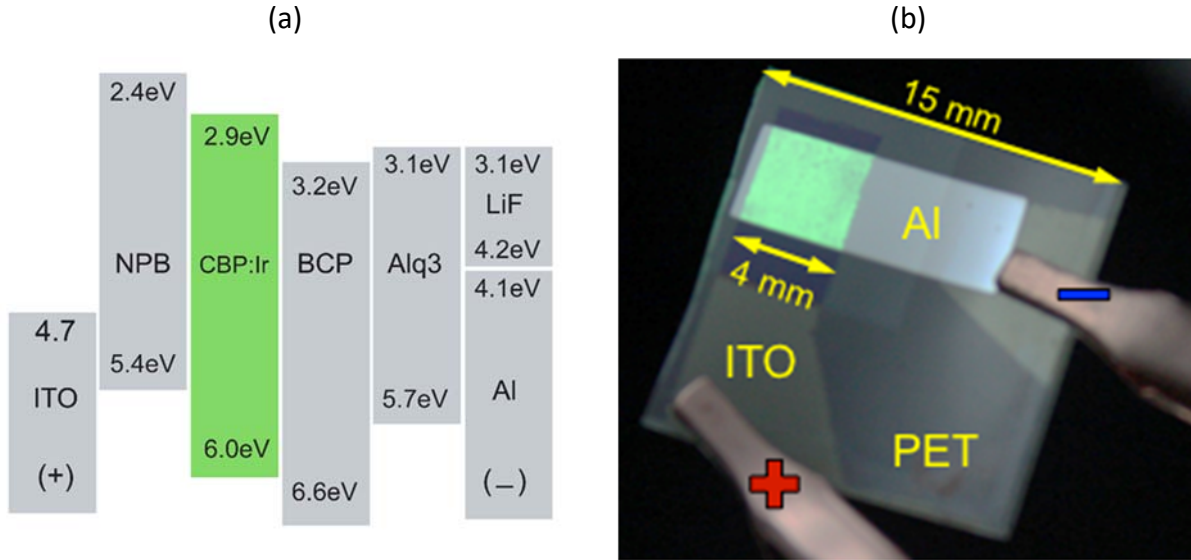


Figure 3-4 OLED details: (a) constituent layers and their respective HOMO/LUMO energy levels; (b) photo of emitting green OLED pixel on a PET substrate

OLED current-voltage (I-V) characteristics were obtained with a variable voltage source in steps of 0.5 V with current values recorded by an HP-6634B DC power source. Brightness was measured using a luminance meter (Konica-Minolta CS-200). The spectral output was obtained using Ocean Optics SD 2000 spectrometer. Figure 3-5 shows the typical current-voltage-brightness and spectral characteristics of the OLEDs fabricated.

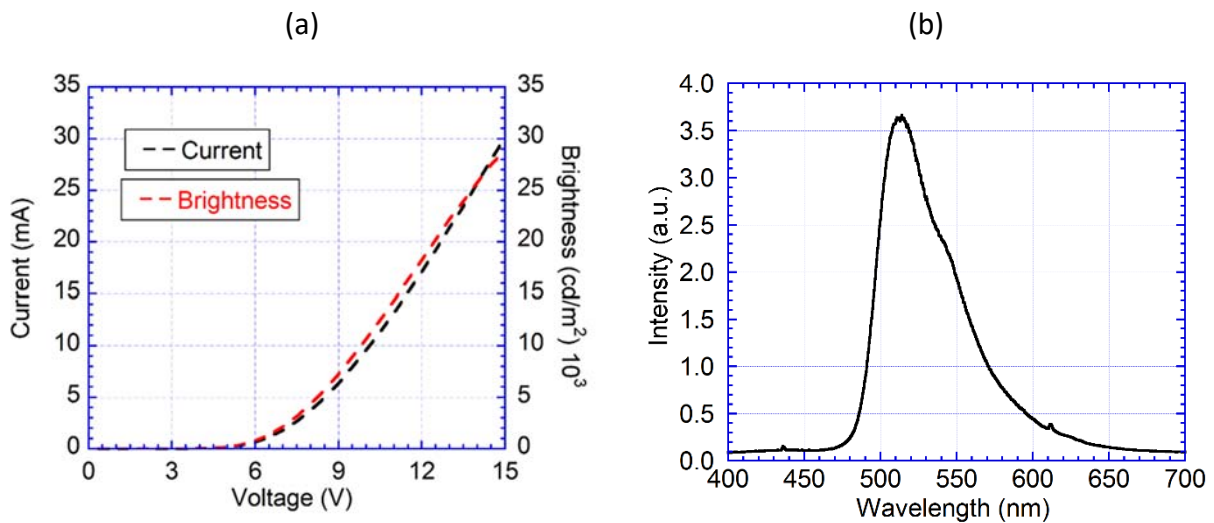


Figure 3-5 OLED characteristics: (a) current and brightness vs. voltage; (b) emission spectrum.

4. LFIA Assay Fabrication

A simple immunoreaction-based fluorescent lateral flow assay was chosen to evaluate the performance of the OLED-integrated LFIA device. The capture mechanism is based on antibody-antibody reaction rather than using a specific analyte to form a sandwich assay. The analytical membrane with test lines (Meridian Biosciences Inc.) measured 60 mm × 6 mm. The quantum dot fluorophore conjugate, Donkey Anti-Mouse QD 655 (Life Technologies) binds to the test lines present in the analytical membrane. Figure 3-6 shows the absorption and emission spectra measured using the Nanodrop instrument. Two thin plastic light filters were integrated in the device to improve the contrast and produce a higher visual sensitivity: an input green filter (to reduce the red component in the OLED emission spectrum) and an output red filter (to remove green OLED emission after QD excitation). As can be seen from Figure 3-7a, the OLED has a long emission tail into the red spectrum, with some emission at ~600-620 nm, which competes with the red emission signal from the test line.

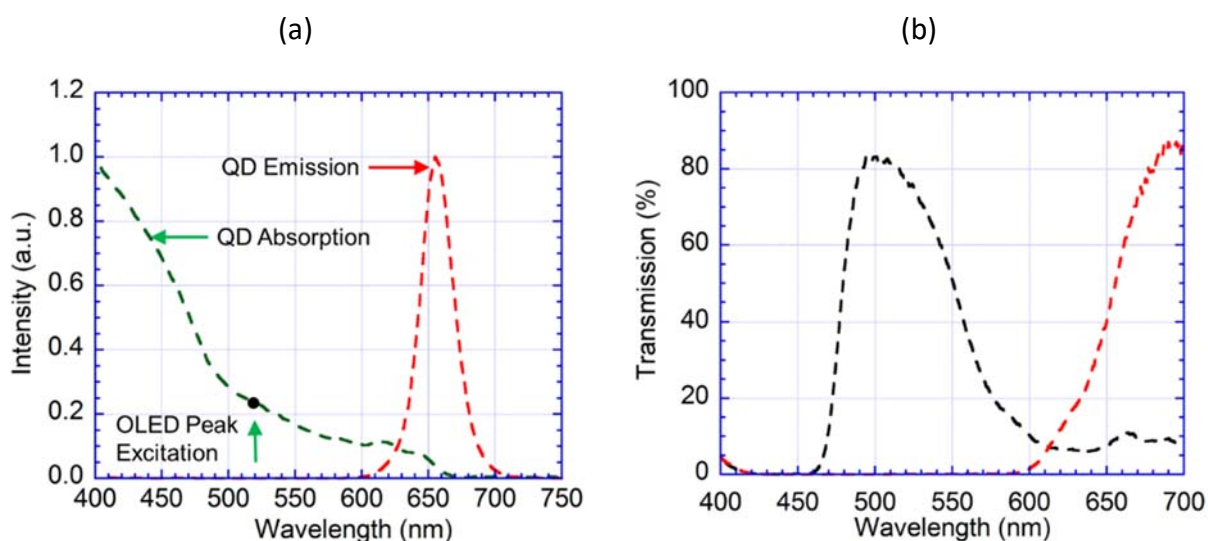


Figure 3-6 Optical spectra of the components of the integrated OLED/QD-LFIA device: (a) Absorption and emission spectra of quantum dots. OLED peak excitation wavelength also indicated; (b) Transmission of green and red filters.

To reduce the red component, a green light filter (Chroma Green, Rosco Laboratories), was used as the input light filter. The spectral shaping is shown in Figure 3-7a. The output red filter (Medium Red, Rosco Laboratories), was used to eliminate the green light from the OLED source, and allow only the light from the QDs, which emit in the deep red region (655 nm) as seen in Figure 3-7b.

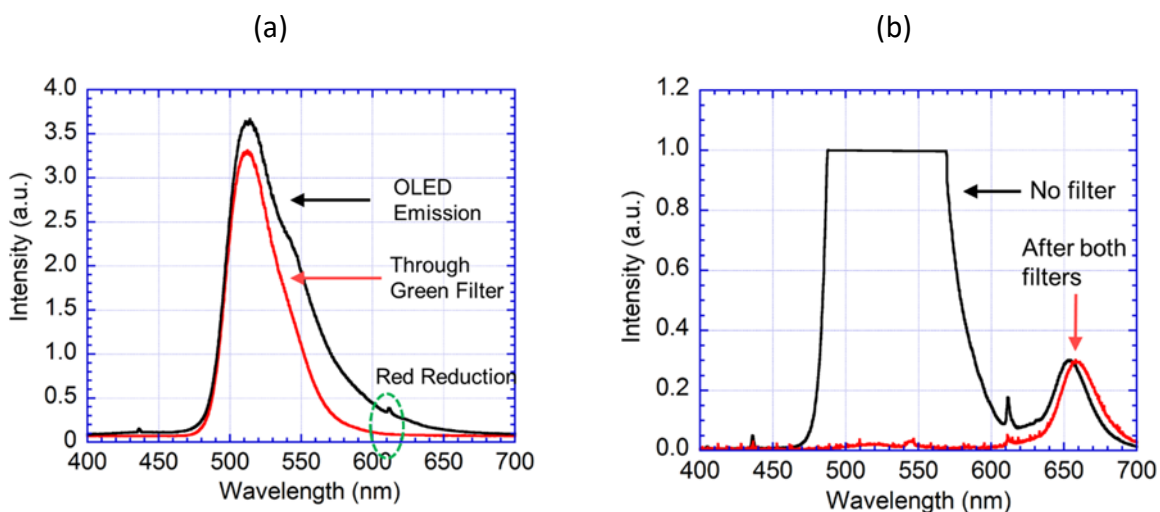


Figure 3-7 Spectral response showing the effect of light filters in the OLED/LFIA device: (a) OLED emission through input light filter; (b) OLED + QD emission through input and output light filter

The LFIA was constructed by attaching the analytical membrane to a backing card, and attaching the sample and wicking pads (Diagnostic Consulting Network Inc.) to the two ends of membrane, with an overlap of ~ 5 mm. The sample and wicking pads measured $20\text{mm} \times 6$ mm. The assay was performed by dipping the LFIA into conjugated QD solutions of various concentrations for a specific amount of time. For conventional Au-NP LFIA, Donkey Anti-Mouse Au solution (from Abcam) was used to perform assays under the same conditions as the QD solution. Figure 3-8 illustrates the basic operation of the LFIA and the capture lines under UV excitation.

(a) DipStick Assay Format

(b) UV Excitation

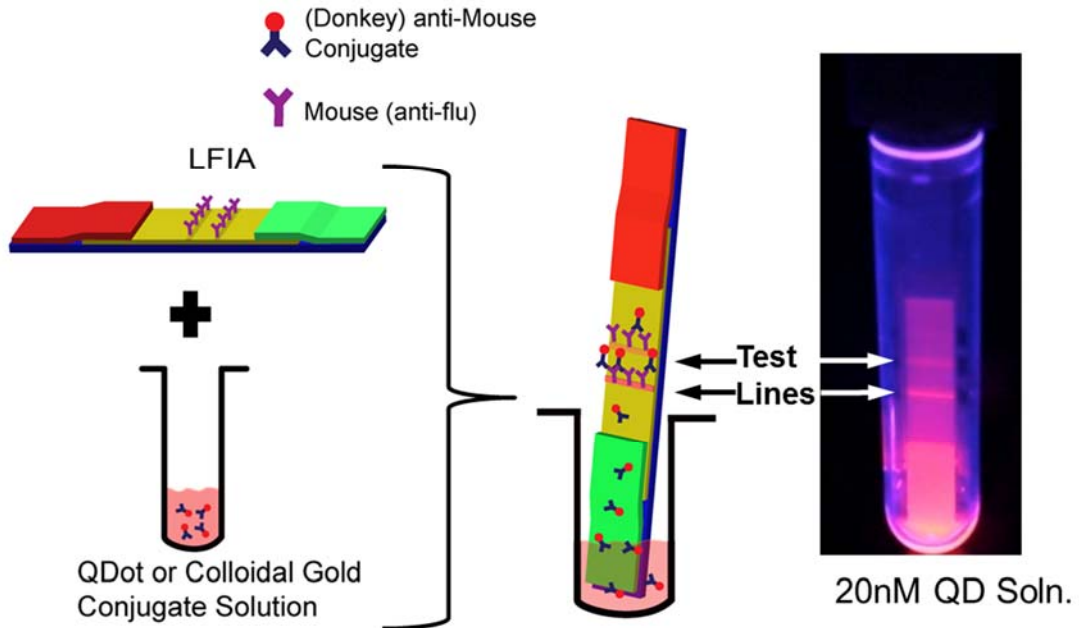


Figure 3-8 LFIA working principle: (a) dipstick assay format; (b) UV excitation after assay process shows emission from QDs captured on test lines

5. Integration

Figure 3-9 illustrates the integration process of the OLED with the QD-LFIA device. The integration starts by attaching the OLED fabricated on PET onto an adhesive backing membrane (DCN). Copper tapes were attached to the OLED to provide external electrical contact. The input (green) plastic filter is then placed on top of the OLED. Next, the analytical membrane is placed on top of the OLED and color filter and aligned such that the position of the test line lies within the device emission area. Adhesives were used between these layers for attachment. The sample and wicking pads were then attached to the analytical membrane for enabling the lateral fluid flow. Finally, the output (red) filter is attached on top of the test line region. The assays were

performed by inserting the LFIA unit into a 100 μ L QD solution of varying concentrations for 10 min. For comparison, the same procedure was used with Au-NP solution at the same concentration and duration. A uniform drying process was used for both assays. Figure 3-10a shows the resulting comparison using photographs under room light conditions of the two types of LFIA at 100 nM concentration. The signal generated by the QD-LFIA is much more visible than that from the Au-NP LFIA, with the QD test line being much brighter and sharper than the NP test line.

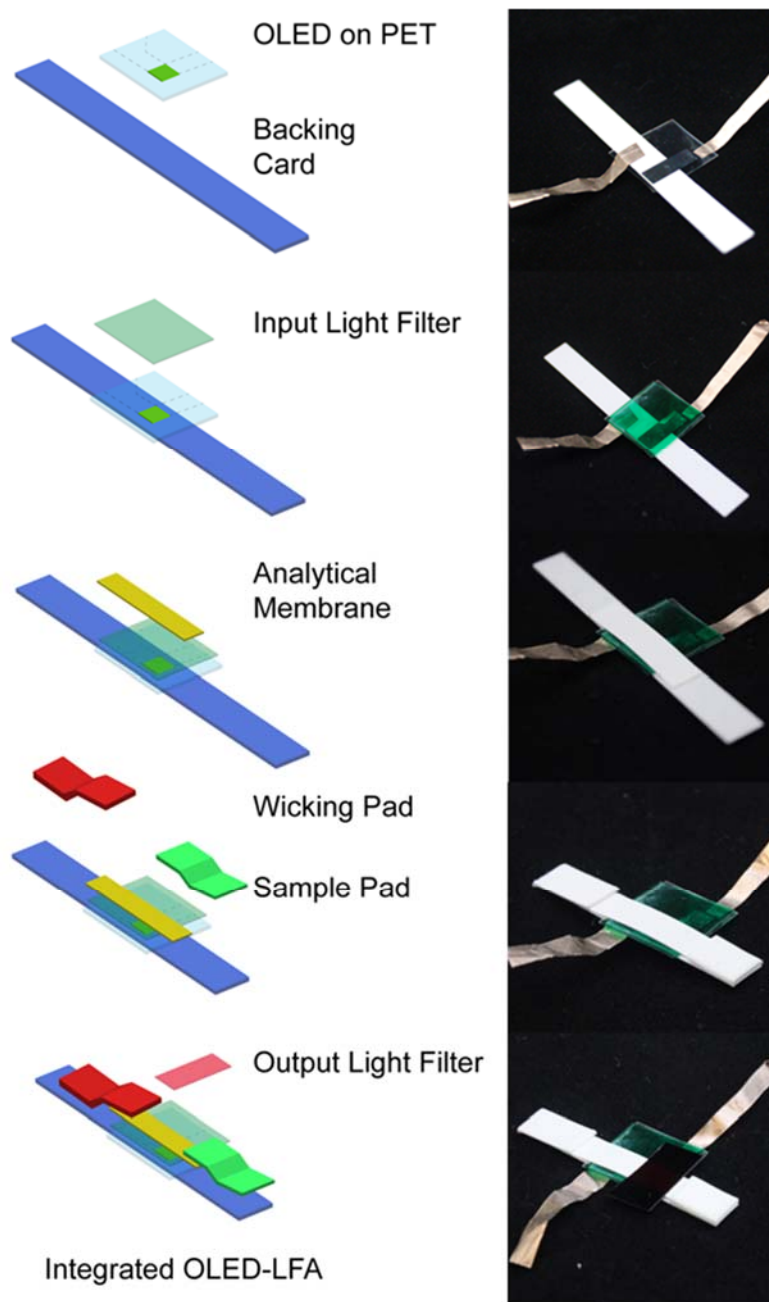


Figure 3-9 Fabrication steps of integrated OLED/LFA device

To quantify the contrast, grey line scans were taken (Image J software) in the test line region. The corresponding data is plotted in Figure 3-10b. The signal from the QD-LFIA is seen to be $\sim 5\times$ larger than from the Au-NP based device. This clearly indicates superior sensitivity of visual detection for the OLED integrated QD-LFIA.

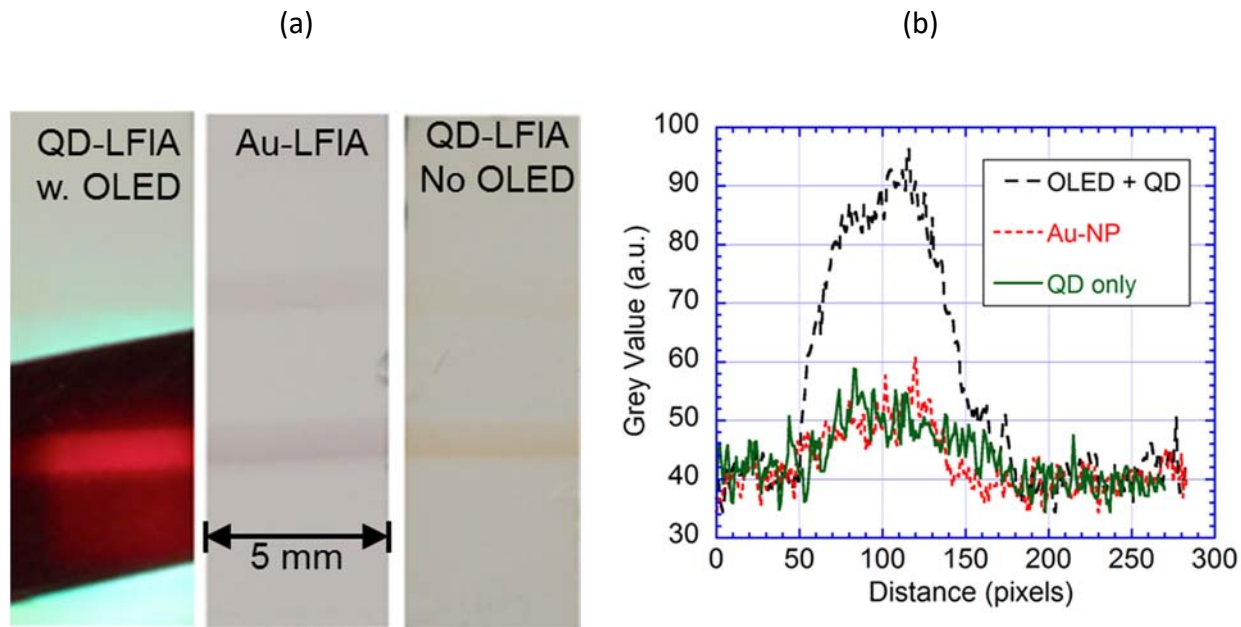
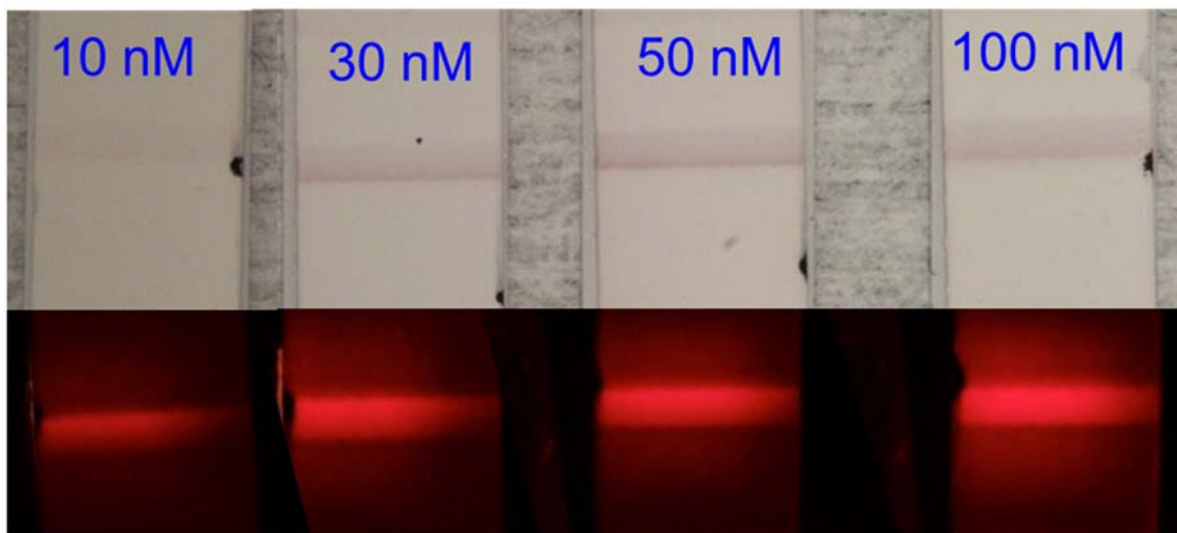


Figure 3-10 Comparison of LFIA operation - emissive integrated OLED-QD approach vs. reflective Au-NP approach: (a) side-by-side photo of the two types of LFIAs; (b) equivalent grey scale contrast comparison

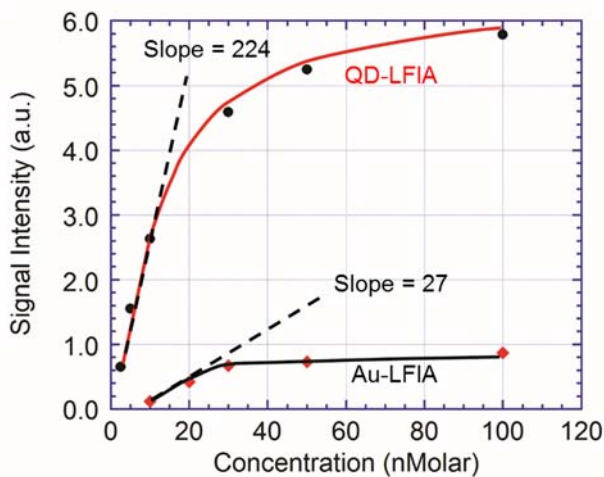
Assays at various concentrations were used to determine the LOD in the two cases, concentrations and images are shown in Figure 3-11b. In all cases, the OLED was biased at the same voltage and the same room lighting conditions were used. Signal-to-noise (S/N) ratios were calculated from the Image J data as follows. Grey scale pixel values in the test line region were averaged and the difference from the average of the background pixel grey values (around the test line region) was calculated. This difference is taken as the signal intensity. The signal is plotted in Figure 3-11a as a function of conjugate concentration. As indicated by the dashed lines, the sensitivity (i.e. change in signal with change in concentration) in the linear region is $\sim 8\text{-}9\times$ higher for the QD-LFIA. While both device types experience some saturation at the higher concentration, the effect is more pronounced for the Au-NP device. The noise intensity was taken as the average of the difference between consecutive grey pixel values in the Image J line scan away from the test line. The S/N ratio is then given by the ratio between the signal and noise

intensities. Figure 3-11c show the S/N ratio for both QD-LFIA and AuNP-LFIA for various conjugate concentrations. A S/N ratio of 3 was chosen to represent the LoD condition, which was reached at 3 nM for the integrated QD-LFIA and at 21 nM for Au-based LFIA.

(a)



(b)



(c)

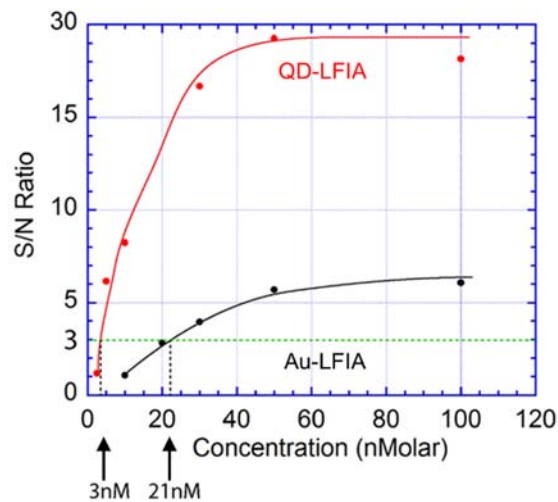


Figure 3-11 Visual characteristics of QD and Au NP-LFIA as a function of concentration of conjugate solution: (a) Photographs of Au based LFIA compared with QD based LFIA at same concentrations; (b) signal intensity; dashed lines indicate signal sensitivity in linear region; (c) signal-to-noise ratio; LoD concentrations indicated by the arrows.

6. Summary

In summary, the integration of OLED-based excitation of QD fluorescent labels in LFIA devices was demonstrated. Integration was achieved by attaching OLEDs fabricated on PET with color plastic filters and the LFIA components. QD-based fluorescent LFIAs were used for proof of concept and visual sensitivity was compared to conventional Au NP-based LFIA. A significant improvement in signal intensity, contrast and limit-of-detection was achieved in integrated OLED devices compared to conventional LFIA. The LoD for OLED excited QD-LFIA was ~ 3 nM compared to 21 nM for the conventional LFIA, or a 7 \times improvement. Combined with other attractive factors of LFIA and OLEDs, such as low cost and large-scale roll-to-roll manufacturability, these results show that integrating OLEDs in paper-based diagnostic system is a high potential path for lab-on-chip device applications.

Chapter 4 : Integrated NFC Power Source in Lateral Flow Immunoassays

1. Introduction

A true LOC can only be realized if all the components including the power source can be also integrated with the diagnostic system. For LFIA diagnostic devices, similar to organic optoelectronics, thin film power harvesting devices will be the ideal candidates. Our first preference was to have zero “on board” power. This can be achieved by harvesting RF signals, NFC⁶³, which is present in several modern day smartphones. Smartphones are ubiquitous computer which can be also used to process the data fed back into it from the integrated optics, making them also a part of POC ecosystem. Similar to optoelectronics, this component will also have to be “thin film” and can be fabricated on plastics and be flexible to enable seamless integration with the LFIA system.

A lab-on-chip vehicle was explored combining RF near field communication (NFC) harvested power and light sources for paper-based lateral flow immunoassay systems (LFIA) with quantum dots (QD) as fluorophores. Such a vehicle has potential applications to point-of-care systems requiring high sensitivity while also being low-cost, disposable and easy to use. Micro-LEDs which provided the excitation source for the test line of a QD-LFIA were surface mounted on plastic substrates using a printed hybrid electronics approach for the fabrication of power harvesting NFC antenna, chip assembly and electronics integration with the LFIA strip. The LFIA is a rotavirus assay kit with Au nanoparticles into which QDs emitting at 655 nm were also incorporated. A

digital camera was used for detecting the fluorescence from QDs and the reflected signal from Au NPs. The signals were compared using gray scale analysis. The NFC-powered LED light source integrated with the QD-LFIA demonstrated $\sim 9\times$ higher sensitivity compared to conventional Au-NP based assays. Such an integrated system can be potentially mass manufactured using roll-to-roll processing making the device cost effective, as well as having high sensitivity.

Given all the desirable characteristics of LFIAs, they still fall behind on sensitivity and limit-of-detection (LOD) in comparison to enzyme-linked immunosorbent assay (ELISA)⁶⁴. A possible approach to improve LFIA sensitivity is the use of fluorescent particles over conventional Au nanoparticles (NP) as the colorimetric indicator in the assays⁴⁶⁻⁴⁹. Specifically, quantum dots (QD) as fluorescent particles have gained considerable interest in medical applications^{55,56,61}. Some of their desirable characteristics over other assay particles are high photoluminescence and simple synthesis using colloidal water soluble methods^{53,54}. The incorporation of QDs in LFIA devices has been reported by several groups. Particularly noteworthy for the application targeted in this article are those of Yang et al.⁶⁰ who have shown a $10\times$ increase in visual signal and Gui et al.⁴⁸ who used CCD sensors to integrate the photo signal for best sensitivity and LOD. Several groups investigated making the assay more quantitative, along with being more sensitive, by using QDs in conjunction with external reader systems^{61,65,66}. Major limitations in the work of these groups for point-of-care (POC) applications were the requirements for external readers, light sources and power supplies. We have previously reported⁶⁷ one solution to this limitation by integrating organic light emitting diodes (OLEDs) as a light source and successfully produced similar improvements in sensitivity. However, there remains the need to integrate the power source into the device as well.

Thin film batteries are possible candidates for this application as they can be flexible, thin and biodegradable^{68,69}. However, an approach having a zero on-board power and harvesting energy from ubiquitous sources may be more desirable⁷⁰. RF harvesting⁷¹ on board is a possibility, however the limitation can be the availability of the source of RF power. The incorporation of smartphones into everyday existence has made their image collection/transmission and computation available for much more than communication. Smartphones have increasingly gained substantial interest as adjunct platforms in diagnostic applications, some are shown below in Figure 4-1⁷²⁻⁷⁴.



Figure 4-1 Smartphone use in diagnostic devices: (a) Smartphone camera microscopy⁷⁵; (b) Colorimetric detection using smartphone's camera⁷⁶.

Shen et al.⁷⁶ used the smartphone's camera and CPU for detection and signal processing applied to colorimetric assays. Many modern smartphones possess near field communications (NFC) which uses RF technology for connecting devices. Lee et al.⁷⁷ used this technology in for communicating data to/from the diagnostic device. In our approach, we use power harvesting from NFC-equipped smartphones. NFC harvesting antennas can be hybrid manufactured on

flexible substrates, which implies that they can ultimately be mass manufactured using large scale roll-to-roll technology, potentially being cheaper than thin film battery options. Of course, in addition to serving as the power source, NFC may also be used for communication between the diagnostic device and smartphone for processing and cloud connectivity.

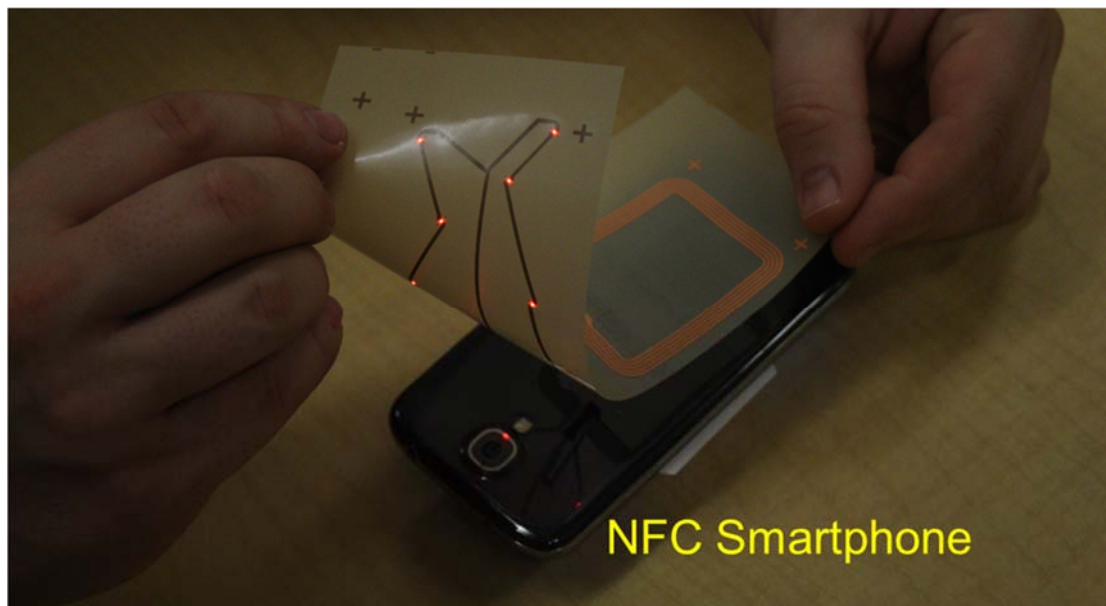


Figure 4-2 Hybrid manufactured flexible NFC powered LED chip (powered using a Samsung smartphone)

In this manuscript, we explore NFC-powered green LEDs (Figure 4-2) as light sources in QD-based LFIA. Suitable optical filters have been selected for maximum sensitivity. A conventional CCD digital camera was used for detection, providing the ability to integrate the fluorescent signal for best sensitivity. Figure 4-3 shows an overall sketch of the LFIA operation, illustrating the integration of the LFIA with the antenna, LEDs and optical filters.

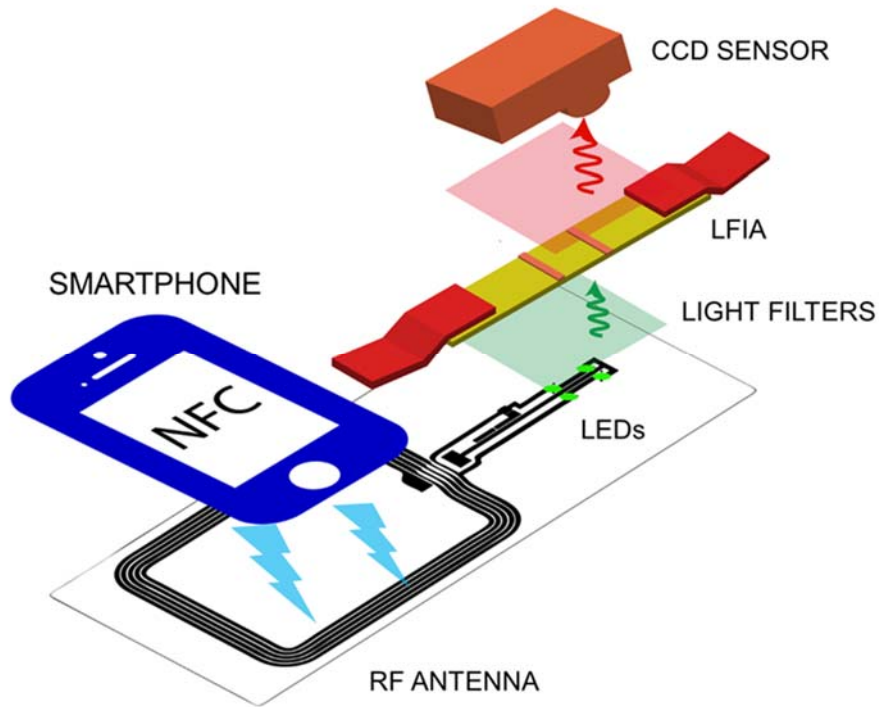


Figure 4-3 Schematic showing NFC power harvesting and integration with LEDs, optical filters and LFIA

For the LFIA, a conventional Au-NP based commercial test kit was used. QDs introduced into the test kit with the sample solution are captured on the test line along with Au NPs. The presence of both types of detector particle in the same test line results in an easier and fair comparison. Since the major focus is to obtain improved sensitivity, the lower concentration region is of more interest. This makes interference of one detector type over the other negligible. To quantify the signal, a gray scale plot of the image was taken and contrast was calculated.

2. NFC LED Chip Fabrication

The electronic backbone circuitry was fabricated using a printed and hybrid electronics manufacturing approach for reduced device cost, waste and footprint. Copper coated PET foil

(Prinel Ltd., Finland) was patterned using wet etching to create the antenna structure and electronic circuit design (**Error! Reference source not found.**).

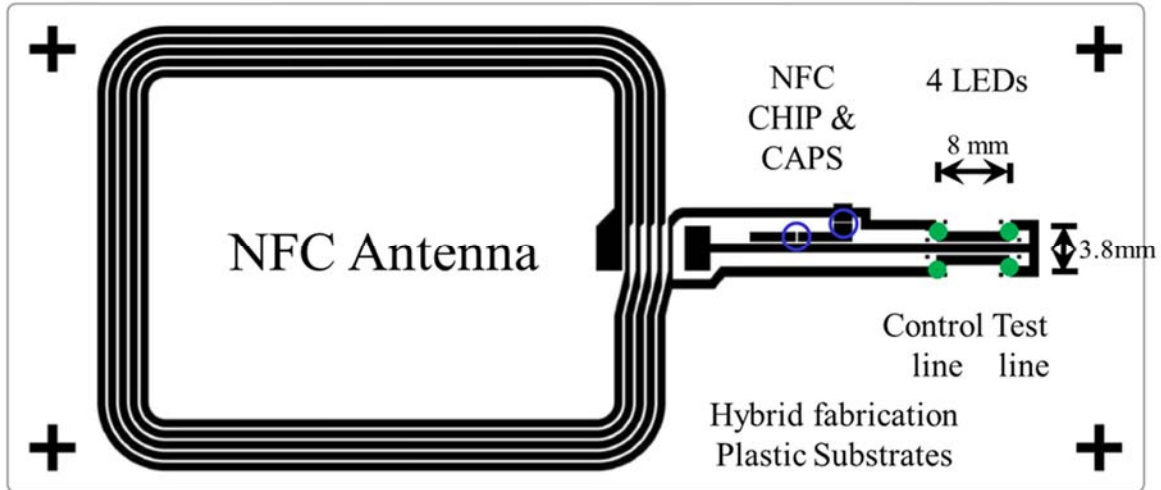


Figure 4-4 NFC chip design tailored to fit dimensions of the LFIA kit test and control lines.

Bare-die green LEDs (ES-CEGHV15B, Epistar Corp., China) and electronic components (RFID chip and capacitors) responsible for the power transfer between mobile phone and the LED chip were assembled using a custom-made roll-to-roll hybrid assembly machine at VTT's printed and hybrid electronics pilot manufacturing environment (Datakon EVO 2200, Austria). Figure 4-5 below shows this pilot manufacturing roll-to-roll facility and the chip bonding.

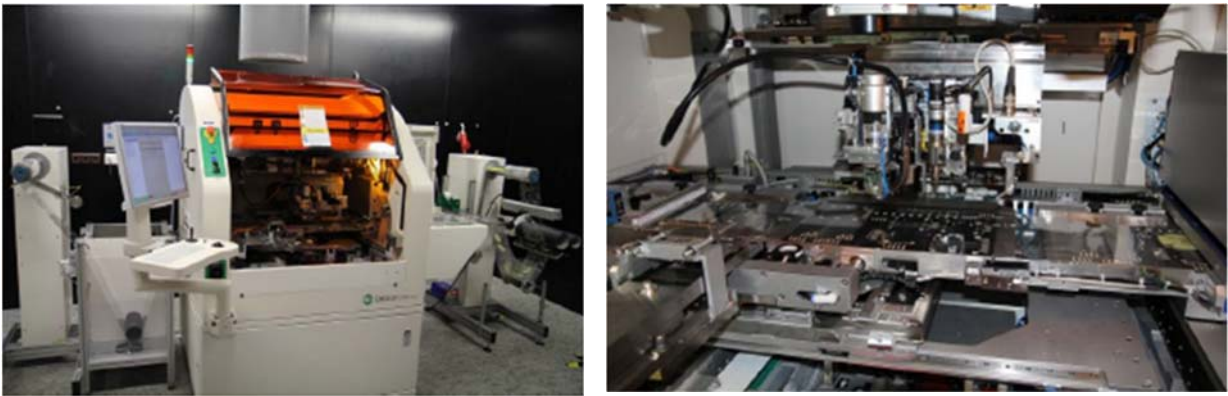
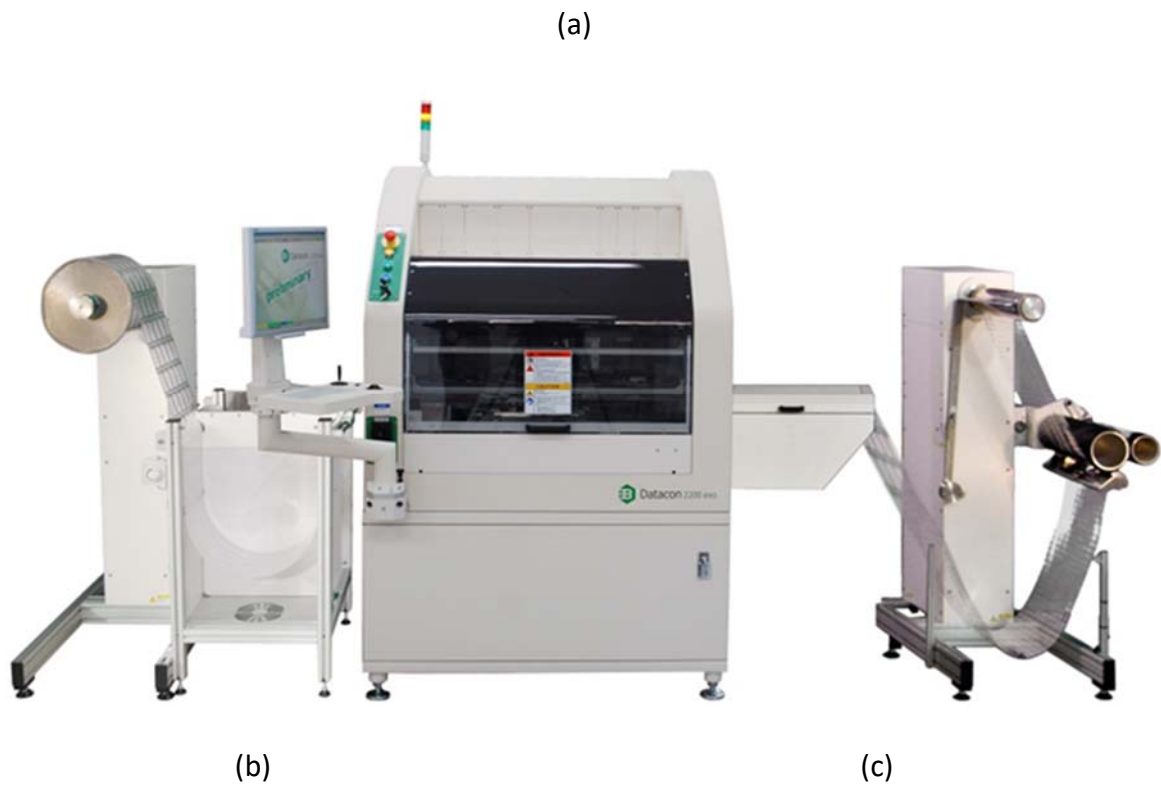


Figure 4-5 Hybrid manufacturing setup at VTT; (a) Roll-to-Roll fabrication equipment; (b) Actual equipment and setup; (c) Die attachment using “pick and place” and adhesive glue.

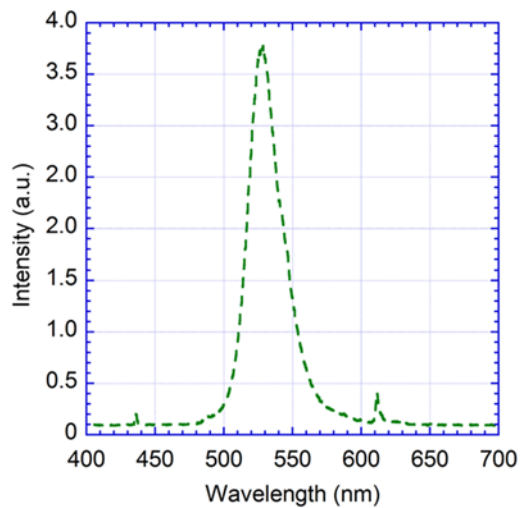
Figure 4-6a illustrates the powering principle of the flexible LED chip using the NFC module of a smartphone. The LEDs were separately characterized electrically and optically using an external DC bias source. Figure 4-6b shows the spectral characteristics of the green LEDs used as measured

using Ocean Optics SD 2000 spectrometer. Optical power output shown in Figure 4-6c was measured (Newport Optical 1918-C) against various input currents (HP-6634B DC power source). This plot was used to calculate a power output value of $80\mu\text{W}$ (per LED) when powered with 6-7 mW using NFC from a smartphone.

(a)



(b)



(c)

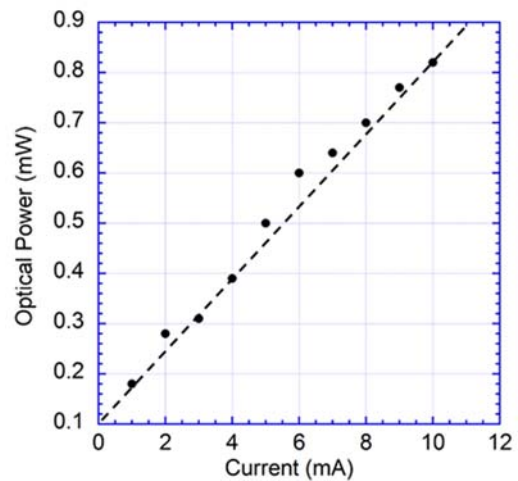


Figure 4-6 NFC power harvesting for LED operation: (a) demonstration of smartphone powering LEDs (insert – photo showing LEDs surface mounted on plastic sheet); (b) emission spectrum of the green LED; (c) LED output optical power vs. input current, separately measured

3. LFIA Assay Fabrication

The LFIA test kits were provided by Meridian Bioscience Inc. (Cincinnati, USA) and designed for detection of rotavirus. The operating principle of the LFIA is illustrated in Figure 4-7a. The test strip contains mouse anti-rotavirus conjugated to Au NPs as detector particles in the conjugate pad. The kit also contains a nitrocellulose analytical membrane with capture antibodies (rabbit anti-rotavirus) embedded in the test line that bind to an epitope of the rotavirus molecule. A control line containing goat anti-mouse Ab is present to validate the test, by capturing the conjugate mouse Abs even in the absence of rotavirus analyte. QD 655 (Life Technologies) QDs conjugated to donkey anti-mouse Ab that target the mouse antibodies in the conjugate pad were introduced with the sample solution. An antibody complex is formed as shown in Figure 4-7a which then migrates toward the test line and is captured in the presence of analyte. Hence, both QDs and Au-NPs are present in the test and control lines, as can be seen in Figure 4-7b,c. The QDs possess wide absorption spectra in the UV-green region, but a very narrow emission line at 655 nm. This large Stokes shift makes it easy to choose simple colored plastic light filters to eliminate the excitation light signal. For the output light filter, a medium red (Rosco Labs) filter was used. Though the LED has a fairly narrow emission spectrum, an input light filter was used to ensure that there is no competing red spectral component from the excitation source. Chroma green light filter (Rosco Labs) was used for this purpose. The spectral characteristics of the QDs and light filters has also been discussed in detail elsewhere⁶⁷.

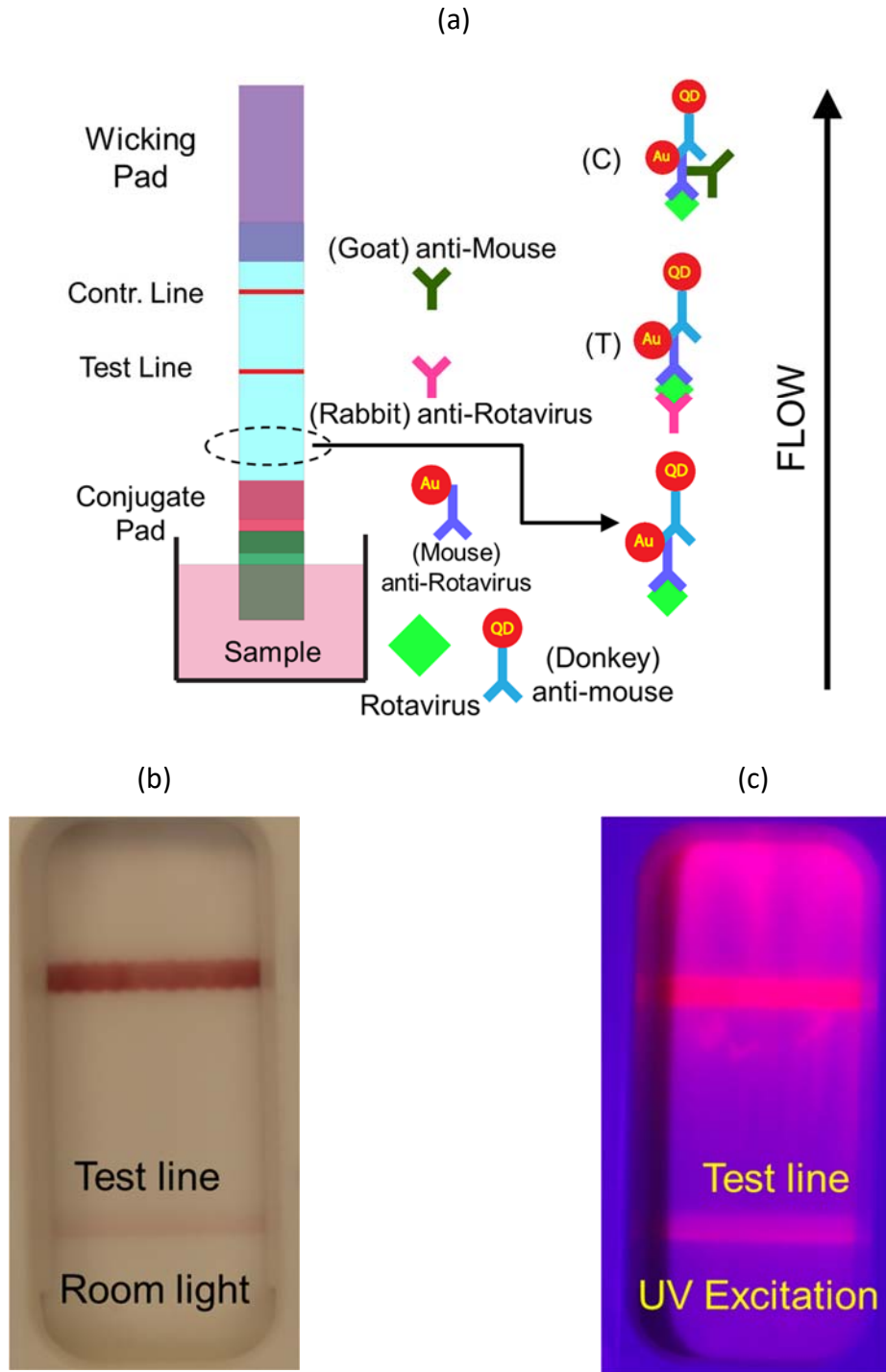


Figure 4-7 LFIA working principle: (a) immunochemistry of the LFIA showing capture of both Au-NP and QD at test and control lines; (b) captured Au-NPs reflection under room light; (c) captured QD particles fluorescence excited under UV light.

4. Results & Discussion

The rotavirus test kit was run with a standard positive solution at a low concentration volume of 10uL to yield a faint looking test line. Such a concentration would represent the LOD of this commercial test kit using Au-NP and considered as the baseline. 3 μ L of QD solution at 1 μ M concentration was added along with the positive control solution (100 μ L) and the test was run. After subject to uniform drying process, the membrane with captured test lines (QD & Au) was separated from the test kit and integrated with the light source. The input and output light filters were attached to either side of the analytical membrane using adhesive. The setup consisted of NFC-powered LED as the light source and a spacer. The spacer was a 5mm thick cardboard with a circular opening. Using a thicker spacer gave more uniform illumination over the entire test line, this can be seen in Figure 4-8 below.

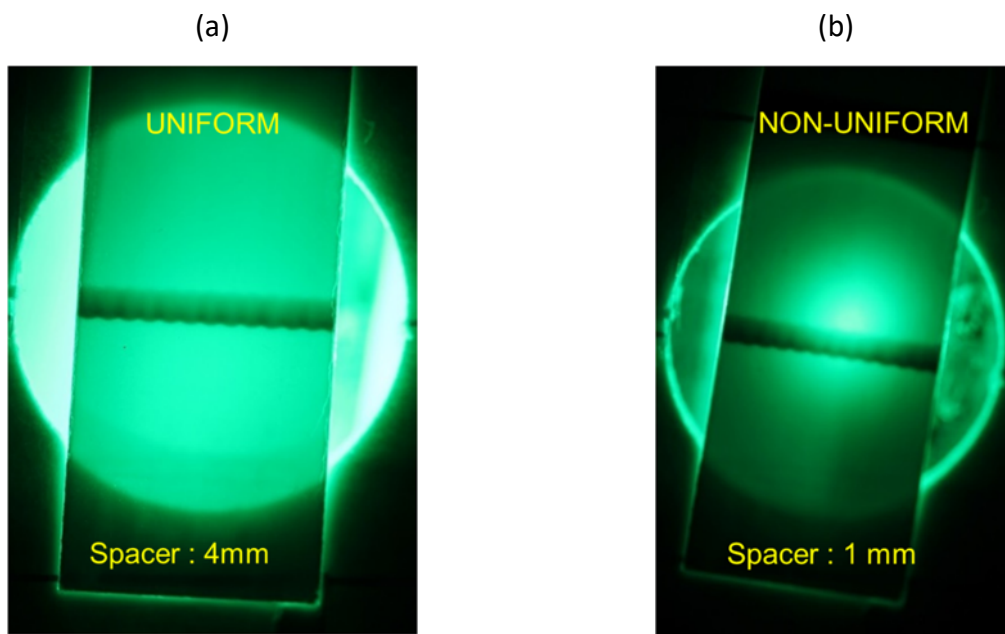


Figure 4-8 Spacers used in integration: (a) Thicker spacer for uniform illumination; (b) Thinner spacer that shows non uniformity due to point source nature of LED.

A digital CCD camera was used as the sensor. The integration capability of the CCD by adjusting the shutter speed settings was used to obtain the maximum signal for the QD-based LFIA. This helped to mitigate the loss in intensity due to spacers.

Figure 4-9a,b shows the test line contrast under optimum conditions for each case: room light conditions for Au NP case, dark fluorescence for QD case. As can be seen from the images, the QDs excited with light powered by the NFC power source exhibit superior performance over Au NPs of the same concentration. The image was converted to its equivalent gray scale image using ImageJ⁷⁸ software and a line contrast plot was measured. For best results, red channel conversion was selected for QD devices. As can be seen in Figure 4-9c the contrast plot is consistent with the images. Signal intensity of the test line was quantified by calculating the area under each curve between 200-350 pixel distance. A $\sim 10\times$ increase in intensity for QD devices compared to conventional Au-NP based diagnostic kit was observed.

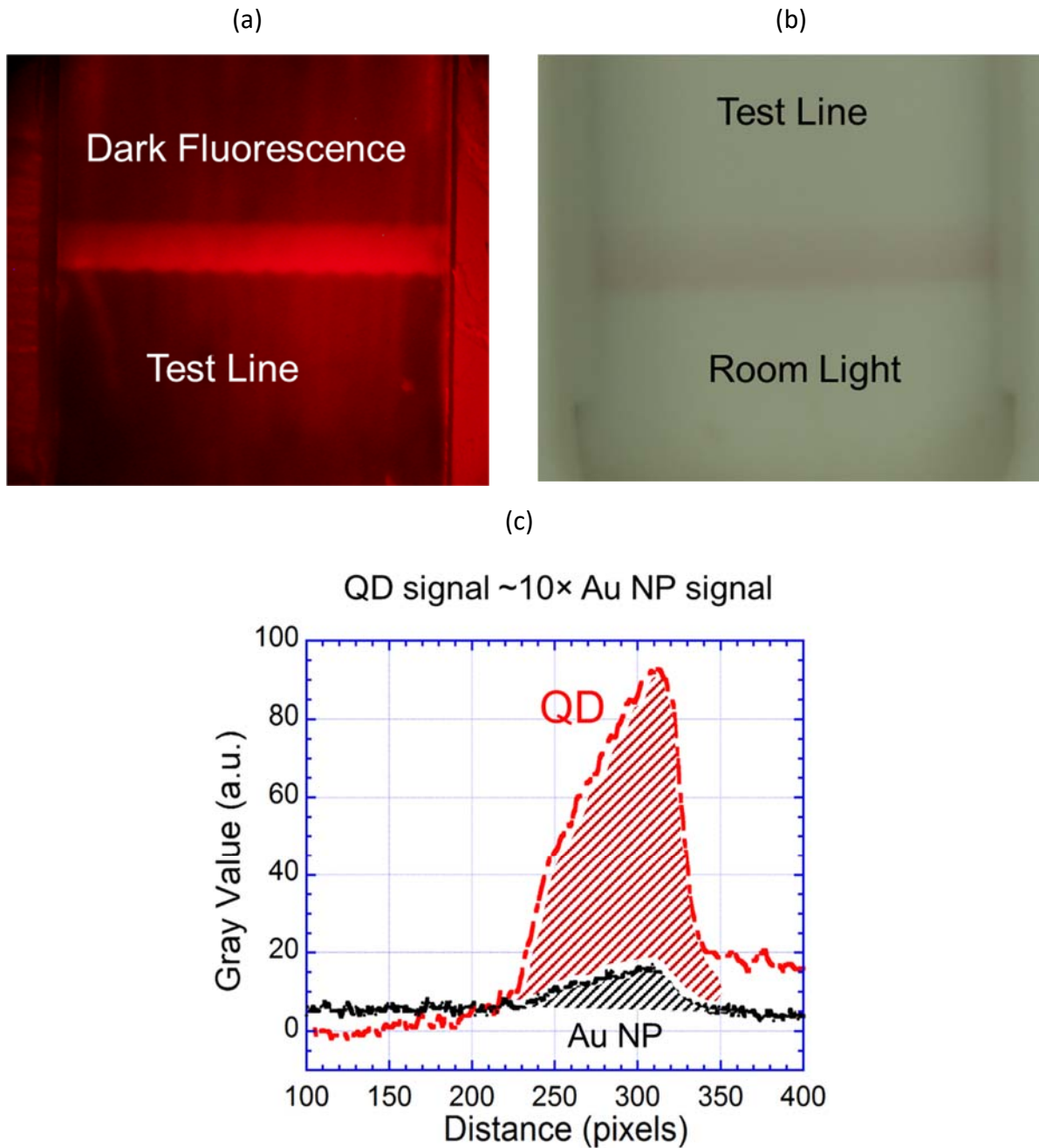


Figure 4-9 LFIA capture test line results: (a) fluorescence of QDs excited using NFC powered LEDs; (b) room light reflectance of Au NPs; (c) gray value contrast comparison between QD and Au-NP as baseline

It should be noted that the signal contrast of the test line is still limited by the amount of non-specific binding around the test line. Hence, in efforts to bring it closer to ideal case, a wash run was also performed to remove the non-bound conjugate, Figure 4-10 below. This step was

performed by replacing the QD soaked sample pad (from run before) with a new pad and adding 150uL of negative dilutant solution.

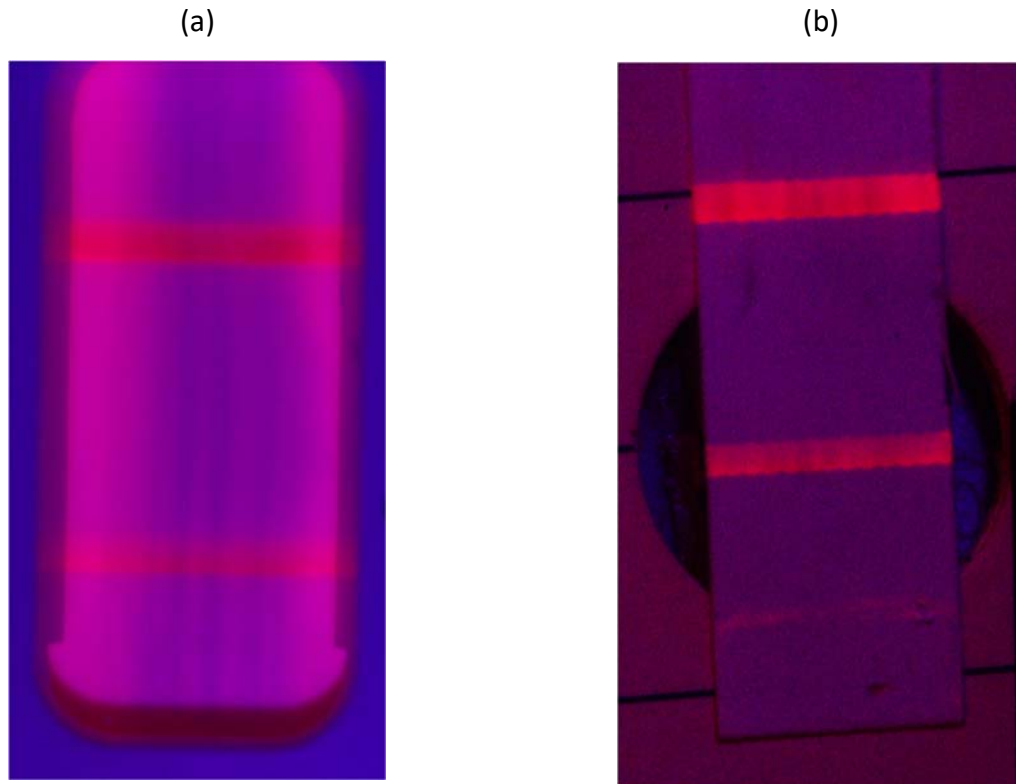


Figure 4-10 Wash step to remove non-specific binding: (a) No wash step performed; (b) Wash step using DI water.

However, in the eventual optimized case (i.e. no non-specific binding), the contrast can be amplified by integration to the saturation level and thereby even higher sensitivity can be achieved.

5. Summary

In summary, a lab-on-chip vehicle powered with NFC RF power from smartphones was demonstrated. Fluorescent QD-based paper LFIAs were excited with NFC-powered LEDs fabricated by hybrid manufacturing processes on plastic substrates. A CCD camera was used as detector that integrated the signal to provide maximum sensitivity. In the future the separate camera may be replaced with the camera of the smartphone that is also acting as a power source. The devices achieved nearly 10× increase in sensitivity in comparison to conventional commercially optimized Au-NP based LFIAs.

Such a high sensitivity device was achieved with a minimal increase in device complexity by using a printed and hybrid electronics approach for fabricating a low-cost, disposable LOC device. The added cost for the printed electronics backbone (plastic substrate, conductive ink, antenna, RFID chip, micro-LEDs) are currently in the range of tens of cents (< 1 \$US) for mid-volume manufacturing (< 1 million devices/year) and have the potential for further cost decrease at higher volumes and continued progress in printed electronics research. These results indicate the potential path for future work, such as integrating a photodiode with the device to obtain electrical output that can then be transferred to the smartphone via the same NFC technology. The optoelectronic part may also be replaced with its organic counterparts (OLEDs and OPDs) for larger area detection, as well as biodegradability and cost effectiveness. Such applications can also bring quantitative detection along with increased sensitivity that are some of the desirable characteristics of Lab-on-Chip diagnostic devices.

Chapter 5 : Integration of OPD Detector in Lateral Flow Immunoassays

1. Introduction

In this chapter, the LFIA was integrated with organic optoelectronics devices on plastic as the detector component as a step toward a fully integrated lab-on-chip device. Organic devices are suited for this purpose as they can be formed on many types of substrates and can have relatively larger active area¹¹. For light emitting component, phosphorescent green emitting organic light emitting diodes (OLED) have been used owing to its high brightness while for the light detector, an organic photodiode (OPD) that absorbs at green wavelengths has been used. The quantitative measurements have utilized optical transmission mode through an LFIA strip with red colored lines formed by the accumulation of gold nanoparticles (AuNP). In such configuration, the amount of transmitted light decreases as the number of Au NPs accumulate on the test line, which directly correlates with the analyte concentration. This change in optical intensity results in as a change in the OPD photocurrent. We have successfully created such a prototype and have done a quantitative measurement of the analyte.

Point of Care (POC) systems have multiple applications in the field of medical diagnostics¹. Lab-on-chip designs are integral components in such systems as they provide portability by miniaturizing laboratory scale equipment. The major goals of lab-on-chip systems is the integration and miniaturization of various components such as sample preparation, sensors and detectors in order to reduce sample size and measurement time³. Rapid paper-based microfluidic

devices, such as lateral flow immunoassays (LFIA), have many such desirable characteristics: (a) capillary action for fluid transport in contrast to PDMS-based microfluidics, which requires external pumps for operation; (b) Use of paper based membranes, such as nitrocellulose, which are bio sustainable⁵⁻⁸. They are also roll-to-roll process compatible, due to the simplicity of construction, and hence the cost of manufacturing is low. LFIAs work on the principle of immunoreaction, capturing Au NP tagged antibodies in the test and control line regions of the membrane. Such capture leads to appearance of red colored lines, which are visually interpreted. The presence of analyte in the fluid sample is indicated by the appearance of both test and control lines⁷⁹. The absence of analyte results in the presence of control line only. Although such type of analysis is simplistic in nature and may be useful for certain analytes such as hCG hormones for pregnancy testing, other diagnostic tests prefer quantitative analysis. Further, the visual interpretation of the lines can also be very subjective in nature and altered by psychological misinterpretation. This problem may be solved by incorporating fluorescence-based nanoparticles, which can give a much brighter visual signal. We have previously reported the integration of OLED as light sources to excite these fluorophores leading to increased sensitivity LFIA devices^{67,80}. However, these devices still do not provide quantitative information.

To offset some of these disadvantages, efforts have been undertaken⁷⁹ to integrate optical detection with the LFIA to make it a quantitative test as well as to remove subjective perceptions. This design uses a light source in the form of a miniature LED and photodiode chips as light detectors. When NPs accumulate at the test or control line, they absorb some of the light and thereby reducing the light intensity incident on the photodiode and hence the photocurrent. The change in photocurrent is processed using analog microelectronic circuits which typically drive

an LCD unit to display a quantitative result. Such optical readers can be stand-alone, into which the LFIA with the formed test lines are inserted and read. External readers provide sophisticated functionality and can be extremely sensitive, they are generally too expensive for POC use and are less portable as well (see Figure 5-1 below).



Figure 5-1 External LFIA reader: (a) Qiagen reader with a LCD display; (b) Reader with slot to insert an LFIA strip.

Fully integrated packaged small devices are also commercially available with far less functionality (Figure 5-2a,c). However, they are predominantly semi-quantitative in nature. They do alleviate the problem of subjective interpretation by providing the results in a digital display. The optical detection scheme in such systems use discrete component inorganic optoelectronics devices, such as surface mounted LEDs and PDs. Such an approach poses a major alignment problem with the test line (Figure 5-2b).

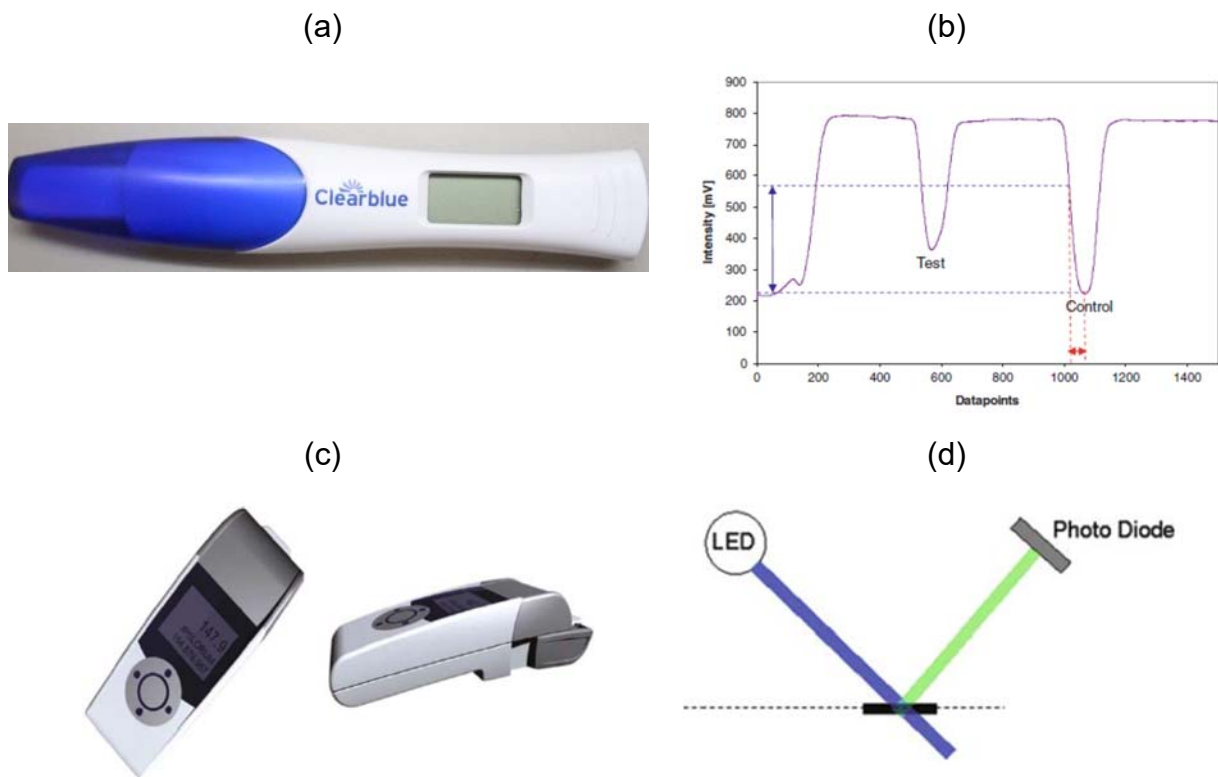


Figure 5-2 Portable POC devices and readers⁵¹: (a) Clearblue packaged LFIA digital device; (b) Alignment error intensity loss; (c) Handheld reader for LFIA strips; (d) Basic underlying reflection mechanism in all the devices.

Also, the detection is usually based on optical reflection, as depicted in Figure 5-2d, which means that the LEDs and PDs are co-planar and hence wave guides are needed to direct light to minimize light intensity loss. Such constraints make the device bulky, less reproducible and prone to errors. Such devices are fairly expensive and not environmentally friendly, as the whole bulky plastic package is disposed after each use.

In this chapter, we describe the use of organic optoelectronics as light sources and detectors for integrating with the LFIA. OLEDs and OPDs use thin films of organic layers to emit and detect light. The advantages of such an approach are several folds and several groups have used them over the years. OLEDs and OPDs can be fabricated on planar substrates such as thin plastics and

integrated as layers directly with the LFIA membranes. Such an integration using optical transmission mode of analysis is illustrated in Figure 5-3.

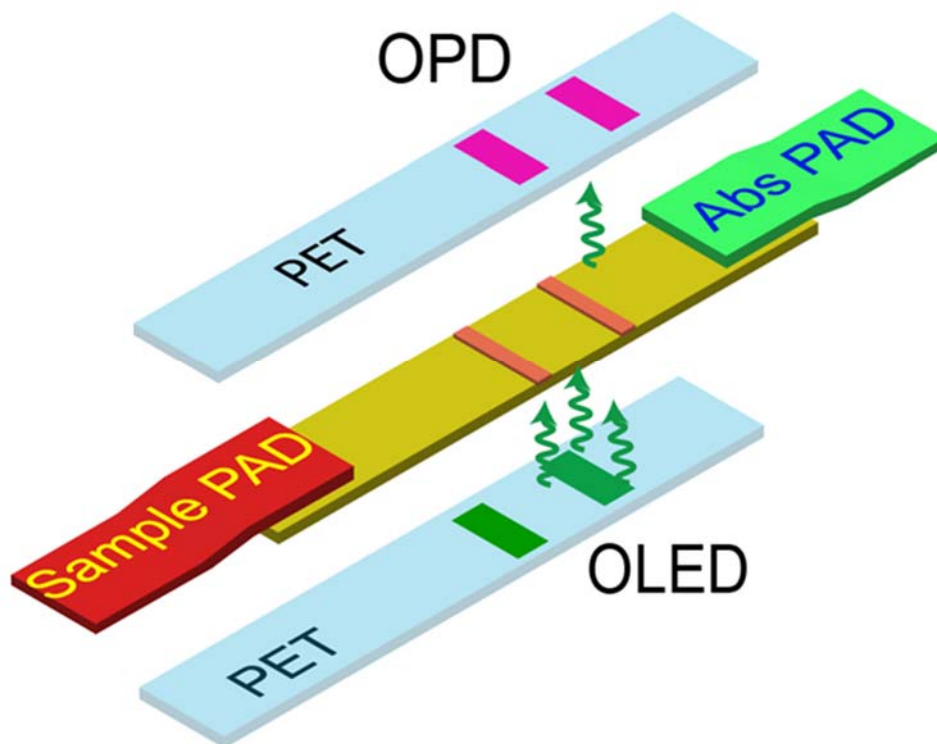


Figure 5-3 Schematic of organic optoelectronics and LFIA integration approach

In this design, the optical alignment between light source, LFIA test line and photodetector is simpler and more accurate than in reflection mode designs. The ability to fabricate the organic electronics on thin plastic substrates facilitates this integration in which majority light transmission through the membrane is detected by the OPD. Such an arrangement has been proposed by Whitesides et al for colorimetric readers²⁵. The light source and detector are in close proximity in such a configuration and hence maximum signal generation/ detection efficiency can be achieved, while the bulk of the overall package can be significantly reduced. The OLED and the OPD can be patterned to match the dimensions of the test lines, which is much more desirable

compared to the point source characteristics of the inorganic LEDs. The associated cost of such approach is significantly lower as the components can be roll-to-roll manufactured and integrated. Finally, the devices can be fabricated with ecofriendly materials and substrates making them environmentally friendly and disposable¹²⁻¹⁴.

In this project, we have chosen a commercial Au NP based LFIA that forms lines that look red in color. Two lines form in the presence of a biomolecule in the sample solution to be detected. The line darkens as the amount of analyte in the sample solution is increased and hence the amount of light (green) transmitted would decrease as the analyte concentration increases. In the following section, we describe the fabrication of these devices on glass as well as plastic substrates. We measure compare and contrast the various device characteristics following the fabrication of these devices. The devices on glass substrates perform superior compared to the one on plastic substrates. Hence, for the best case quantitative analysis, we fabricate the devices on glass and integrate with the LFIAs with already formed test lines. However, for integrating the devices within the LFIA, the devices will have to be fabricated on thin plastic substrates, explanations of which are in the integration section. Instead of using analytes of different concentration, we do its equivalent process by measuring the intensity over time instead. Finally, in the conclusions and future section, we describe how the signal can be analyzed using microelectronics and propose a prototype with promising results.

2. Device Fabrication & Characterization

OLEDs were fabricated with a multi-layer structure containing a phosphorescence emission layer and other layers for charge transport and blocking. This organic stack was chosen due to its high efficiency and brightness demonstrated by Forrest et al. group. In contrast for OPDs, a simple single layer stack was chosen.

Device fabrication on glass started by cleaning pre-patterned ITO-coated 30mm x 30mm substrates of 900um thickness. The patterned ITO stripes were 2mm wide and had a sheet resistance of 10 ohm/sq. This dimension fits well with the typical LFIA test line width (~ 1-1.5 mm). Solvent cleaning in an ultrasonic bath was performed followed by mechanical scrubbing using tech wipes. Next, substrates were then baked at 120 C to remove any residual solvents. The surface was then cleaned using exposure to an O₂ plasma (250W power) for 2 min. For devices on plastic (PET), ITO coated sheets (60 ohm/square) were purchased from Sigma Aldrich and patterned using photolithography. Details of this fabrication process is found elsewhere⁶⁷. The patterned ITO on plastic substrates, had 4 mm wide stripes, for reasons explained in later sections.

The deposition procedure of the organic layers and metal cathode is same for both glass and PET substrates. The layers were vacuum deposited in a high vacuum system (SVT associates) sequentially at operating pressures of $\sim 5 \times 10^{-7}$ Torr. The stack and thickness of the organic layers were ITO[90 nm]/ CuPC (40nm)/ NPB[17 nm]/CBP:Ir(ppy)₃(10 wt%)[30 nm]/BCP[12 nm]/Alq₃[25 nm]/LiF[<1 nm]/Al[40 nm]. The thickness and deposition parameters were characterized using an in situ quartz crystal monitor. The organic layers were deposited through a shadow mask with

a square opening to prevent deposition in unwanted areas, specifically, the contact pads. For OLEDs, the combined organic layers had a total thickness of ~ 100 nm. For the OPD, a single thick layer of CuPC (500nm) was deposited using a similar shadow mask as for the OLED. The cathode (LiF/Al) was then deposited through a second shadow mask to create contact stripes with 4mm width. The devices fabricated on glass had an active area of 2mm x 4 mm and 4 mm x 4mm for the devices on PET substrates. The Al cathode (top electrode) is reflective and hence the emitted light exists the ITO electrode and substrate. The OLED bottom emitting configuration needs to be taken into consideration when integrating with the LFIA. For OPDs, the transmitted light also enters through the substrate and is absorbed in the CuPC layer, generating photocurrent in the device. Figure 5-4 shows the devices fabricated on PET substrates and corresponding energy diagrams (devices on PET only shown). OLED devices were characterized under ambient room conditions for current – voltage (I-V) and brightness-voltage (L-V) characteristics. A luminance meter (Konica-Minolta CS-200) was used to measure the brightness while the applied voltage was swept at intervals of 0.25V from an Agilent DC power source controlled by LabVIEW software. The characteristics of devices on PET and glass are compared in Figure 5-5a,b (same dimensions of 2mm x 4mm). They exhibited high brightness as can be expected from such devices⁴⁰. The devices on PET did not perform quite as the devices on glass primarily owing to the high resistance of ITO on PET compared to that of glass. Hence, the devices on glass were used to determine the best-case scenario results when integrating with the LFIA. Lifetime performance is an important parameter for this particular application to produce reproducible results and organic devices, particularly OLEDs, are susceptible to environmental moisture conditions.

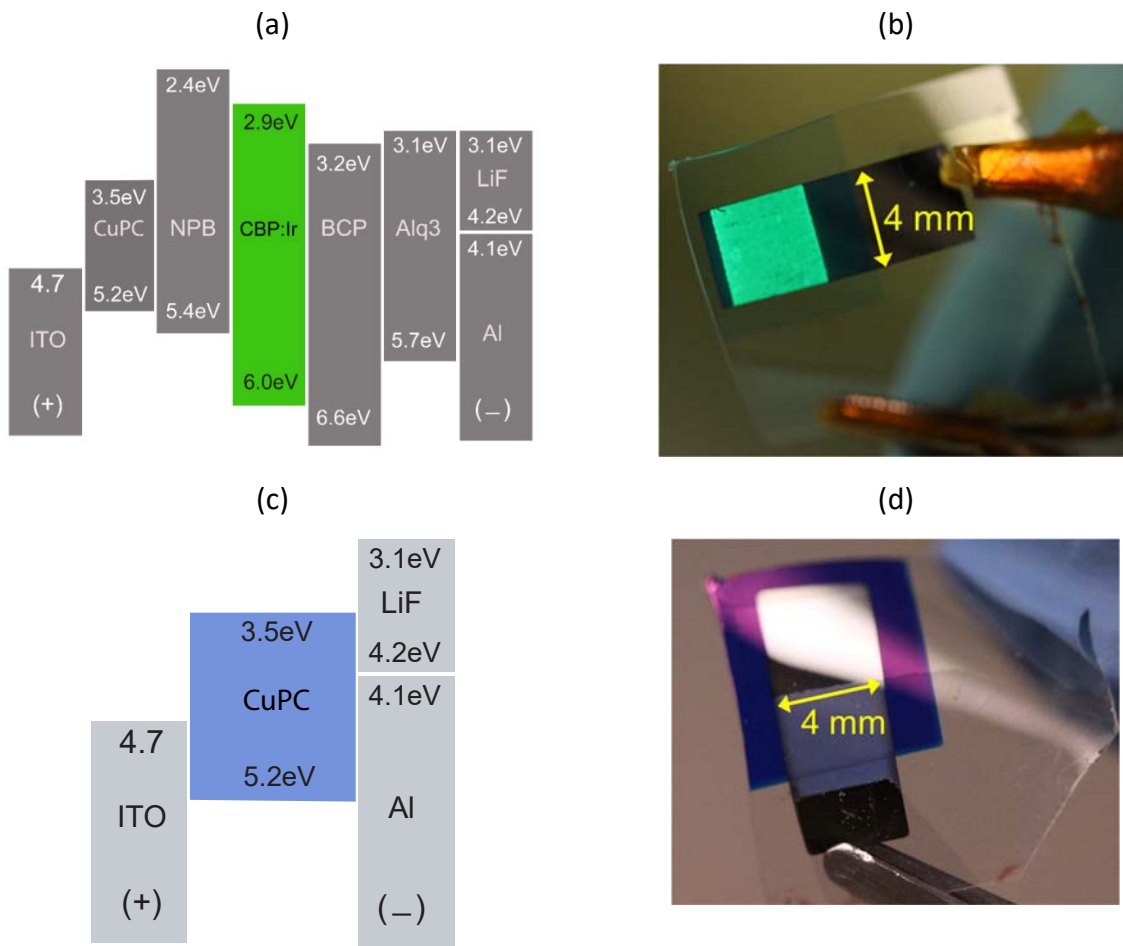


Figure 5-4 Organic devices details: (a,c) Energy band diagrams for devices used in this project; (b,d) OLED and OPD devices fabricated on PET.

To improve the OLED lifetime performance, we incorporated a CuPC (40nm) capping layer, which has been reported in the literature⁸¹. A comparison of lifetime of OLED, with and without CuPC layer is shown in Figure 5-5c. The addition resulted in a reduction in brightness by ~10%. However, this is outweighed by the significant improvement in lifetime.

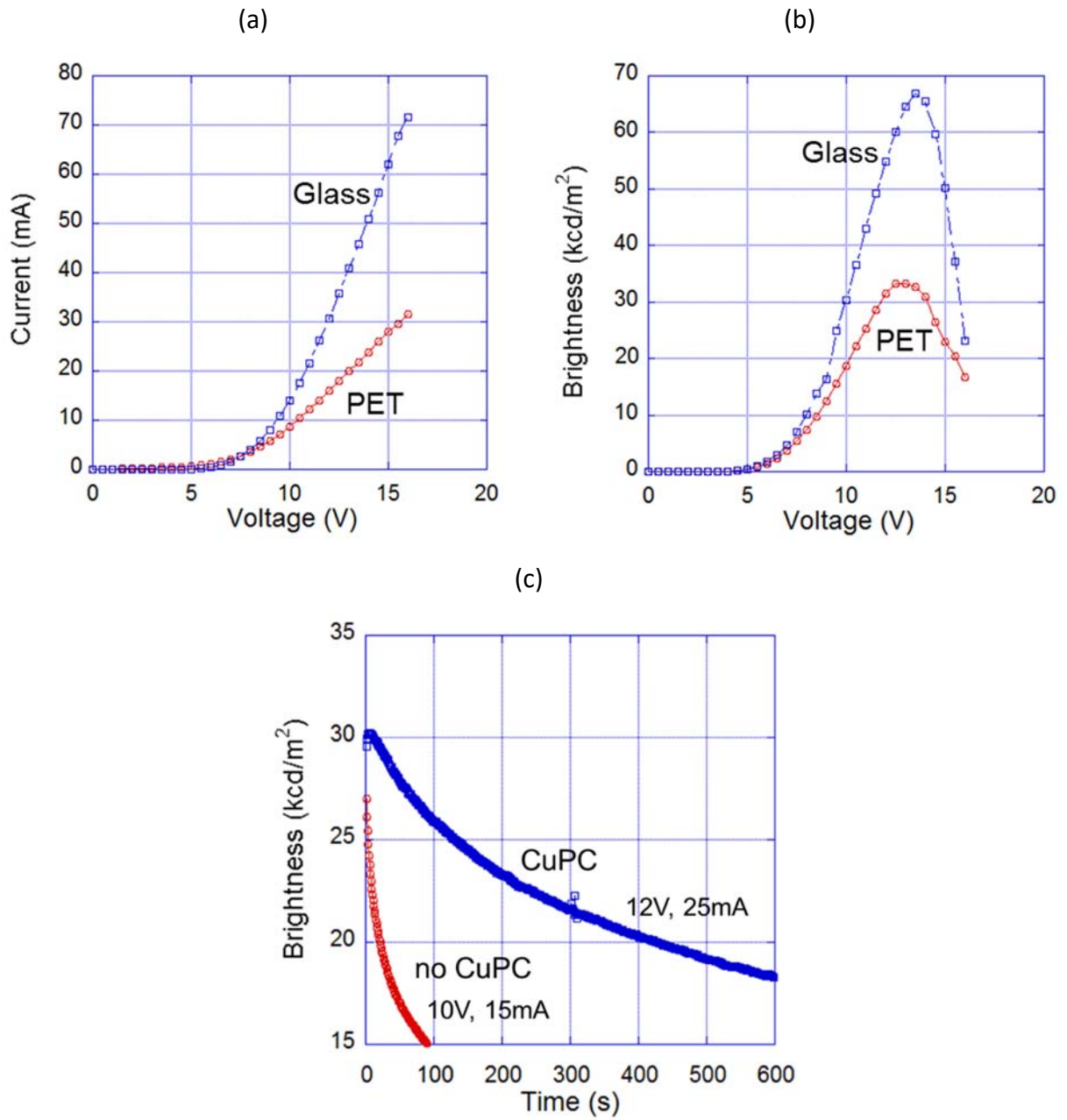


Figure 5-5 OLED characteristics: (a) Current vs. Voltage; (b) Brightness vs. Voltage; (c) Lifetime testing measuring Brightness over time.

For OPD characterization, the I-V was measured with a HP picoammeter using a probe station with voltage steps of 0.1V. The absorption spectra of the active layer (deposited on quartz substrates) were measured using Perkin Elmer system, see Figure 5-6a. The layer absorbs significantly in the green region which can be expected based on the color of the layer.

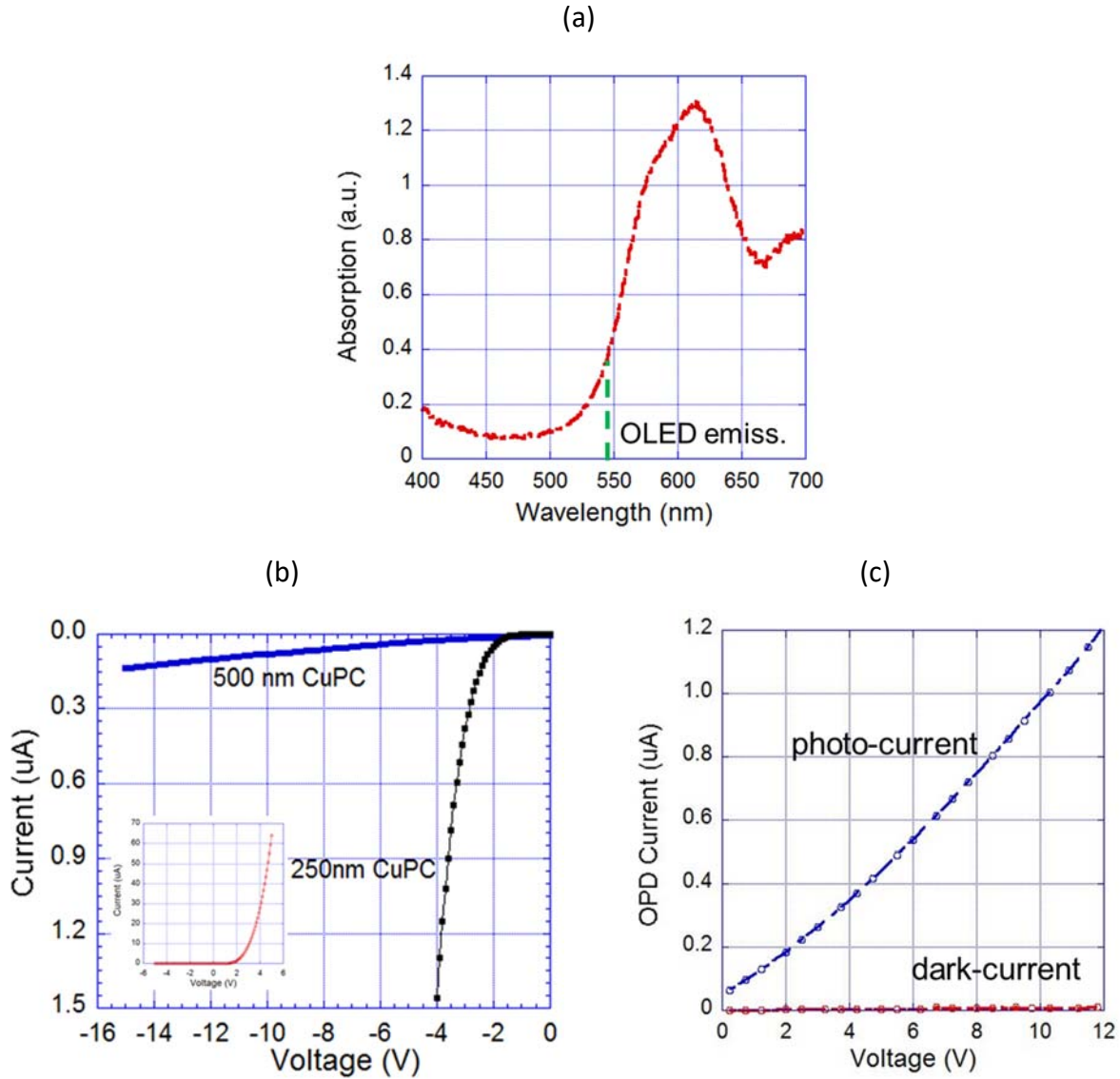


Figure 5-6 OPD characteristics: (a) Absorption spectra of the active layer; (b) Reverse bias dark current characteristics and breakdown; (c) Photo-current response of the OPD in reverse bias excited with a green laser source.

The I-V characteristics of OPD with CuPC layers of 250 and 500 nm are shown in Figure 5-6b. Not unexpectedly, the OPD with the thicker layer had a lower dark current and a higher breakdown voltage was much higher and hence we chose 500nm as the device thickness. Green laser (power specs) was used to measure the responsivity and we were able to obtain a responsivity of 1.2 mA/W Figure 5-6c. The device performance was similar for both glass and PET devices.

3. LFIA Diagnostics

We used rotavirus test kits manufactured by Meridian Bioscience Inc. (Cincinnati, OH). The antigen, rotavirus, is detected using a sandwich immunoreaction at a specific location in the strip (test line) which contains antibodies impregnated in the nitrocellulose membrane that bind to an epitope of the rotavirus protein. Conjugate pad of the assay strip contains gold nanoparticle (Au NPs) conjugated antibodies that attached to a different epitope of the virus protein. The sample solution is transported through capillary wicking through the assay kit. In the presence of the virus an antibody sandwich with the antigen is formed, which leads to the accumulation of the Au NPs in the narrow region of the test line. This results in a dark red line, whose intensity is roughly proportional to the amount of conjugated antibodies captured, which in turn depends on the concentration of the rotavirus protein in the sample solution. To validate a successful test, these devices contain a second stripe (the “control” line), which contains immobilized secondary antibodies that can bind to the flowing conjugated antibodies. This process occurs even in the absence of the analyte protein. Absence of this line invalidates the assay results (irrespective of formation of test lines). Ultimately, it is important to detect both lines with optoelectronic circuits, however, in this manuscript only one line is detected at a time. This is done to reduce complexity for a proof-of-concept device, with visual verification of the performance of LFIA as intended. Such an assumption is still very reasonable as currently LFIAs have a large commercial market and reproducible sensitivities close to 100%. In a LFIA, these lines are visually interpreted, where, more than one line, must include the control line, mean positive result (presence of the analyte). An example of a positive test result is shown in the photograph of Figure 5-7(a), i.e, two

lines. The optoelectronic detection of these lines uses light scattering by the Au NPs. The use of light transmission through the assay membrane has been used to enable vertical integration with optoelectronic components as illustrated previously in Figure 5-3. The amount of light scattering increases with the number of captured Au NPs, which is related to an increasing analyte concentration. This, in turn, reduces the transmitted light intensity. To validate this approach, a commercial LED package was utilized to illuminate test line with various analyte concentrations. As observed in the photos of Figure 5-7b, increasing the analyte concentration decreases the amount of green light passing through the test line, resulting in darker looking lines. This effect was quantified by measuring the transmitted light intensity (brightness) as a function of LED bias voltage, as shown in Figure 5-7c. Another important observation that can be inferred from the brightness graph is that as the voltage to LED is increased, brighter LED, the sensitivity also increases (more difference between the three cases).

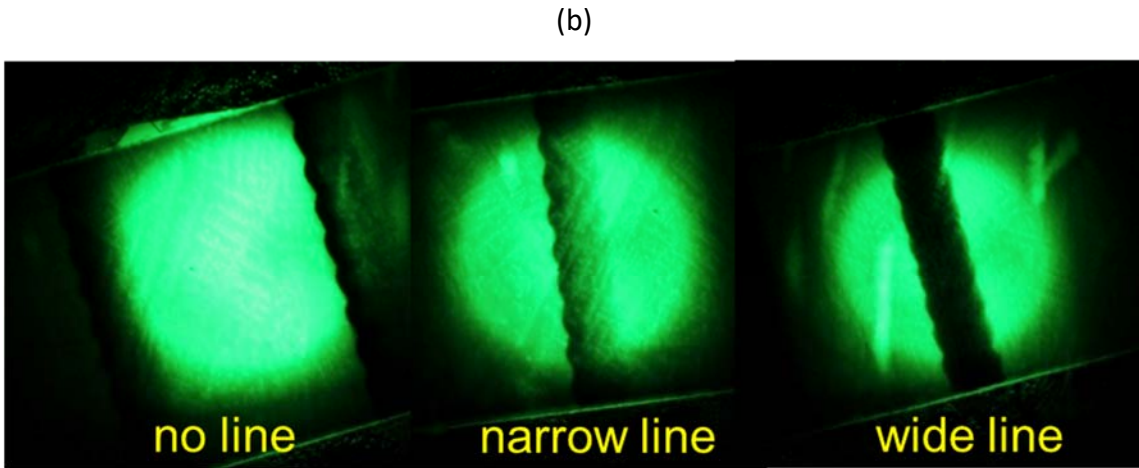
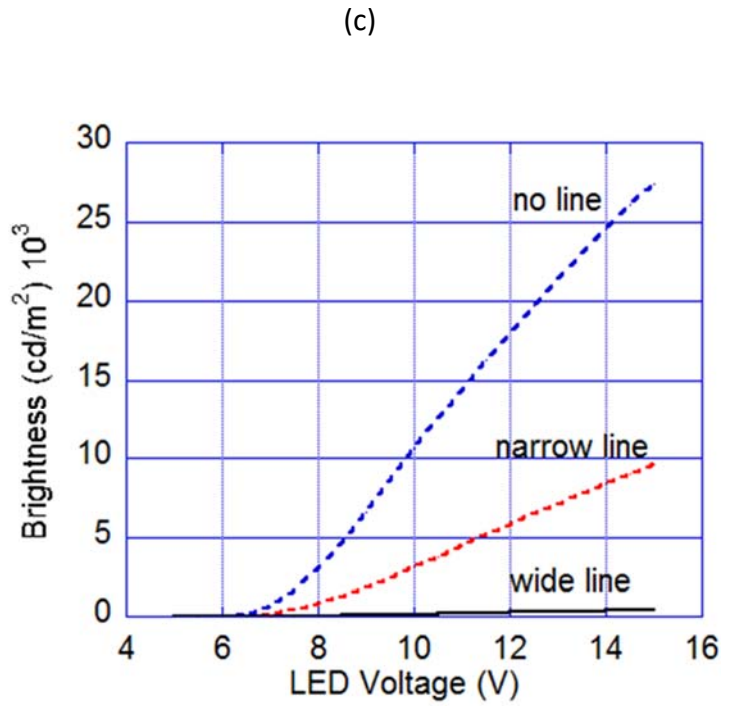


Figure 5-7 LFIA details: (a) Test and control lines formation in an LFIA; (b) Different densities of test line illuminated under green light; (c) Measured brightness of light transmitted through different densities of LFIA lines.

4. Integration

The initial integration of the organic optoelectronics and LFIA used OLEDs and OPDs fabricated on glass substrates due to their superior performance. The device dimensions used were 2 x 4 mm². Assays were first run in original LFIA cassettes with various rotavirus concentrations in the analyte solution so as to obtain lines of varying density. The LFIAs were run for 30 min. Then the active membrane with the formed test line with various concentration (Figure 5-8a) was removed from the cassette and sandwiched between devices fabricated on glass. Alignment of the test line to the OLED and OPD was done under an optical microscope. Alignment errors are compensated by having device width (2 mm) larger than the typical test line width (1.2-1.5 mm). OLEDs were biased to obtain maximum brightness to improve sensitivity (evident from figure before).

Figure 5-8b shows the plot of OPD currents measured as the voltage to the OLED was swept from 0 to 15V for different analyte concentrations. The devices were biased well beyond the peak emission intensity, bell curve, to get best sensitivity results. These curves are characteristics of OLED devices which when biased over the peak intensity voltage starts to degrade, brightness decrease, due to intense current levels. The trends of the results were as expected. First, the peak OPD photocurrent decreases as the analyte concentration increases owing to less transmitted light passing through the sample. Secondly, the maximum difference between the concentrations, i.e sensitivity, happens at the maximum brightness peak. The area under the curves were then calculated and plotted against the concentrations. A linear trend with good correlation was observed as can be seen in Figure 5-8c. Results were fairly reproducible with

repeated iterations (n) greater than or equal to 3. The level of current difference between the no analyte case and 100 % analyte was ~ 200 nA. Such current differences can generally be detected with several microelectronic sensing circuits.

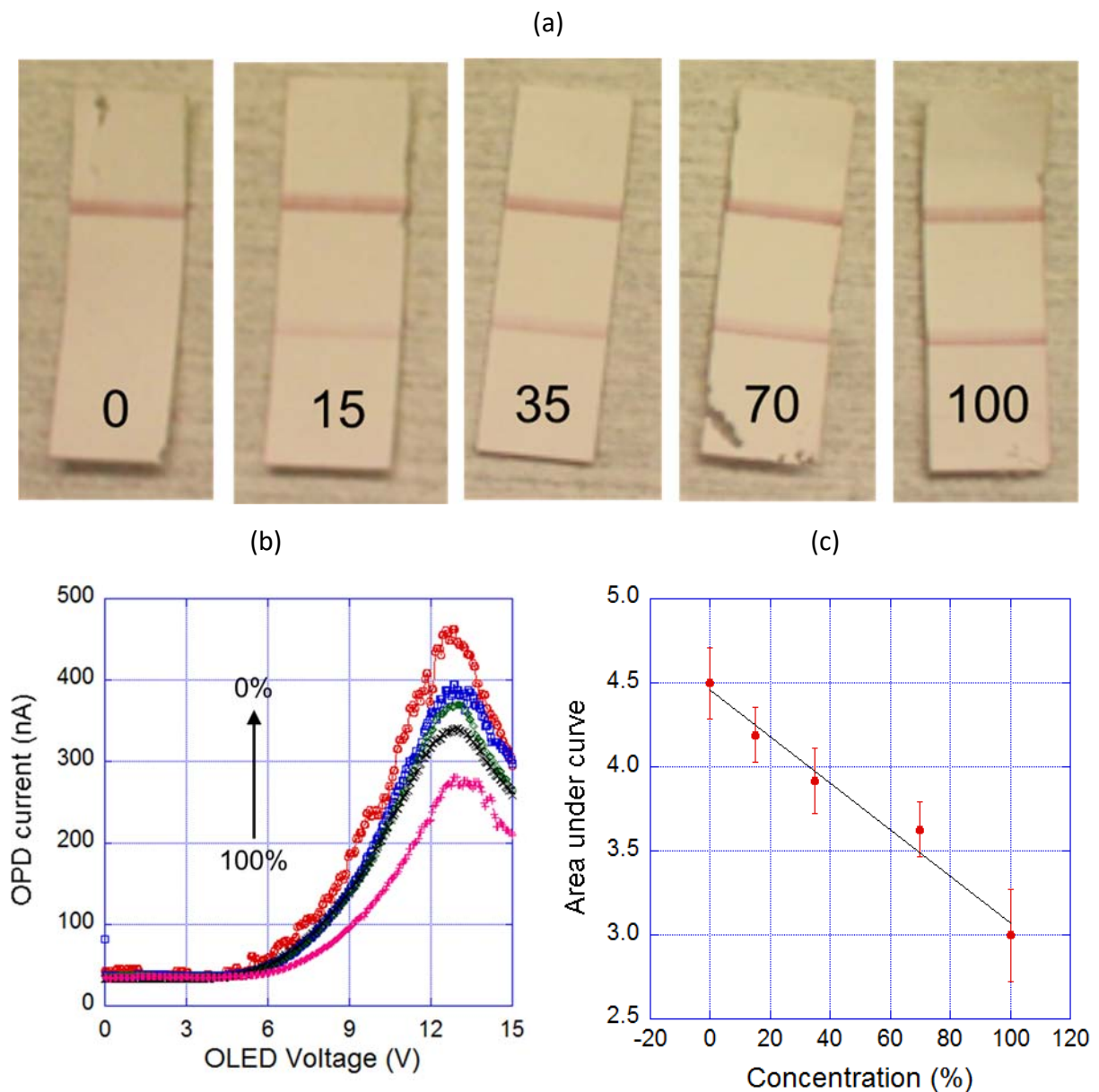


Figure 5-8 Quantitative LFIA measurements: (a) LFIA strip with test lines of various concentration of analyte (in %); (b) Measured OPD photocurrent for various concentration of analyte; (c) Intensity of photocurrent (area under curve) plotted for various concentrations of analyte.

After performance analysis experiments with devices fabricated on glass, the integration into the LFIA packaging was done. This can be possible only with devices fabricated on thin plastics which can be then be sandwiched within the cassette. This integration began first by disassembling the various components from the LFIA such as the sample pad, NC membrane and conjugating pad from the backing card. The position of the to-be formed test lines were marked on the outer plastic packaging based on which the OLED and OPD were then aligned later. This was necessary, as, in contrast to the experiments performed with devices on glass, the test line has not yet formed for alignment visually. Further, the exact position of the line may vary considerably with respect to the markings on the packaging which indicate only an approximate location of the lines. Due to these errors, the device size for these experiments were chosen to be 4mm x 4mm. This width is substantially larger than the typical test line width of 1.5 mm and the hence the alignment is easier. However, this also causes a large light leakage which may cause results in increased background signal.

The integration process begins by first attaching the OLED (device side) onto an adhesive backing. Each PET with the devices measured $15 \times 15 \text{ mm}^2$. Copper tapes were attached to the OLED devices to make contact after the integration process. The NC membrane was then placed on top the PET containing the OLED with the control line aligning to the middle of device area. The sample and the conjugate pads were then attached to the ends of the NC membrane. Finally, the PET containing OPD (same dimensions as the OLED) was attached to the top of the NC membrane, using double sided adhesive tapes. Experiments were conducted to see the effect of the adhesive tape on the membrane and no significant changes were observed in the fluid flow as well as in the line formation. Finally, the top plastic casing of the LFIA cassette was attached to impart

pressure on the sample pad and to hold the sample area. The steps of the integration and photograph of the integrated package is illustrated in Figure 5-9.

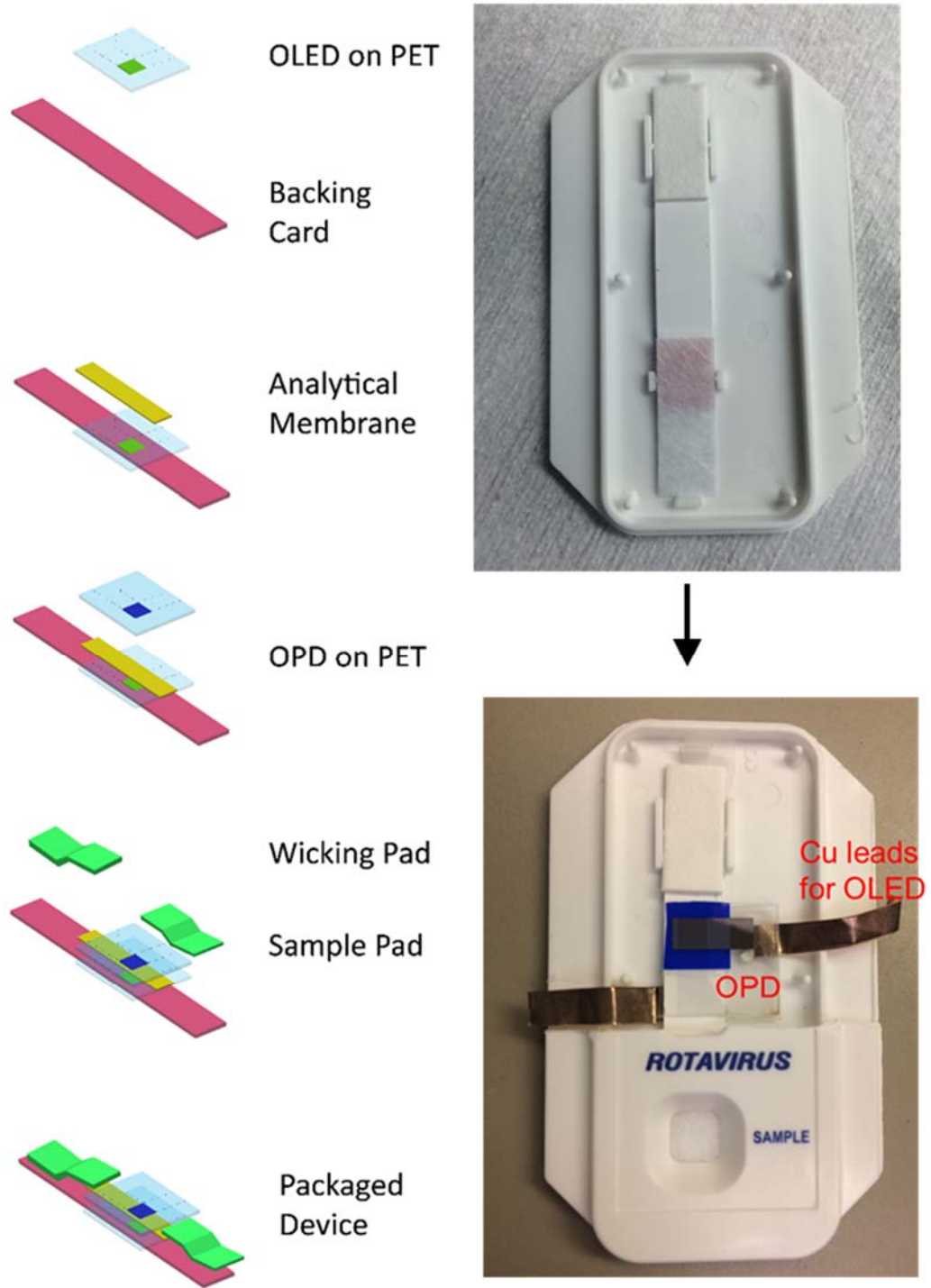


Figure 5-9 Integration of organic devices with LFI strip inside the cassette.

The device was then tested in a dark ambient environment optical room. A probe station equipped with a microscope was used to measure the photo and dark-currents of the OPD, with the OLED powered using a LabVIEW controlled DC power source. The test was initiated by adding a “negative” sample solution (150 μ L) which leads to formation of only the control line. As the line became denser over time, the OLED was pulsed every 0.1 seconds and the corresponding OPD photo-current was measured. Both the OLED and OPD devices were biased at a voltage of 10 V. As the line formed over time the OPD photo-current decreased due to decreased light transmission as is evident in Figure 5-10a. For baseline experiments, the devices were integrated and photo-current measured in an area where no line would form. In this case there should be no decrease in light intensity transmitted, and, hence the photo-current. However, some minor decrease was observed, attributed to either drying effects of the LFIA and/or organic device performance degradation over time. The successful results confirmed the concepts and shows the potential of such integration. The relative intensity was plotted by subtracting the “no test” line data from the test line data and plotted over time Figure 5-10b. To correlate this to the visual formation of the line, gray scale contrast of the line formation (photographed) over time was measured and plotted in Figure 5-10c. The measured OPD current correlates well with the visual signal curve. One minor difference is that the OPD current seems to saturate more strongly after ~1000s. This could be also be due to variation in drying effects and/or the device performance degradation over time.

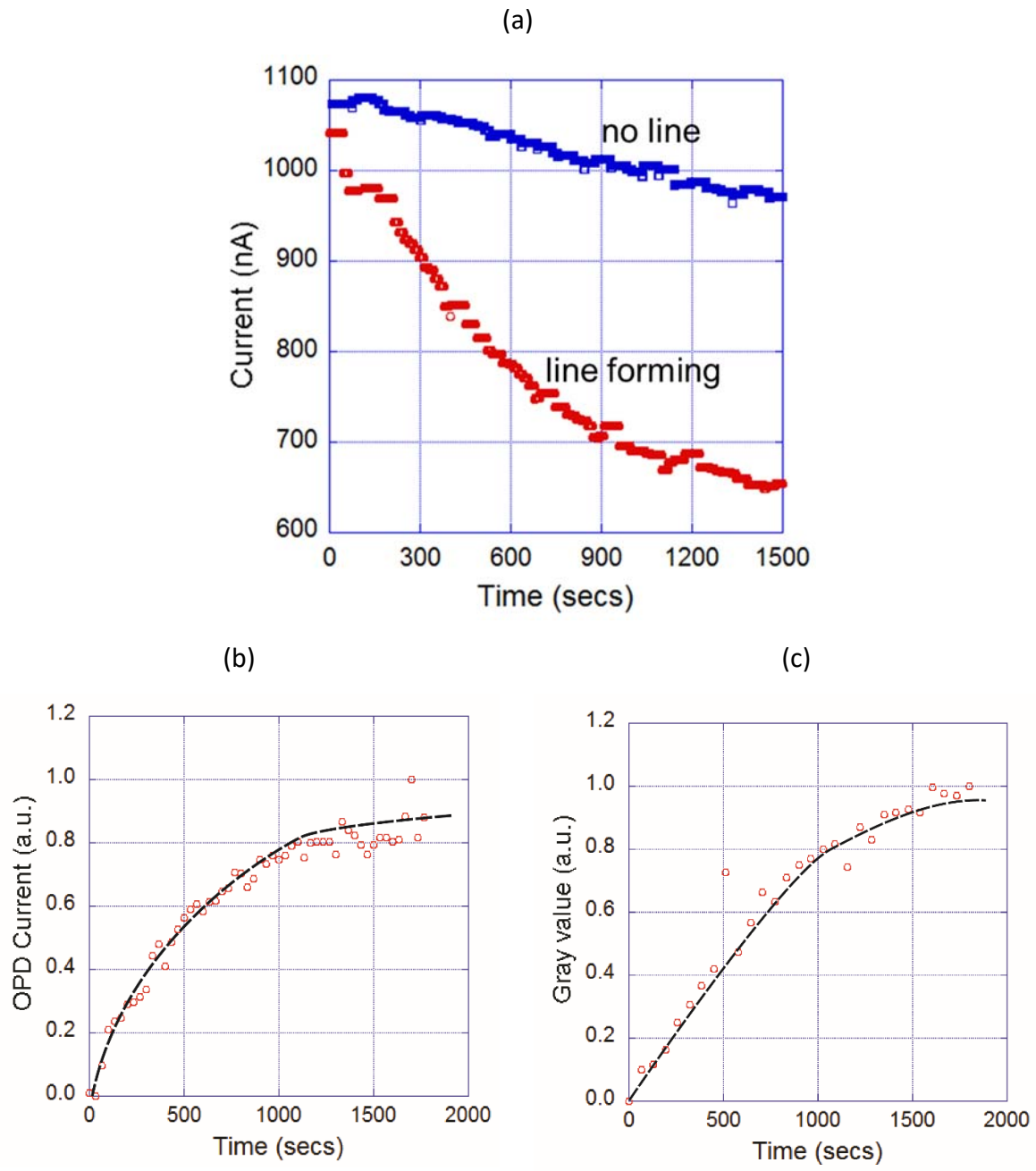


Figure 5-10 Integrated device results; (a) Measure OPD photocurrent as the line in the LFIA forms over time; (b) Relative OPD photocurrent plotted over time; (c) Gray value measure as a line forms over time (visual contrast).

5. Conclusions

In summary, a prototype of organic optoelectronics integrated with LFIA for quantitative detection has been demonstrated. This integration was possible by fabricating the devices on thin plastic and sandwiching within the LFIA packaging. The integration was designed to enable operation in optical in transmission mode, such that the intensity of transmitted light decreases with increasing analyte concentration, resulting in decreasing OPD photo-current.

In addition to the optical source and detector being integrated, there are other necessary components such as microelectronic circuits, power sources etc. which are currently external and should be investigated for integration in the future. With fabrication techniques, such as hybrid assembly, and the ever-decreasing size of IC chips, they can also be fabricated on plastics. For the power source, we have previously integrated a hybrid manufactured NFC antenna circuit that harvests RF power from smartphones. Flat/flexible batteries are also an important option for providing electrical power in a package form factor that can be readily integrated.

Chapter 6 : Conclusions and Future Work

1. Concluding Remark

In this project, focus was on research to create a sensitive, quantitative, cheap & disposable lab on chip (LOC) system. Such a system has been realized by integrating organic optoelectronics as reader and RF harvesting as power sources with paper based microfluidic systems. Paper based microfluidic systems by itself have several desirable characteristics such as an integrated capillary pump, natural filtration, at the same time being cost effective and disposable. Lateral flow immunoassays (LFIAs) are widely applied paper microfluidic systems and hence was chosen as the research vehicle for this work. Organic light emitting diodes and photo-diodes (OLEDs & OPDs) have been integrated as optics in LOC systems by several research groups and hence its integration with LFIAs will create a device for point of care applications with several attractive features of a LOC device.

This research of integrating active components with LFIAs was pursued through three specific goals. The first goal was to integrate just a light source, OLED, with fluorescent based LFIAs. OLEDs fabricated on plastic was integrated with Quantum dot based LFIA with plastic light filters to achieve better visual sensitivity and limit of detection in comparison to calorimetric based LFIA system. A 7× lower LOD (limit of detection) in comparison to gold based LFIA was achieved. This POC system can hence achieve sensitivities in the range of 10-100 pM for well optimized LFIA systems⁸².

Following this integration, focus was then given to power source integration, goal 2, in which power was extracted from the NFC signals of a smartphone (RF). Antennas fabricated on plastic using hybrid manufacturing powered green LEDs from the NFC signals of a smartphone. This setup can then be used as a light source for fluorescent based LFIAs, a continuation of goal 1. We collaborated with VTT Inc. at Finland who specializes at hybrid manufacturing for this project. It was integrated with the LFIA with similar setup as in Goal 1 and achieved a 10 × improvement in signal intensity.

Finally, in goal 3, focus was given on detector integration which would make the system more quantitative as well as digitized. Organic photodiodes (OPDs) fabricated on plastic substrates was a desirable candidate. OPD as detector and OLED as light source all fabricated on plastic substrates integrated with LFIA was pursued. Colorimetric based LFIA was on focus here, unlike the first two goals, due to their well-established industry as well as well optimized LFIAs out of shelf. We were successfully able to quantify five levels of the analyte and integrated devices fabricated on glass into the LFIA packaging. Though integration of all the components is beyond the scope of this thesis, individual integration or partial combination still can provide valuable stepping stones for any future work in this area. Such a fully integrated device would have desirable features and performance as can be seen in Figure 6-1.

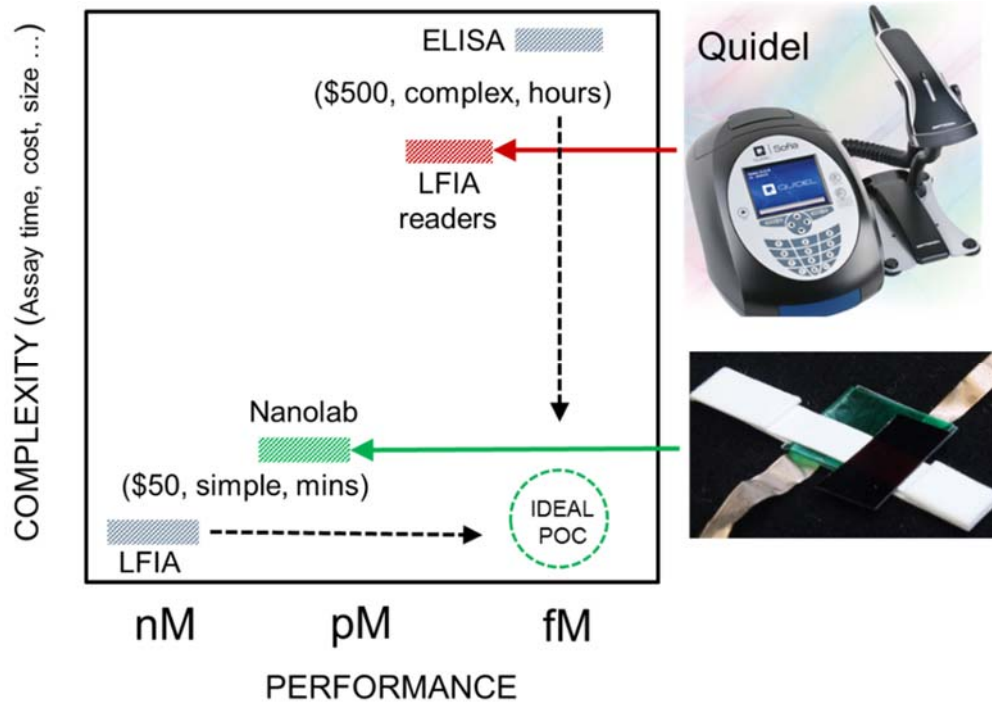


Figure 6-1 Attractive feature of POC designed at Nanolab.

2. Future Work

2.1 Flat Battery Power Source

An attractive alternative to NFC power source are flat batteries (Figure 6-2a). This is because, unlike conventional batteries, including button cells, these batteries can be extremely thin (few hundreds of microns), Figure 6-2b. The NFC power source has currently the limitation of not well standardized and hence fabricating antennas with precise specifications is an issue. Due to this we experienced several problems such as blinking of LEDs due to bad syncing. This may be possibly solved in the future by using software prompts in the smartphone. Using flat battery instead also simplifies the circuitry requirement since the NFC power source, on top of coils,

require IC chips to communicate with smartphone. The coils can also take up more real estate area as the power requirement grows.

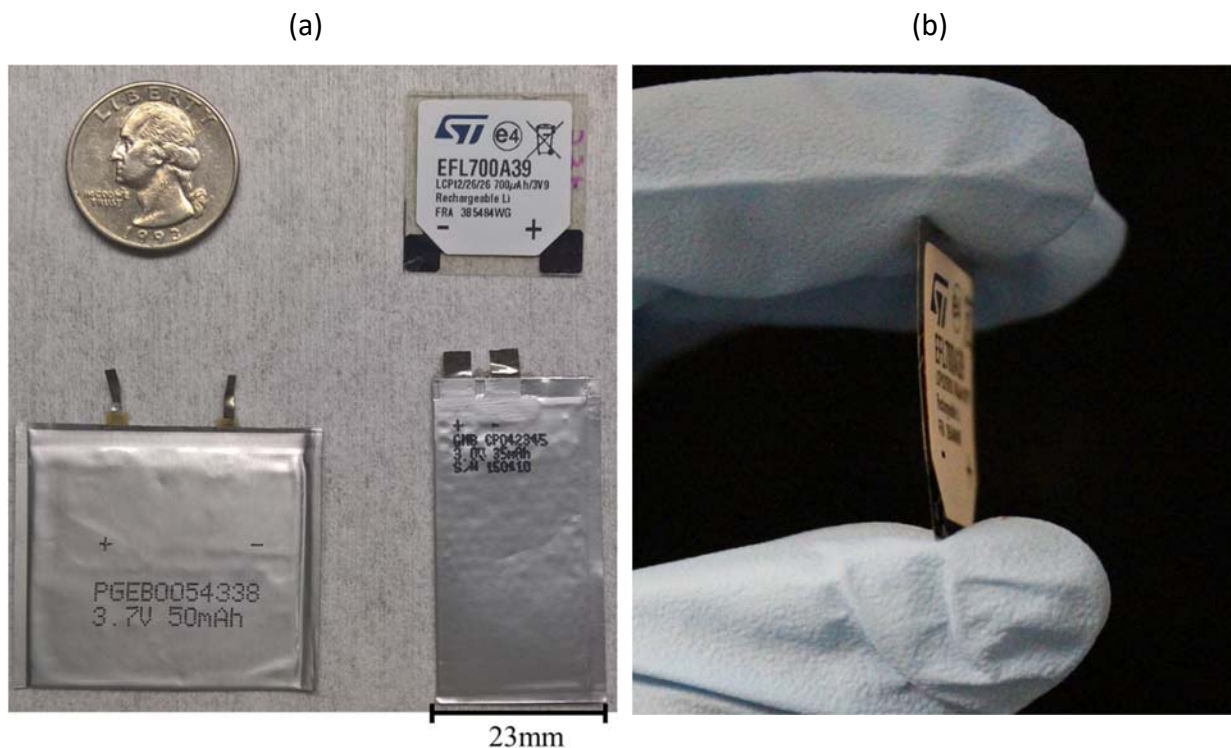


Figure 6-2 Flat battery options (Credit: Eric Frantz): (a) Few options of batteries available in the market; (b) Side view of extremely thin STMicron battery.

However, using NFC as a data transfer option can still be a good choice as such a data transfer has been well established and a combination with flat battery as power source is a viable design. Further, flat batteries can also be made eco-friendly and biodegradable, and as a planar component, it also integrates well with the rest of the components in the LFIA system. Such a design has been depicted in Figure 6-3.

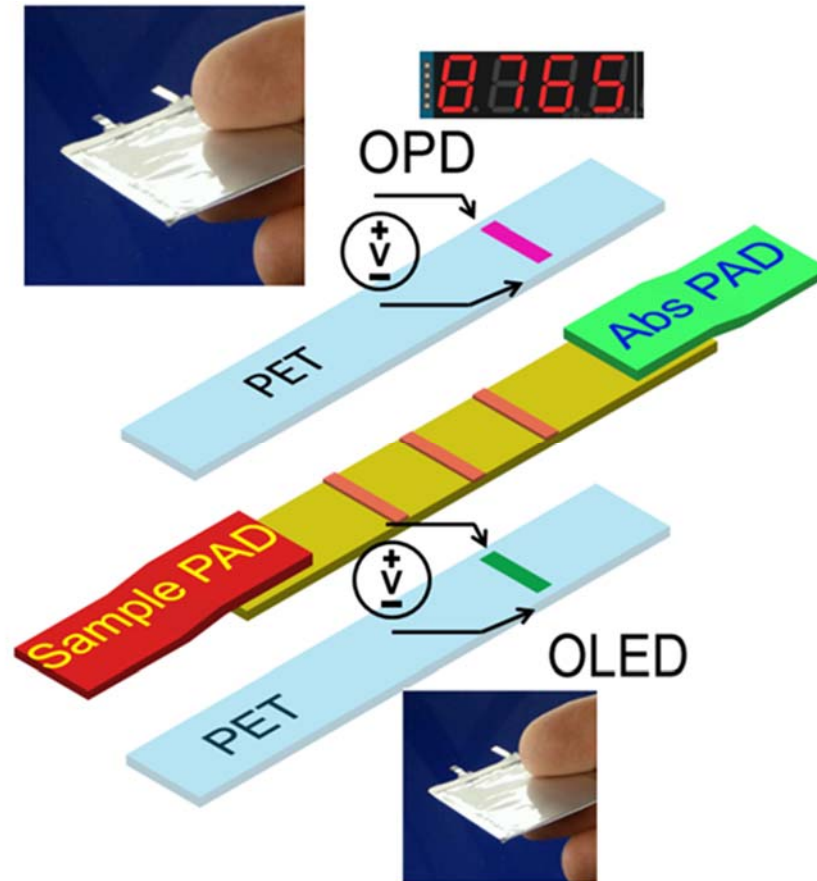


Figure 6-3 Flat battery integration concept

Further, due to the thin nature of such batteries, they can also be stacked one over the other without much compromise on the total dimensions to improve the power output. This is not possible with a conventional button battery as stacking them would alter severely the device dimensions by increase the footprint. Making contacts with thin battery (due to planar contacts) is easier as well and can be achieved with copper tapes to create interconnects in the circuit. Table below shows some of the characteristics of these batteries. As can be seen from the voltage and power specs, a single battery cannot be sufficient for applications described in Goals 1 and 3. The organic devices were powered 10V and requires at least 30mA of current. Hence

stacking of multiple thin battery is a requirement and choosing the thinnest might be a viable choice than a high-power battery.

Brand	Volts (V) I_{peak} (mA)	Capacity	Size (min) (mm)	Price (\$)	Eco friendly
BrightVolt	3.0	10 - 48 mAh	25x29x0.45	NA	Yes
Enfucell	1.5 - 3.0 20	10 - 90 mAh	46x36x0.7	10 (bundled)	Yes
FlexEI	1.1 – 1.45 100mA	10 – 15 mAh/cm ²	NA	NA	Yes
Powerstream	3.7 200	10 mAh – 2 Ah	12x12.5x2	7.5 (min)	Li-Ion
BlueSpark	1.5 – 3.0 2	5 – 37 mAh	40x30x0.62	Asked	Yes (no HM)
STMicro.	3.9 5	0.7mAh	25x25x0.22	11	Li-Ion

Table 6-1 Details of some flat batteries available in the market (Credit: Eric Frantz).

As a first step, we powered the LFIA integrated with OLED and OPD fabricated on PET with the flat battery (STMicro) and measured the output current from the OPD (Chapter 5 experimental setup). Figure 6-4a below shows the setup with the thin batteries, they were used as an external component for preliminary testing. From the table in Figure 6-4b, it is clear that, the difference between the test and no test line case is not significant and hence this test result is not promising. This could have happened due to many factors. One major factor, we believe, is variability in the OPD device fabrication. With the devices powered using the flat battery, low powered, the tolerance for any such variation is low. Hence, organic devices fabrication parameters may need to be precisely monitored and standardized to create devices that have low variance in the

expected performance. In such cases, other factors as well such as drying effects and measurement procedures may also need be well controlled and standardized.

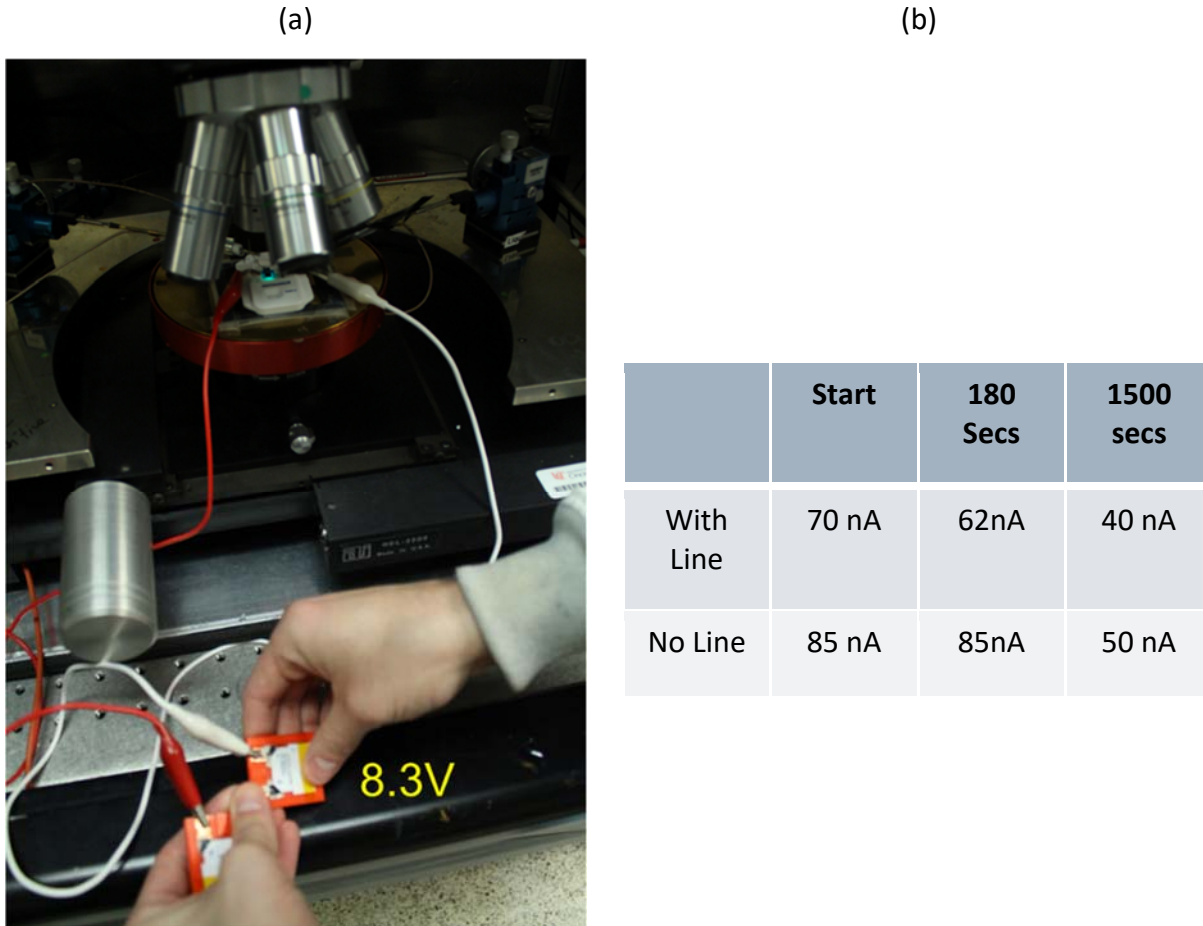


Figure 6-4 Preliminary experiment with flat battery powering integrated device; (a) Experimental setup showing series connection of flat battery; (b) OPD current response with and without test line case.

2.2 Hybrid Microelectronics Circuits

Electronic circuits are integral component of any system in the modern age of digital electronics and their applications in computation and day to day activities. Such circuits are also necessary in this project. With the semiconductor fabrication processing technologies putting efforts to decrease the size of transistors, it is now possible to reduce the footprint of Integrated Circuits (ICs) to perform any specific task.

In the NFC project hybrid manufacturing was used to attach bare die components including ICs on PET substrates. A microelectronic indicator circuit can be designed and fabricated on plastic substrates and integrated with the OPD to read the current output. The read current maybe displayed in the form of a simple yes/no using an indicator LED or made semi quantitative by using multiple LEDs. Below Figure 6-5 shows one such circuit and how it maybe be fabricated on a plastic using hybrid manufacturing (fabricated by VTT Finland).

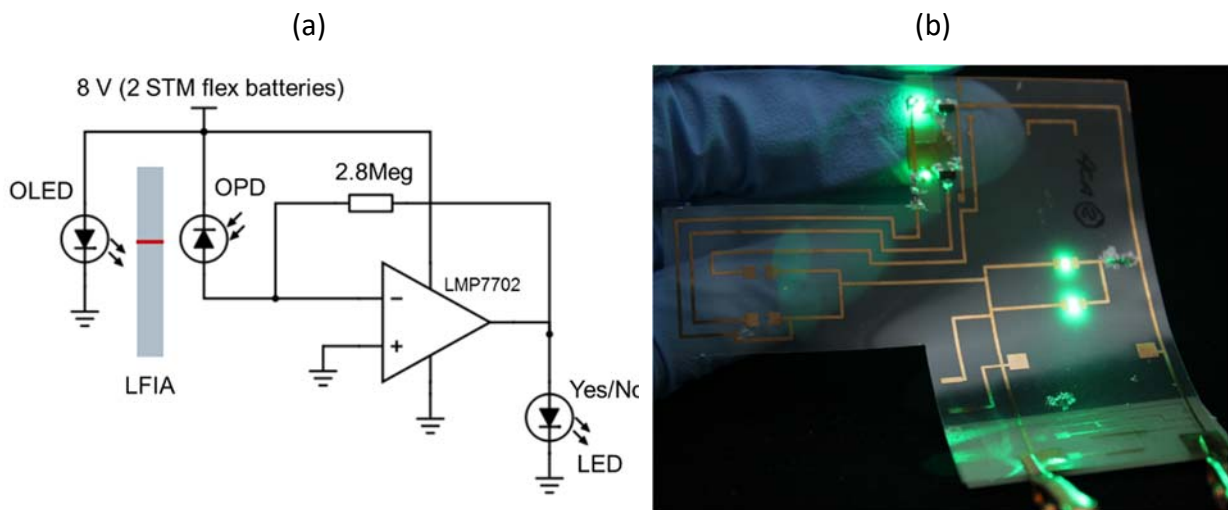
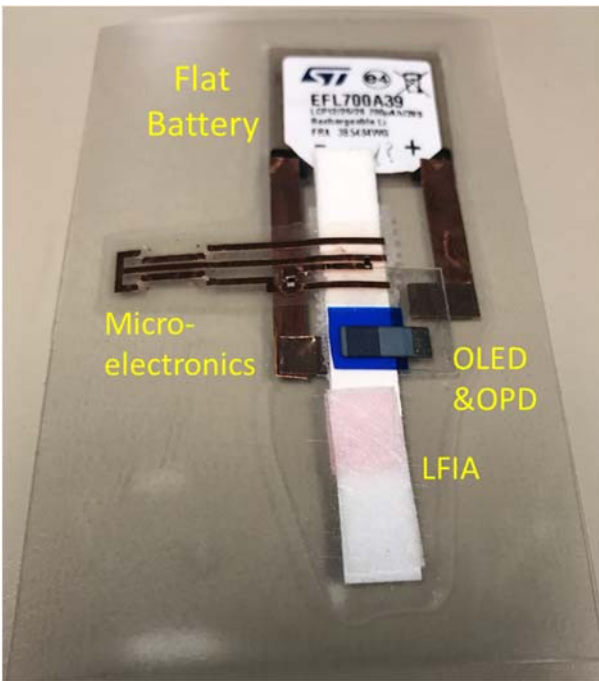


Figure 6-5 All component integrated concept: (a) Microelectronic reader circuit with indicator LED for qualitative readout; (b) A similar microelectronic circuit hybrid manufactured on plastic (Credit: Eric Frantz).

Such a fabricated microelectronic circuit can be integrated along with organic optoelectronics to create device with much smaller form factor at the same time be disposable, cheap and bio degradable. Such a design would compare with the current device in market as shown in the Figure 6-6 below. Though the attractive device in the above Figure 6-6 (a) is not very far from future, it still requires significant amount of work. At Nanolab, we are working in this direction with collaborations with VTT, Finland and CADMIM at Irvine

(a)



(b)

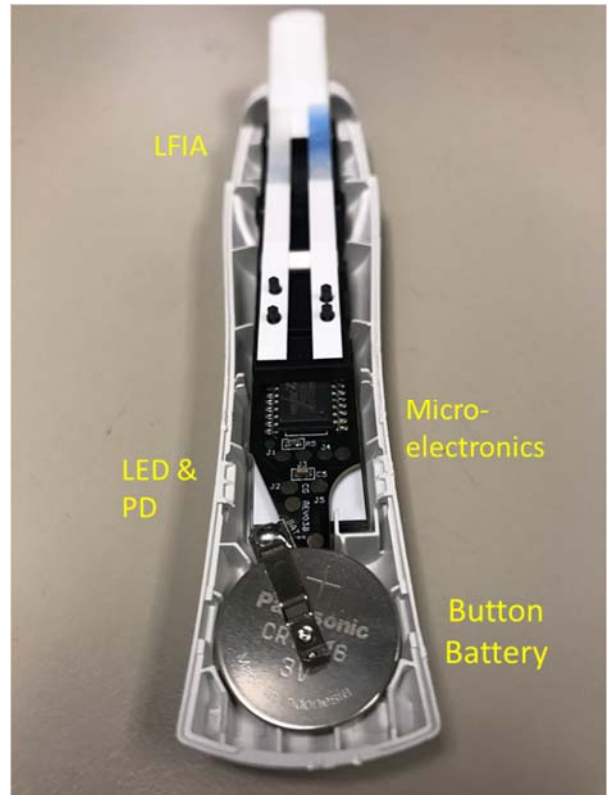


Figure 6-6 All integrated package concept: (a) Approach at Nanolab; (b) Commercially available device with same components.

Appendix A – Devices on NC Membrane

One other way this project could have proceeded is by fabricating the organic devices directly on the Nitro-Cellulose (NC) membrane of the LFIA. This would constitute as a true integration for a LOC diagnostic device. The NC membrane has a plastic backing sheet in which the OLED can be fabricated. One such device was fabricated on circular NC membrane and is shown in the Figure A-1 below. In this case, blue OLEDs were fabricated (initial approach). Shown also the blue OLED exciting drop casted QDs particles drop casted on the paper side of the NC membrane.

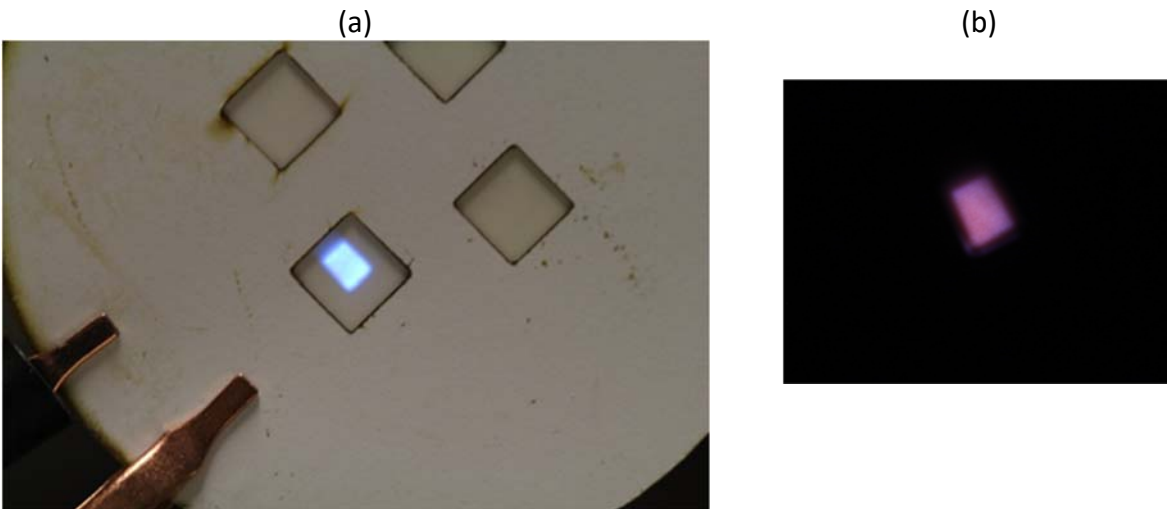


Figure A-1 Blue OLEDs fabricated directly on NC membrane: (a) Device photograph; (b) Blue OLED exciting QD dispensed on top of the membrane.

Though such an approach can be a viable option for a LOC device, it suffers from several practical issues. First, the NC membrane needs to be subject to vacuum processing step that can modify the fibers of the material and/or destroy the active bio-molecules impregnated on the test and control line. This may be circumvented by first fabricating the organic device followed by printing the test and control lines or solution processing (non-vacuum) the devices. This interconnection

of the device fabrication and LFIA fabrication can make processes complicated and not practical at the moment.

Secondly, the surface may not be optimum for fabricating these devices. Though the backing of the NC membrane may help fabricating the OLEDs, it can be impossible to make OPDs directly on the membrane side. A different substrate would be necessary in that case. Hence in this project, the two sides, LFIA and organic devices, were separated out by fabricating them individually. This procedure not only reduces the complexity of the procedure but also brings the best of the two together with little to no compromise. That being said, the above-mentioned pathway is theoretically viable and can be considered as a future step toward the project

Appendix B – Clearblue device teardown

1. Components inside the device:

One of the competing technologies for the idea proposed in this thesis, which is also commercially available, is the Clearblue pregnancy test strip. It comes in a relatively small packaging with the optics and the electronics integrated. It is very interesting that these devices are fairly cheap, retailing at \$6-\$10 per device. Below Figure B-1 shows the packaged device and the test strip inside.

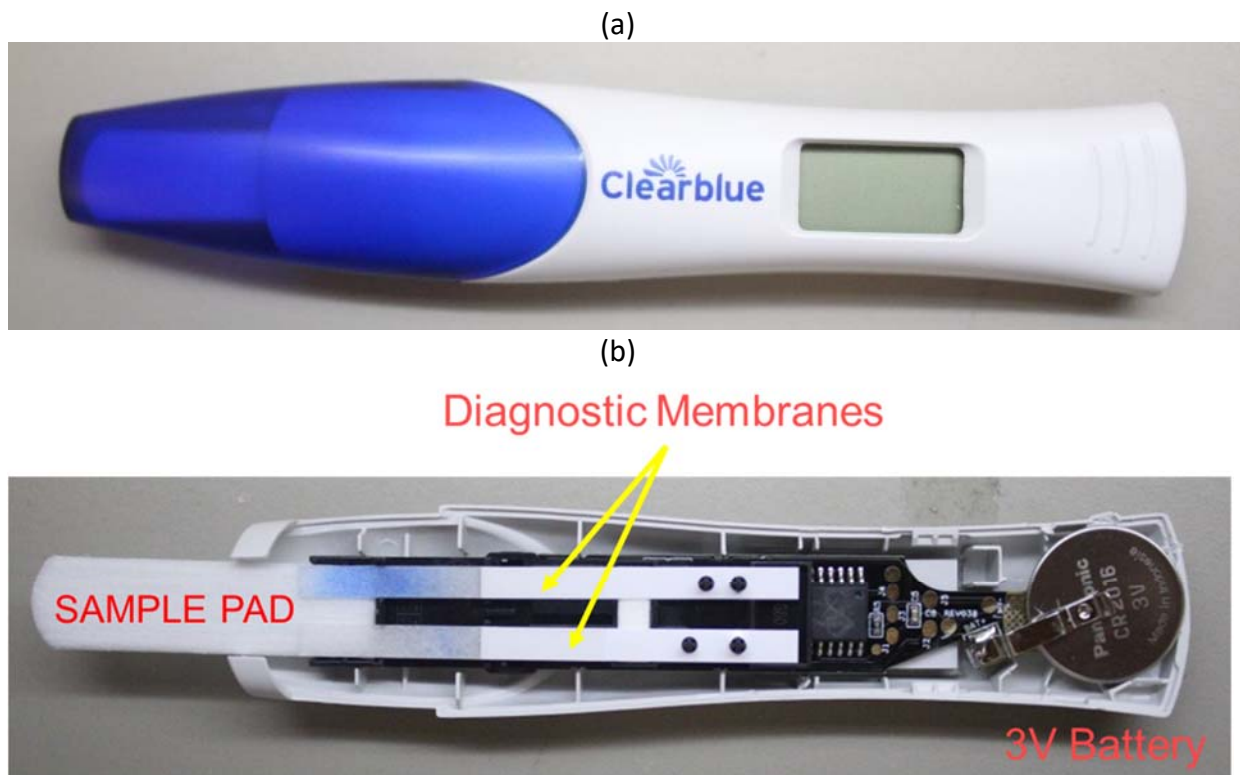


Figure B-1 Clearblue test device: (a) As packaged device; (b) Top cover removed to reveal the test strips inside.

When further disassembled, it was found that the test strips lay on top of a waveguide (plastic) for the light from LED to be guided. There were 4 LEDs and one large photodiode as detector. The whole circuit was powered using a 3V battery. The device contained an LCD screen and a driver IC. These components are shown in the Figure B-2 below.

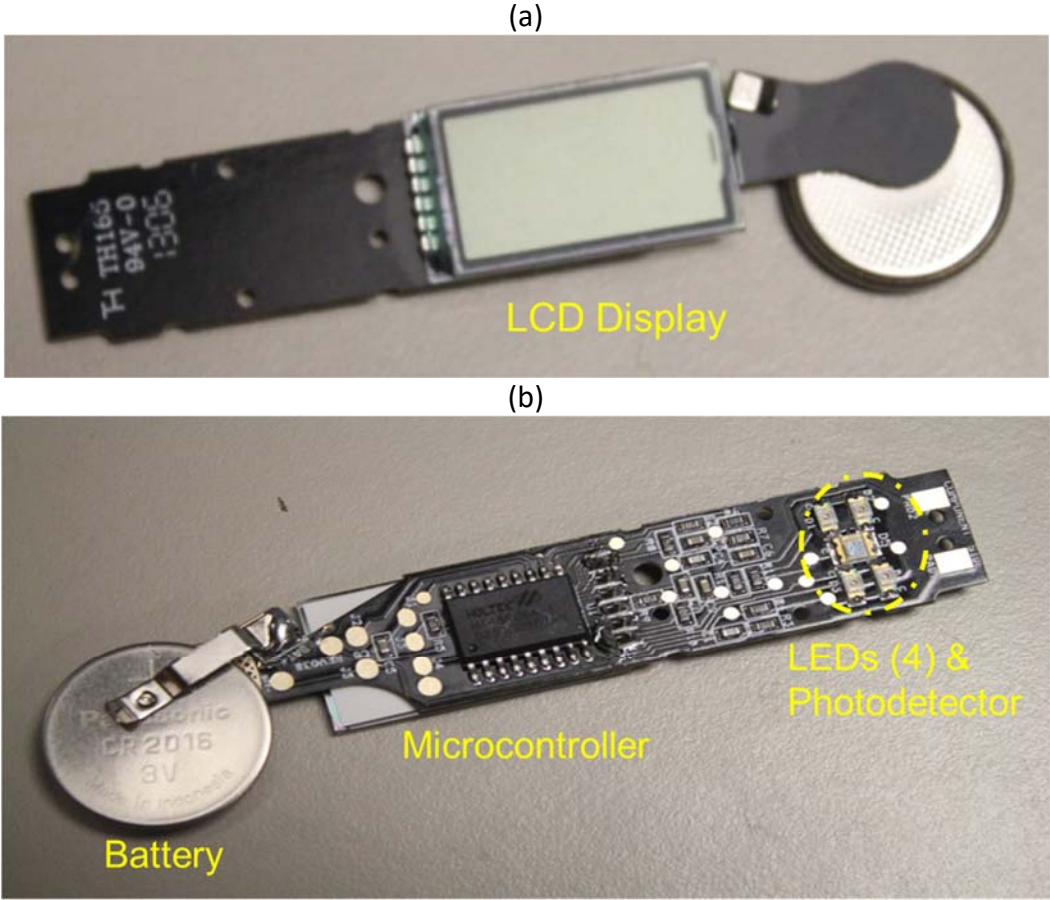


Figure B-2 Optoelectronics inside the device: (a) LCD screen and battery; (b) LEDs and photodetector and microelectronics.

2. Cost analysis:

One of the interesting and curious aspects of this device is its low cost. We looked up for costs of the components inside for small scale manufacturing and came up with the following table.

Part Name	Manufacturer	Vendor	Price \$ (low qnt)	Price \$ (large qnt)
Battery 3V (1)	Panasonic	DK # : P138-ND	0.31	0.15
Micro controller (1)	Holtek	ic-online: ht48r06a-1	1.22	1.0
LCD display (1)	Lumex Opto	DK #: 67-1799-ND	2.28	0.79
LEDs (4)	OSRAM Opto	DK #: 475-1278-2-ND	not listed	0.03
Photodiode (1)	Adv Photonix	DK # : PDB-C154SMTR-ND	0.46	0.42
Chip resistors (10)	Stackpole Electronics	RNCP0603FTD10R0TR-ND	0.0034	0.0023
Chip capacitors (6)	Yageo Electronics	311-1343-2-ND	0.0032	0.0019

Table B-1 Various parts and their details inside a clearblue test device.

The total price for large quantity (>1000) components came to about \$2.5. Considering the retail price of the product, \$6 for 3, the component cost alone is quite high. Further other expenses such as labor and marketing have not been considered. Hence the retail cost of this device may seem perplexing, however, considering the current progress of microelectronics, power of ICs and its lower costs, a rational sense can be drawn.

A simple pregnancy test strip (bare) costs only tens of cents and hence the price of Clearblue device can still be considered relatively high. With the organic optoelectronics roll to roll fabrication we believe our device manufacturing cost can significantly be lower as well. The NFC chip when hybrid manufactured over large quantities (>1 million units) can be as low as tens of cents and can be potentially lowered on setting up a constant fabrication procedure.

Appendix C: Cost analysis of proposed approach

1. OLED and OPD Fabrication cost

1.1 Layers Cost

An estimate can be presented for the fabrication expense of a single device. Only an estimate is possible as the amount of material consumed while depositing a layer is unknown and can only best be predicted based on the frequency of replenishing of the material. This was predicted as 1mg per nanometer of the deposited material (irrespective of the material) in Dr. Gomez's thesis⁸³. The lead to a cost of organic and thin film deposition cost of \$13.04 (no substrate and anode) per run based on the cost of material shown in the Table C-1 below for the OLED. For OPD, the consumption rate could not be predicted and hence a quote is not presented here.

Material	Price/g	OLED thickness (nm)	OLED Type
Al	\$2.80	40	Electrode
LiF	\$4.00	1	EIL
Alq3	\$62.00	35	EIL
CBP	\$170.00	30	EL
Ir(ppy)3	\$620.00	3	EL
BCP	\$260.00	12	HBL
NPB	\$40.00	17	HBL

Table C-1 Cost of each material used for OLED and OPD⁸³

1.2 Substrate Cost

Our substrates for devices in plastic were ITO coated PET sheets purchased from Sigma-Aldrich. It is quoted at \$30 for a 1 ft² sheet. Which translates to \$0.1 per device (15 × 15 mm²). This cost of course does not include the expenses of photolithography to pattern these devices.

Hence the total cost for an OLED device (4 × 4 mm²) fabricated on PET sheet of 15 × 15 mm² is ~ \$1.1. This cost does not include other expenses such as labor, wet chemical processes, equipment setup and maintenance costs and the facility costs.

Further, this cost can further be decreased by using solution processing and a roll-to-roll manufacturing setup.

2. Microelectronics on PET Fabrication

We have previously described in Chapter 4, the fabrication of the NFC antenna circuitry using hybrid manufacturing. Such a manufacturing process is roll-to-roll compatible and for a medium size manufacturing (< 1 million units), the cost is tens of cents. With more components, such as photodiodes, other ICs and indicator LEDs, it would be safe to assume the total cost as ~\$1 for the NFC and the detector circuits.

3. LFIA Test kits:

All the test kits used in this research work were in kind donation from Meridian Bioscience Inc. based in Cincinnati, OH, USA. The two major kits used in this work were the Tru-flu kit and the Rotavirus kit. Each kit contained multiple tests inside them (~ 30 counts). And each device costs

roughly ~\$10. These kits are for specialized applications and hence the reason for their high prices. However, for common tests like pregnancy test strips, can be obtained for much lower price of 10-50 cents per piece and also on larger quantities for test repetition. The clearblue digital test strip on the other hand costs moderate at \$6 per piece, which can become of significant concern as the number of tests need to be performed increase, which is typically done to ensure the results of the device.

Our optoelectronics fabricated all on plastic, integrated with individual strips as described above can cost about \$2-\$3, if manufactured in our lab. The major cost consuming portion, currently is the flat battery retiling at at least \$5. However, this cost may potentially be significantly reduced by using low cost as well as larger manufacturing using roll-to-roll processing. Table C-2 below summarizes the cost.

Vendor	Cost per test	Analyte
Meridian Bioscience	\$10	HCG, Rotavirus
Easy@Home Pregnancy	\$0.4	HCG
Clearblue Pregnancy	\$6	HCG
Nanolab Integrated device	\$7	HCG or others

Table C-2 Commercial device costs and Nanolab's proposed design cost

REFERENCES

- 1 Tüdős, A. J., Besselink, G. A. & Schasfoort, R. B. Trends in miniaturized total analysis systems for point-of-care testing in clinical chemistry. *Lab on a Chip* **1**, 83-95 (2001).
- 2 Martinez, A. W., Phillips, S. T., Whitesides, G. M. & Carrilho, E. (ACS Publications, 2009).
- 3 Abgrall, P. & Gue, A. Lab-on-chip technologies: making a microfluidic network and coupling it into a complete microsystem—a review. *Journal of Micromechanics and Microengineering* **17**, R15 (2007).
- 4 Gervais, L., De Rooij, N. & Delamarche, E. Microfluidic chips for point-of-care immunodiagnosics. *Advanced Materials* **23** (2011).
- 5 Martinez, A. W., Phillips, S. T., Whitesides, G. M. & Carrilho, E. Diagnostics for the developing world: microfluidic paper-based analytical devices. *Analytical chemistry* **82**, 3-10 (2009).
- 6 Parolo, C. & Merkoçi, A. Paper-based nanobiosensors for diagnostics. *Chemical Society Reviews* **42**, 450-457 (2013).
- 7 Fu, E., Ramsey, S. A., Kauffman, P., Lutz, B. & Yager, P. Transport in two-dimensional paper networks. *Microfluidics and nanofluidics* **10**, 29-35 (2011).
- 8 Yetisen, A. K., Akram, M. S. & Lowe, C. R. Paper-based microfluidic point-of-care diagnostic devices. *Lab on a Chip* **13**, 2210-2251 (2013).

- 9 Posthuma-Trumpie, G. A., Wichers, J. H., Koets, M., Berendsen, L. B. J. M. & van Amerongen, A. Amorphous carbon nanoparticles: a versatile label for rapid diagnostic (immuno)assays. *Analytical and bioanalytical chemistry* **402**, 593-600, doi:10.1007/s00216-011-5340-5 (2012).
- 10 Rohrman, B. A., Leautaud, V., Molyneux, E. & Richards-Kortum, R. R. A Lateral Flow Assay for Quantitative Detection of Amplified HIV-1 RNA. *PLoS ONE* **7**, e45611, doi:10.1371/journal.pone.0045611 (2012).
- 11 Williams, G., Backhouse, C. & Aziz, H. Integration of organic light emitting diodes and organic photodetectors for lab-on-a-chip bio-detection systems. *Electronics* **3**, 43-75 (2014).
- 12 Gomez, E. F., Venkatraman, V., Grote, J. G. & Steckl, A. J. Exploring the potential of nucleic acid bases in organic light emitting diodes. *Advanced Materials* (2014).
- 13 Gomez, E. F., Venkatraman, V., Grote, J. G. & Steckl, A. J. DNA bases thymine and adenine in bio-organic light emitting diodes. *Scientific reports* **4** (2014).
- 14 Purandare, S., Gomez, E. F. & Steckl, A. J. High brightness phosphorescent organic light emitting diodes on transparent and flexible cellulose films. *Nanotechnology* **25**, 094012 (2014).
- 15 Zocco, A. T., You, H., Hagen, J. A. & Steckl, A. J. Pentacene organic thin-film transistors on flexible paper and glass substrates. *Nanotechnology* **25**, 094005 (2014).
- 16 Acharya, T., Daar, A. S., Thorsteinsdottir, H., Dowdeswell, E. & Singer, P. A. Strengthening the role of genomics in global health. *PLoS medicine* **1**, 195 (2004).

- 17 Posthuma-Trumpie, G. A., Korf, J. & van Amerongen, A. Lateral flow (immuno) assay: its strengths, weaknesses, opportunities and threats. A literature survey. *Analytical and bioanalytical chemistry* **393**, 569-582 (2009).
- 18 Carrilho, E., Martinez, A. W. & Whitesides, G. M. Understanding wax printing: a simple micropatterning process for paper-based microfluidics. *Analytical chemistry* **81**, 7091-7095 (2009).
- 19 Nie, Z. *et al.* Electrochemical sensing in paper-based microfluidic devices. *Lab on a Chip* **10**, 477-483 (2010).
- 20 Martinez, A. W., Phillips, S. T., Wiley, B. J., Gupta, M. & Whitesides, G. M. FLASH: a rapid method for prototyping paper-based microfluidic devices. *Lab on a Chip* **8**, 2146-2150 (2008).
- 21 Nie, Z., Deiss, F., Liu, X., Akbulut, O. & Whitesides, G. M. Integration of paper-based microfluidic devices with commercial electrochemical readers. *Lab on a Chip* **10**, 3163-3169 (2010).
- 22 Cheng, C. M. *et al.* Paper-Based ELISA. *Angewandte Chemie International Edition* **49**, 4771-4774 (2010).
- 23 Pollock, N. R. *et al.* A paper-based multiplexed transaminase test for low-cost, point-of-care liver function testing. *Science translational medicine* **4**, 152ra129-152ra129 (2012).
- 24 Martinez, A. W., Phillips, S. T., Butte, M. J. & Whitesides, G. M. Patterned paper as a platform for inexpensive, low-volume, portable bioassays. *Angewandte Chemie International Edition* **46**, 1318-1320 (2007).

- 25 Ellerbee, A. K. *et al.* Quantifying colorimetric assays in paper-based microfluidic devices by measuring the transmission of light through paper. *Analytical chemistry* **81**, 8447-8452 (2009).
- 26 Martinez, A. W. *et al.* Simple telemedicine for developing regions: camera phones and paper-based microfluidic devices for real-time, off-site diagnosis. *Analytical chemistry* **80**, 3699-3707 (2008).
- 27 Mark, D., Haeberle, S., Roth, G., von Stetten, F. & Zengerle, R. Microfluidic lab-on-a-chip platforms: requirements, characteristics and applications. *Chemical Society Reviews* **39**, 1153-1182 (2010).
- 28 Chou, S.-F. Development of a manual self-assembled colloidal gold nanoparticle-immunochromatographic strip for rapid determination of human interferon- γ . *Analyst* **138**, 2620-2623, doi:10.1039/c3an36547f (2013).
- 29 Tang, C. W. & VanSlyke, S. Organic electroluminescent diodes. *Applied physics letters* **51**, 913-915 (1987).
- 30 Steckl, A. J. Circuits on cellulose. *Spectrum, IEEE* **50**, 48-61 (2013).
- 31 Craig Freudenrich, P. D. "How OLEDs Work" (2005).
- 32 OLED.
- 33 Hicks/NREL, A. Organic photovoltaic cell structure.
- 34 Galagan, Y. & Andriessen, R. *Organic photovoltaics: technologies and manufacturing*. (InTech, 2012).

- 35 Shin, K.-S. *et al.* Characterization of an integrated fluorescence-detection hybrid device with photodiode and organic light-emitting diode. *IEEE Electron device letters* **27**, 746-748 (2006).
- 36 Kim, Y.-H. *et al.* Poly (dimethylsiloxane)-based packaging technique for microchip fluorescence detection system applications. *Journal of microelectromechanical systems* **15**, 1152-1158 (2006).
- 37 Pais, A., Banerjee, A., Klotzkin, D. & Papautsky, I. High-sensitivity, disposable lab-on-a-chip with thin-film organic electronics for fluorescence detection. *Lab on a Chip* **8**, 794-800 (2008).
- 38 Helfrich, W. & Schneider, W. Recombination radiation in anthracene crystals. *Physical Review Letters* **14**, 229 (1965).
- 39 Tang, C. W. & VanSlyke, S. A. Organic electroluminescent diodes. *Applied physics letters* **51**, 913-915 (1987).
- 40 Adachi, C., Baldo, M. A., Thompson, M. E. & Forrest, S. R. Nearly 100% internal phosphorescence efficiency in an organic light-emitting device. *Journal of Applied Physics* **90**, 5048-5051 (2001).
- 41 Yu, G., Gao, J., Hummelen, J. C., Wudl, F. & Heeger, A. J. Polymer photovoltaic cells: Enhanced efficiencies via a network of internal donor-acceptor heterojunctions. *Science* **270**, 1789 (1995).
- 42 Brabec, C. J., Dyakonov, V., Parisi, J. & Sariciftci, N. S. *Organic photovoltaics: concepts and realization*. Vol. 60 (Springer Science & Business Media, 2013).

- 43 Forrest, S. R. The path to ubiquitous and low-cost organic electronic appliances on plastic. *Nature* **428**, 911-918 (2004).
- 44 Lab, U. Physical Vapor Deposition.
- 45 Sony Develops a "Rollable" OTFT-driven OLED Display that can wrap around a Pencil.
- 46 Bamrungsap, S., Apiwat, C., Chantima, W., Dharakul, T. & Wiriyaichaiorn, N. Rapid and sensitive lateral flow immunoassay for influenza antigen using fluorescently-doped silica nanoparticles. *Microchimica Acta* **181**, 223-230 (2014).
- 47 Corstjens, P. L. *et al.* Up-converting phosphor technology-based lateral flow assay for detection of Schistosoma circulating anodic antigen in serum. *Journal of clinical microbiology* **46**, 171-176 (2008).
- 48 Gui, C., Wang, K., Li, C., Dai, X. & Cui, D. A CCD-based reader combined with CdS quantum dot-labeled lateral flow strips for ultrasensitive quantitative detection of CagA. *Nanoscale research letters* **9**, 1-8 (2014).
- 49 Xia, X., Xu, Y., Zhao, X. & Li, Q. Lateral flow immunoassay using europium chelate-loaded silica nanoparticles as labels. *Clinical chemistry* **55**, 179-182 (2009).
- 50 Xie, Q.-Y. *et al.* Advantages of fluorescent microspheres compared with colloidal gold as a label in immunochromatographic lateral flow assays. *Biosensors and Bioelectronics* **54**, 262-265 (2014).
- 51 Faulstich, K., Gruler, R., Eberhard, M., Lentzsch, D. & Haberstroh, K. in *Lateral flow immunoassay* 1-27 (Springer, 2009).

- 52 Dunn, J. *et al.* Prompt detection of influenza A and B viruses using the BD Veritor™ System Flu A+ B, Quidel® Sofia® Influenza A+ B FIA, and Alere BinaxNOW® Influenza A&B compared to real-time reverse transcription-polymerase chain reaction (RT-PCR). *Diagnostic microbiology and infectious disease* **79**, 10-13 (2014).
- 53 Lu, W., Ji, Z., Pfeiffer, L., West, K. & Rimberg, A. Real-time detection of electron tunnelling in a quantum dot. *Nature* **423**, 422-425 (2003).
- 54 He, R. *et al.* Core/shell fluorescent magnetic silica-coated composite nanoparticles for bioconjugation. *Nanotechnology* **18**, 315601 (2007).
- 55 Cui, D. *et al.* Self-assembly of quantum dots and carbon nanotubes for ultrasensitive DNA and antigen detection. *Analytical chemistry* **80**, 7996-8001 (2008).
- 56 Han, M., Gao, X., Su, J. Z. & Nie, S. Quantum-dot-tagged microbeads for multiplexed optical coding of biomolecules. *Nature biotechnology* **19**, 631-635 (2001).
- 57 Li, Z. *et al.* Arginine-glycine-aspartic acid-conjugated dendrimer-modified quantum dots for targeting and imaging melanoma. *Journal of nanoscience and nanotechnology* **10**, 4859-4867 (2010).
- 58 Montón, H. *et al.* in *Nanoparticles in Biology and Medicine* 185-192 (Springer, 2012).
- 59 Taranova, N., Berlina, A., Zherdev, A. & Dzantiev, B. 'Traffic light' immunochromatographic test based on multicolor quantum dots for the simultaneous detection of several antibiotics in milk. *Biosensors and Bioelectronics* **63**, 255-261 (2015).

- 60 Yang, H. *et al.* A novel quantum dots–based point of care test for syphilis. *Nanoscale research letters* **5**, 875-881 (2010).
- 61 Li, Z. *et al.* Rapid and sensitive detection of protein biomarker using a portable fluorescence biosensor based on quantum dots and a lateral flow test strip. *Analytical chemistry* **82**, 7008-7014 (2010).
- 62 Tang, C. & VanSlyke, S. Organic electroluminescent diodes. *Applied Physics Letters* **51**, 913-915 (1987).
- 63 Freudenthal, E. *et al.* in *Engineering in Medicine and Biology Workshop, 2007 IEEE Dallas*. 51-54 (IEEE).
- 64 Chin, C. D., Linder, V. & Sia, S. K. Commercialization of microfluidic point-of-care diagnostic devices. *Lab on a Chip* **12**, 2118-2134 (2012).
- 65 Berlina, A. N., Taranova, N. A., Zherdev, A. V., Vengerov, Y. Y. & Dzantiev, B. B. Quantum dot-based lateral flow immunoassay for detection of chloramphenicol in milk. *Analytical and bioanalytical chemistry* **405**, 4997-5000 (2013).
- 66 Qu, H. *et al.* Rapid lateral-flow immunoassay for the quantum dot-based detection of puerarin. *Biosensors and Bioelectronics* **81**, 358-362 (2016).
- 67 Venkatraman, V. & Steckl, A. J. Integrated OLED as excitation light source in fluorescent lateral flow immunoassays. *Biosensors and Bioelectronics* **74**, 150-155 (2015).
- 68 Koo, M. *et al.* Bendable inorganic thin-film battery for fully flexible electronic systems. *Nano letters* **12**, 4810-4816 (2012).

- 69 Yin, L. *et al.* Materials, designs, and operational characteristics for fully biodegradable primary batteries. *Advanced Materials* **26**, 3879-3884 (2014).
- 70 Choi, S. Powering point-of-care diagnostic devices. *Biotechnology advances* **34**, 321-330 (2016).
- 71 Qiao, W., Cho, G. & Lo, Y.-H. Wirelessly powered microfluidic dielectrophoresis devices using printable RF circuits. *Lab on a Chip* **11**, 1074-1080 (2011).
- 72 García, A. *et al.* Mobile phone platform as portable chemical analyzer. *Sensors and Actuators B: Chemical* **156**, 350-359 (2011).
- 73 Martinez, A. W. *et al.* Simple Telemedicine for Developing Regions: Camera Phones and Paper-Based Microfluidic Devices for Real-Time, Off-Site Diagnosis. *Analytical Chemistry* **80**, 3699-3707, doi:10.1021/ac800112r (2008).
- 74 Wang, S. *et al.* Integration of cell phone imaging with microchip ELISA to detect ovarian cancer HE4 biomarker in urine at the point-of-care. *Lab on a Chip* **11**, 3411-3418, doi:10.1039/c1lc20479c (2011).
- 75 Erickson, D. *et al.* Smartphone technology can be transformative to the deployment of lab-on-chip diagnostics. *Lab on a Chip* **14**, 3159-3164 (2014).
- 76 Shen, L., Hagen, J. A. & Papautsky, I. Point-of-care colorimetric detection with a smartphone. *Lab on a Chip* **12**, 4240-4243 (2012).

- 77 Lee, S. *et al.* Flexible opto-electronics enabled microfluidics systems with cloud connectivity for point-of-care micronutrient analysis. *Biosensors and Bioelectronics* **78**, 290-299 (2016).
- 78 Hobby, A. SCREEN PRINTING FOR THE INDUSTRIAL USER.
- 79 Kim, S. & Park, J.-K. Development of a test strip reader for a lateral flow membrane-based immunochromatographic assay. *Biotechnology and Bioprocess Engineering* **9**, 127-131 (2004).
- 80 Vishak, V., Ralph, L., Kenneth, K. & Andrew, J. S. Integrated NFC power source for zero on-board power in fluorescent paper-based lateral flow immunoassays. *Flexible and Printed Electronics* **1**, 044001 (2016).
- 81 Aziz, H., Popovic, Z. D., Hu, N.-X., Hor, A.-M. & Xu, G. Degradation mechanism of small molecule-based organic light-emitting devices. *Science* **283**, 1900-1902 (1999).
- 82 Sajid, M., Kawde, A.-N. & Daud, M. Designs, formats and applications of lateral flow assay: A literature review. *Journal of Saudi Chemical Society* (2014).
- 83 Gomez, E. F. *Investigation of DNA Nucleobases for Bio-Organic Light Emitting Diodes*, University of Cincinnati, (2015).